The influence of rotational speed in the Friction Stir Welding of 6082-T6 aluminium alloy joints

By

Busiswa Tracey Jantjies

Thesis submitted towards the degree

Master of Engineering in Mechanical Engineering

in the Faculty of Engineering and Built Environment

at the Cape Peninsula University of Technology

Supervisor:
Dr V. Msomi

Bellville
September 2019

DECLARATION

I, Busiswa Tracey Jantjies, declare that the contents of this dissertation/thesis represent my own unaided work, and that the dissertation/thesis has not previously been submitted for academic examination towards any qualification. Furthermore, it represents my own opinions and not necessarily those of the Cape Peninsula University of Technology.

13/09/2019

Signed **Date**

ABSTRACT

Friction Stir Welding is regarded as a great welding technique compared to other welding processes. As a welding technique, it has good advantages as well as lesser disadvantages. It is categorised as a solid-joining technique with the aid of applied force and friction. A non-deteriorating rotating tool is plunged between two materials (similar or dissimilar) to be joined at a specific rotational and welding speed. The tool is moved through the material rubbing against them, causing them to soften and fuse before they solidify. This technique is mostly used in the welding of aluminium alloys especially in the automotive, aerospace and marine industries; as it produces high-quality welds with very low porosity, lesser change in material, low distortion and low shrinkage.

This research reports on the influence of rotational speeds on friction stir welded 6082-T6 Aluminium Alloy plates of 6 mm thickness. The different rotational speeds tested were, 600, 700, 800, 900, 1000 and 1200 rotation per minute (rpm). The microstructure and macrostructure were also evaluated under optical microscopes and compared. The 6082 aluminium alloy specimens were tensile tested, using the Hounsfield machine. The fractured tensile specimens underwent fracture analysis taking fractographs using the Scanning Electron Microscope (SEM). The material's hardness was tested using the Rockwell B hardness (HRB). Results show that high rotational speeds with a welding speed of 80 mm/min have a negative effect on the welds at the start and middle of weld but positive effect at the end for tensile properties and grain sizes. Rotational speed of 600 rpm was found to produce welds with higher tensile properties with smaller grain sizes. While 1000 rpm was found to be suitable to get high hardness values.

ACKNOWLEDGEMENTS

It would not have been possible to complete this thesis without the encouragement and guidance that I have received throughout. I was able to garner the strength and ability needed to conduct the research and write a full dissertation.

Firstly, I would like to extend my gratitude to my supervisor Dr V. Msomi for his supervision, guidance, assistance and giving me this opportunity to do my research with him at the Cape Peninsula University of Technology. I also wish to extend my gratitude specifically to the Department of Mechanical Engineering at the University; for providing the research equipment and facilities necessary for this research.

To the people working at the Department of Mechanical Engineering from the workshop to the management team, your assistance and guidance is much appreciated. Thank you so much for your time and efforts. The research would not have been possible without your combined efforts.

To my dear friend and mentor Ms K. S-G Brown, I would like to thank you for your valuable advice, encouragement and assistance throughout this study.

Finally, I would like to thank the National Research Foundation (NRF) for their financial assistance provided in support of my fulfilment of the degree Master of Engineering.

Declaration

Opinions expressed in this thesis and the conclusions arrived at, are those of the author, and are not necessarily to be attributed to the National Research Foundation.

I am forever grateful for all your contributions in helping me to achieve this goal. Thank you.

DEDICATION

To my dearest mother and primary source of strength, Nombuyiselo Virginia Jantjies. Thank you for your support, tolerance and inspiration throughout my study period.

TABLE OF CONTENTS

DECLARATION ii
ABSTRACT iii
ACKNOWLEDGEMENTS iv
DEDICATION v
TABLE OF CONTENTS vi
LIST OF FIGURES viii
LIST OF TABLES x
GLOSSARY xi
CHAPTER 1: INTRODUCTION 1
1.1 Introduction 1
1.2 Problem statement 2
1.3 Background 2
1.4 Research Objectives 5
1.5. Organization of the dissertation 5
CHAPTER 2: LITERATURE REVIEW 6
2.1 Variation of welding parameters 6
2.2 Impact of rotational speed in dissimilar materials 7
2.2.1 Impact of rotational speed on tensile properties of the weld 7
2.2.2 Effect of rotational speed variation on hardness 8
2.2.3 Effect of rotational speed variation on microstructure 9
2.3 Impact of rotational speed in similar materials 10
2.3.1 Impact of rotational speed on tensile properties of the weld 10
2.3.2 Effect of rotational speed variation on hardness 11
2.3.3 Effect of rotational speed variation on microstructure 12
2.4 Summary 13
CHAPTER 3: EXPERIMENTAL SETUP AND PERFORMANCE 14
3.1 Equipment used for producing welds 14
3.1.1 TA Shear Master guillotine 14
3.1.2 Semi-automated milling machine (LAGUN FA. 1-LA)/ FSW Machine 15
3.2 Welding performance 15
3.2.1 Friction Stir Welding 16
3.3 Weld preparation for analysis 18
3.3.1 Accutex AU-500iA EDM wire cutter 18
3.3.2 Mounting equipment 18
3.3.3 Grinding and polishing equipment for metallurgical specimens 19
3.4 Performance of specimen preparation 20
3.4.1 Tensile tests specimens 20
3.4.1.1 Cutting of specimens 21

3.4.2 Microstructure and macro-structure specimens 22
3.4.2.1 Mounting of specimens 23
3.4.2.2 Grinding and polishing of specimens 24
3.4.2.3 Etching of specimens 25
3.5 List of Tests performed 26
3.6 Mechanical Tests 27
3.6.1 Tensile tests 27
3.6.2 Rockwell Hardness tests 28
3.7 Microstructure and Macrostructure Tests 29
3.7.1 Fractography Analysis 29
3.7.2 Microstructure analysis 30
3.7.3 Macro-structure analysis 31
CHAPTER 4: RESULTS AND DISCUSSIONS 32
4.1 Tensile Tests 32
4.1.1 Micro-fractography analysis 35
4.2 Microstructure 42
4.2.1 Grains at rotational speed of 600 rpm 44
4.2.1.1 Stir Zone (SZ) 45
4.2.1.2 Thermo-Mechanically Affected Zone (TMAZ) 45
4.2.1.3 Heat Affected Zone (HAZ) 46
4.2.2 Grains at rotational speed of 700 rpm 46
4.2.2.1 Stir Zone (SZ) 47
4.2.2.2 Thermo-Mechanically Affected Zone (TMAZ) 47
4.2.2.3 Heat Affected Zone (HAZ) 48
4.2.3 Grains at rotational speed of 800 rpm 48
4.2.3.1 Stir Zone (SZ) 49
4.2.3.2 Thermo-Mechanically Affected Zone (TMAZ) 49
4.2.3.3 Heat Affected Zone (HAZ) 50
4.2.4 Grains at rotational speed of 900 rpm 50
4.2.4.1 Stir Zone (SZ) 51
4.2.4.2 Thermo-Mechanically Affected Zone (TMAZ) 51
4.2.4.3 Heat Affected Zone (HAZ) 52
4.2.5 Grains at rotational speed of 1000 rpm 52
4.2.5.1 Stir Zone (SZ) 52
4.2.5.2 Thermo-Mechanically Affected Zone (TMAZ) 53
4.2.5.3 Heat Affected Zone (HAZ) 54
4.2.6 Grains at rotational speed of 1200 rpm 54
4.2.6.1 Stir Zone (SZ) 54
4.2.6.2 Thermo-Mechanically Affected Zone (TMAZ) 55
4.2.6.3 Heat Affected Zone (HAZ) 56
4.3 Macrostructure 56
4.4 Rockwell Hardness 61
4.5 Summary 63
CHAPTER 5: CONCLUSION AND FUTURE WORK 64
5.1 Conclusion 64
5.2 Future work 65
Bibliography 66

APPENDICES **72**
APPENDIX A **73**
FSW Stress-Strain test results at different speeds **73**
Appendix B **79**
Hardness Scale Conversion Table **79**

LIST OF FIGURES

Figure 1.1 Two different types of friction stir welding, (a) Conventional and (b) Bobbin, [Esmaily et al., 2016] 2
Figure 1.3: Microstructure and mechanical properties of friction stir welded 2060 aluminium alloy at different rotational speeds, [Mao et al., 2015] 3
Figure 1.4: Forces found in material flow in the weld beneath the shoulder. (a) Vertical section. (b) cross-section, [Huang et al., 2016] 4
Figure 3.1: Guillotine Machine 14
Figure 3.2: Friction Stir Welding Machine used 15
Figure 3.3: H13 Tool 16
Figure 3.4: FSW setup of two 6082-T6 Al alloy plates 17
Figure 3.5: Welded plates 17
Figure 3.6: The Accutex AU-500iA EDM Wire Cutter 18
Figure 3.7: The Struers LaboPress-3 mounting machine with specimen after mounting 19
Figure 3.8: Grinding and polishing tools 20
Figure 3.9: Dimensioned Tensile testing specimen according to the ASTM E8M-04 standards without weld 20
Figure 3.10: Plate placed and clamped in the wire cutter. 21
Figure 3.11: Marked and cut 1000 rpm work piece 22
Figure 3.12: Cut out tensile specimens of 600 rpm from start and middle 22
Figure 3.13: Dimensioned microstructure and micro-hardness testing specimen without weld 22
Figure 3.14: Cut out microstructure specimen. 23
Figure 3.15: Mounted specimens for 1200 rpm 24
Figure 3.16: Mounted and etched specimens with (a) Weck's reagent and (b) Keller's reagent 26
Figure 3.17: Bench top Hounsfield tensile tester 27
Figure 3.18: The Future-Tech Rockwell hardness tester 28
Figure 3.19: Indented macro hardness specimens 29
Figure 3.20: Desktop Phanom Pro SEM (Kaplonek & Nadolny, 2013) 30
Figure 3.21: Cut off fractured tensile specimens 30
Figure 3.22: Nikon Eclipse L150 microscope and working desktop 31
Figure 3.23: Olympus microscope 31
Figure 4.1: Fractured tensile specimens 33
Figure 4.2: SEM fractograph for parent material 35

Figure 4.3: Fractured SEM photographs at the start of the weld for specimens (a) S1, (b) S2 and (C) S3 36
Figure 4.4: SEM fractographs at the start of the weld for specimens (a) S4, (b) S5 and (c) S6 37
Figure 4.5: SEM fractographs at the middle of the weld for specimens (a) M1, (b) M2 and (c) M3 38
Figure 4.6: SEM fractographs at the middle of the weld for specimens (a) M4, (b) M5 and (c) M6 39
Figure 4.7: SEM fractographs at the end of the weld for specimens (a) E1, (b) E2 and (c) E3 40
Figure 4.8: SEM fractographs at the end of the weld for specimens (a) E4, (b) E5 and (c) E6 41
Figure 4.9: Comparison of grain sizes in the stir zone 43
Figure 4.10: Comparison of grain sizes in the thermo-mechanically affected zone 43
Figure 4.11: Comparison of grain sizes in the heat affected zone 44
Figure 4.12: Microstructural grains in the centre of the Stir Zone, from the start (S1), middle (M1) and end (E1) of weld at 600rpm 45
Figure 4.13: Microstructural grains at the retreating and advancing sides of the Thermo-Mechanically Affected Zone, taken from the start (S1), middle (M1) and end (E1) of weld at 600rpm 45
Figure 4.14: Microstructural grains at the retreating and advancing sides of the Heat Affected Zone, taken from the start (S1), middle (M1) and end (E1) of weld at 600rpm 46
Figure 4.15: Microstructural grains in the centre of the Stir Zone, from the start (S2), middle (M2) and end (E2) of weld at 700rpm 47
Figure 4.16: Microstructural grains at the retreating and advancing sides of the Thermo-Mechanically Affected Zone, taken from the start (S2), middle (M2) and end (E2) of weld at 700rpm 47
Figure 4.17: Microstructural grains at the retreating and advancing sides of the Heat Affected Zone, taken from the start (S2), middle (M2) and end (E2) of weld at 700rpm 48
Figure 4.18: Microstructural grains in the centre of the Stir Zone, from the start (S3), middle (M3) and end (E3) of weld at 800rpm 49
Figure 4.19: Microstructural grains at the retreating and advancing sides of the Thermo-Mechanically Affected Zone, taken from the start (S3), middle (M3) and end (E3) of weld at 800rpm 49
Figure 4.20: Microstructural grains at the retreating and advancing sides of the Heat Affected Zone, taken from the start (S3), middle (M3) and end (E3) of weld at 800rpm 50
Figure 4.21: Microstructural grains in the centre of the Stir Zone, from the start (S4), middle (M4) and end (E4) of weld at 900rpm 51
Figure 4.22: Microstructural grains at the retreating and advancing sides of the Thermo-Mechanically Affected Zone, taken from the start (S4), middle (M4) and end (E4) of weld at 900rpm 51
Figure 4.23: Microstructural grains at the retreating and advancing sides of the Heat Affected Zone, taken from the start (S4), middle (M4) and end (E4) of weld at 900rpm 52
Figure 4.24: Microstructural grains in the centre of the Stir Zone, from the start (S5), middle (M5) and end (E5) of weld at 1000rpm 52
Figure 4.25: Microstructural grains at the retreating and advancing sides of the Thermo-Mechanically Affected Zone, taken from the start (S5), middle (M5) and end (E5) of weld at 1000rpm 53
Figure 4.26: Microstructural grains at the retreating and advancing sides of the Heat Affected Zone, taken from the start (S5), middle (M5) and end (E5) of weld at 1000rpm 54
Figure 4.27: Microstructural grains in the centre of the Stir Zone, from the start (S6), middle (M6) and end (E6) of weld at 1200rpm 55

Figure 4.28: Microstructural grains at the retreating and advancing sides of the Thermo-Mechanically Affected Zone, taken from the start (S6), middle (M6) and end (E6) of weld at 1200rpm 55
Figure 4.29: Microstructural grains at the retreating and advancing sides of the Heat Affected Zone, taken from the start (S6), middle (M6) and end (E6) of weld at 1200rpm 56
Figure 4.30: Lack of fill on 600, 800 and 1200 rpm welds 57
Figure 4.31: Macrostructure of FSW specimens taken from the start of the weld, welded at six different rotational speeds 58
Figure 4.32: Macrostructure of FSW specimens taken from the middle of the weld, welded at six different rotational speeds 59
Figure 4.33: Macrostructure of FSW specimens taken from the end of the weld, welded at six different rotational speeds 60
Figure 4.34: Rockwell hardness at the start of the weld for all rotational speeds 61
Figure 4.35: Rockwell hardness results at the middle of the weld for all rotational speeds 62
Figure 4.36: Rockwell hardness at the end of the weld for all rotational speeds 62

LIST OF TABLES

Table 3.1: Tool process parameters 17
Table 3.2: The AKASEL four polishing steps for preparing aluminium specimens 24
Table 3.3: NaOH Pre-Etch and Weck's Etchant concentration 25
Table 3.4: Keller's reagent concentration 25
Table 3.5: Parameters applied to tensile test machine 27
Table 4.1: FSW tensile property results for 6082-T6 Al alloys at the beginning of weld 33
Table 4.2: FSW tensile property results for 6082-T6 Al alloys at the middle of the weld 34
Table 4.3: FSW tensile property results for 6082-T6 Al alloys at the end of the weld ... 34

GLOSSARY

Terms/Acronyms/Abbreviations	Definition/Explanation
FSW: Friction Stir Welding	**Tool Rotational speed**: This is the speed at which the tool is rotating, measured in revolutions per minute (rpm)
FSP: Friction Stir Processing	
Al: Aluminium	**Travel speed**: This is the velocity at which the two aluminium alloy plates are fed, against the tool measured in millimetre per minute (mm/min).
TWI: The Welding Institute	
NASA: National Aeronautics and Space Administration	**Mechanical Properties**: Are the properties used to classify and identify the material, like strength, toughness and ductility.
HAZ: Heat Affected Zone	
TMAZ: Thermo-Mechanical Affected Zone	**Metallurgy**: The science of working or heating metals so as to give them certain desired mechanical properties.
XRD: X-Ray Diffraction	**6082-T6 Aluminium Alloy**: This is a medium strength aluminium alloy belonging to the 6000 series alloys.
SEM: Scanning Electron Microscope	**Stir-zone**: Is a region of heavily deformed material that roughly corresponds to the location of the pin during welding.
UTS: Ultimate Tensile Strength	
H13 Tool: Chromium hot work steel tool	**Grains**: Are small or even microscopic crystals which form during the cooling of many materials.
ASTM: American Society for Testing and Materials	**Workpiece**: Two friction stir welded 6082- T6 aluminium alloys
E8M-04 Standard: Standard Test Methods for Tension Testing of Metallic Materials	**Parent**: Is the 6082-T6 aluminium alloy specimen that is not welded

CHAPTER 1: INTRODUCTION

1.1 Introduction

There are mainly two categories of welding, namely; fusion and solid-state welding. Friction stir welding (FSW) falls under the solid-state welding category. This welding technique was invented by The Welding Institute (TWI) in the United Kingdom in the early 1990s, [Unnikrishnan & Dhas, 2017]. Friction Stir Welding (FSW) is a solid-state joining technique used in the joining of materials such as aluminium alloys that are not easy to join using fusion welding, [Adamowski et al., 2007]. It is an energy efficient technique that is environmentally friendly and can be joined to any metal without worrying about metals compatibility, [Mishra & Ma, 2005]. Friction stir welding is viewed as the solution towards the evaporation problem faced by the fusion as it has low joining temperatures, [Bozorgzadeh & Idris, 2015].

Friction stir welding comprises of two types; conventional welding and self-reacting welding as shown in Figure 1.1. Conventional FSW is the standard FSW and is more widely used. It uses a non-consumable rotating tool with a shoulder consisting of a specially designed pin. This rotating tool is plunged in between the joined materials. It moves from the beginning of the joint to the end producing welds of good quality, [Kallee et al., 2001]. As it moves, the heat is generated by the pin and plasticizes the material causing it to bond. The shoulder helps to keep the plasticized material from escaping, [Sakthivel et al., 2009]. Friction stir welding is considered to have reached a stationary state when the quality of the weld is the same through a long distance, [Tongne et al., 2016].

Self-reacting FSW on the other hand uses a double-sided tool, with one side of the tool consisting of a pin and a shoulder and the other side having only a shoulder. In this type of FSW, the pin is plunged at the top of the material while the second shoulder is plunged under the material to connect right under the pin with both sides moving together and welding both sides, [Wan et al., 2014]. There is a tool invented and patented by NASA for self-reacting FSW, which can be used for conventional FSW too by removing the modified bobbin pin and replacing it with the conventional FSW pin, [Venable & Bucher, 2004].

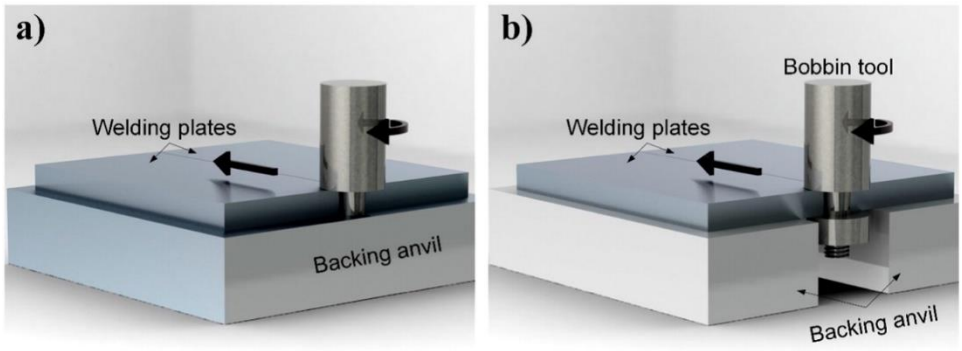

Figure 1.1 Shows two different types of friction stir welding, (a) Conventional and (b) Bobbin, [Esmaily et al., 2016]

1.2 Problem statement

Rotational speed in friction stir welding is one of the most important parameters which needs to be optimized in order to attain hot weld conditions and quality, [Rodrigues et al., 2010]. In order to perform Friction Stir Welding (FSW) on 6082-T6 aluminium alloy plates, the rotational speed of the tool should correlate with the material to achieve good results; taking into consideration that different aluminium alloys react differently to varying welding speeds. It remains a challenge to find optimum parameters for welding similar 6082-T6 aluminium alloy. Literature shows that there is a lot of work that has been done with the purpose of improving the quality of the welds. Most of the works vary the rotational speed together with the welding speed. This type of analysis does not really give a concrete conclusion around these parameters. This study investigates the impact of varying rotational speeds while keeping the welding speed constant during FSW of 6082-T6 aluminium alloy bought at Non-Ferous Metal Works Cape Town.

1.3 Background

The rotation of the tool in friction stir welding completely breaks down the stir zones microstructure to form finer and more equally spaced microstructure, [Moshwan et al., 2015]. Due to the high temperature during the friction stir welding in the stir zone, the grains change in geometry and size from those in the parent material, [Ahmadi et al., 2012]. As the grain sizes decrease, the hardness and tensile properties of the metal improves, [Ramnath et al., 2018]. These grains are said to be facing approximately in the same direction and have almost the same size, [Sharma & Dwivedi, 2017]. Singarapu et al. (2015) identified rotational speed and tool geometry as the cause of such change as they affect the stirring of a material at the stir zone. Onion rings become less visible as the rotational speed is increased, [Sharma et al., 2012].

Mao et al. (2015) investigated the effects of welding parameters that affect the friction stir welding of 2060 aluminium alloys focusing on welding and rotational speeds. The rotational speed of 1180 rpm at a welding speed of 118 mm/min was found to be the best suitable parameters (see figure 1.2). The rotational speed gave the highest mechanical properties and produced the smallest grain sizes.

Ugender et al. (2014) investigated the influence of process parameters on the friction stir welding of 6061 aluminium alloy joints by using different rotational and welding speeds. It was found that joints welded at a rotational speed of 1120 rpm and a welding speed of 40 mm/min had higher ultimate tensile strength, impact strength, yield strength and percentage of elongation.

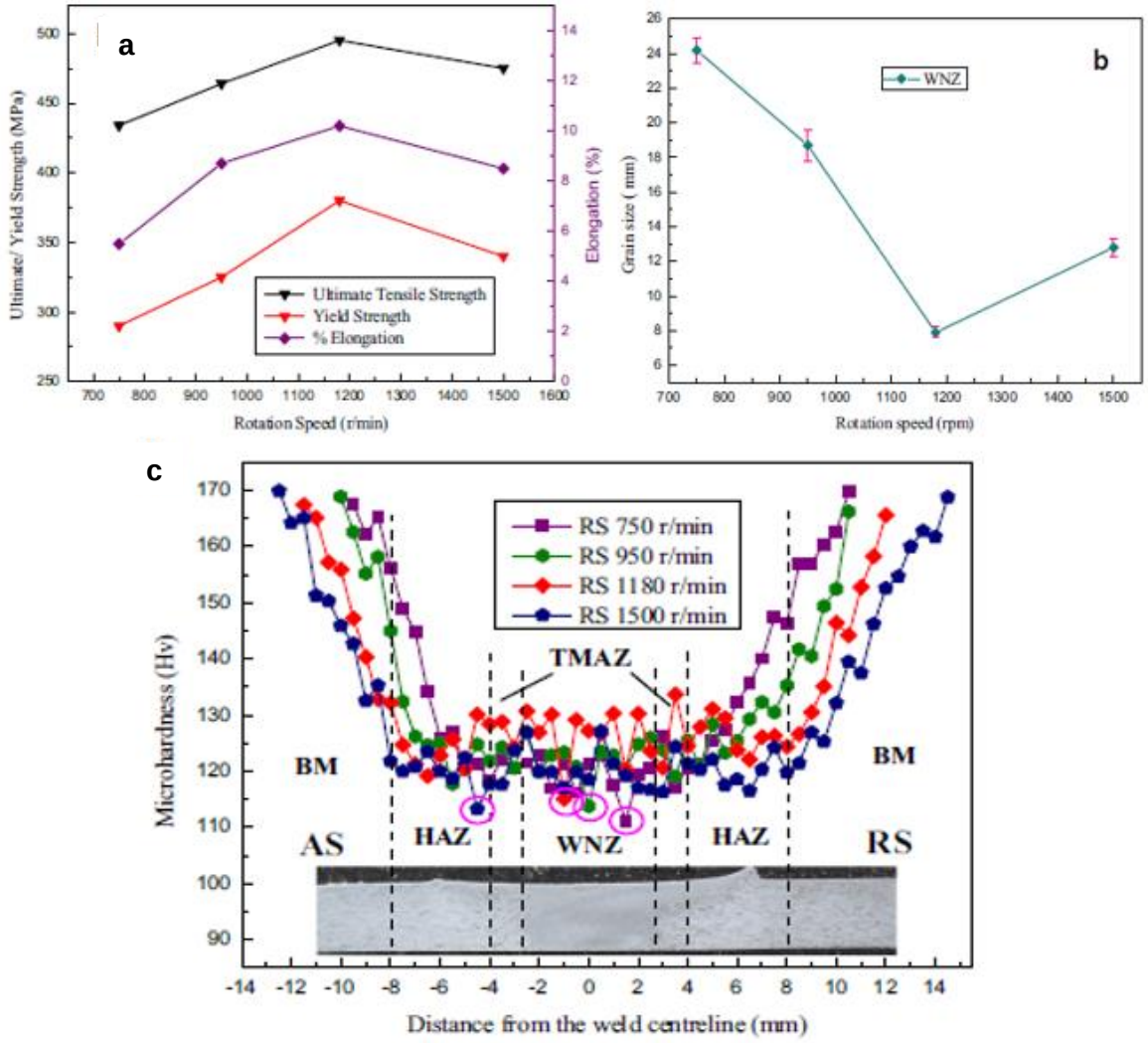

Figure 1.2: Shows microstructure and mechanical properties of friction stir welded 2060 aluminium alloy at different rotational speeds, [Mao et al., 2015]

Gemme et al. (2011) investigated the effects of welding parameters such as the rotational speed and welding speed in the friction stir welding of 2.3 mm thick AA7075-T6 aluminium

alloy joints. Higher rotational speed was found to increase the concavity of the nugget creating insufficient recrystallization but had the highest tensile property values.

Dawood et al. (2013) investigated the effect of rotational speed on flow behaviour and weld properties in friction stir welding of 2 mm thick pure aluminium by using three different rotational speed (1000, 1500 and 2000 rpm) with all other parameters kept constant, i.e. welding speed 60 mm/min. The rotational speed of 1500 rpm appeared to have the highest tensile strength higher than that of the base metal and had a defect-free and smoother surface. Higher rotational speeds cause more material to escape during the stirring process having a negative impact on the recrystallization of the weld to have insufficient material, [Elangovan & Balasubramanian, 2007].

Figure 1.3 shows the forces involved in generating material flow during friction stir welding. During welding, the tool is tilted by a specific angle creating an obliquely downward force that results from the downward force and a forward force. As the tool rotates, moving downward and forward ring vortex flow is created causing material to move from the retreating side to the advancing side, [Huang et al., 2016].

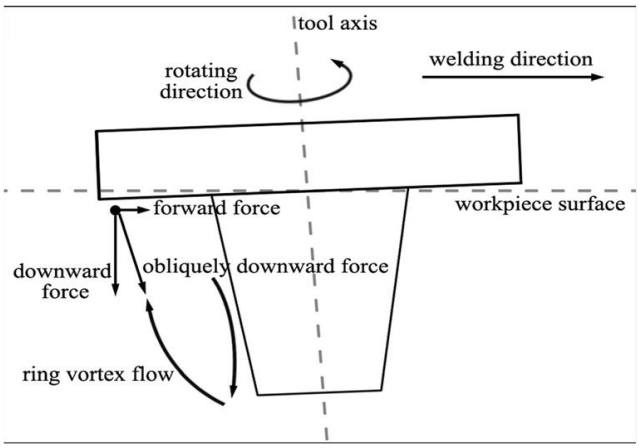

Figure 1.3: Shows the vertical section of forces found in material flow in the weld beneath the shoulder, [Huang et al., 2016]

The axial force on the weld will be weaker at the start and stronger as it progresses towards the end, [Ahmadi et al., 2012]. This is caused by the tool shoulder area not contacting the welded material 100% at the beginning and therefore not creating enough heat to bond the material. These axial forces are normally in the range between 20 KN to 60 KN depending on the process parameters, [Kumar & Noor, 2012]. This heat is caused by the friction pressure between the tool and material and the time taken to weld, [Torun, 2016]. As the welding force increases, the void defects decrease, [Tongne et al., 2016]. Hasan et al. (2015) discovered

that in order to have better-welded joints, the forces that control the joining of workpiece need to be increased.

This research seek to investigate the influence of varying rotational speed in FSW of 6082-T6 aluminium alloy. The mechanical properties of low speed welded joints are compared with the high speed welded joints.

1.4 Research Objectives

The main aim of this study is to analyse the impact of the welding speed variation on the mechanical properties of the 6082-T6 welded joint. This aim will be accomplished through the following objectives:

- To compare the tensile and bending properties of the welds obtained from low rotational speeds with those obtained from high rotational speeds
- To analyse hardness properties of the welds obtained at low speed against the welds obtained at higher speeds.
- To analyse the speed influence on the microstructure of the welds.

1.5. Organization of the dissertation

This dissertation is organized as follows:

- Chapter one introduces the entire study. It encompasses the introduction to FSW technique, the background of the study, problem statement and study objectives.
- Chapter two gives a detailed literature review related to this research.
- Chapter Three deals with the experimental setup and performance. This includes the list of equipment used and their description.
- Chapter four contains an analysis of research results and discussions.
- Chapter Five has the drawn conclusions of the research and further possible work.

CHAPTER 2: LITERATURE REVIEW

Numerous research on the study of Friction Stir Welding (FSW) has been conducted. This chapter reviews some of the reported studies on Friction Stir Welding with the focus on the effects of rotational speeds on similar and dissimilar materials.

2.1 Variation of welding parameters

Rotational speed and welding speed need to complement each other during FSW. This then suggests that a good combination between the two parameters is required for the attainment of a good weld. These two fundamental parameters conjointly work with numerous other parameters. This includes penetration depth, the joint type, tool geometry, dwell time and clamping of material. It is rather a requirement to understand how all these parameters conjointly operate. This sub-section reviews works that have been published with varying welding parameters.

Singarapu et al. (2015) investigated the influence of friction stir welding parameters on the mechanical properties of 6061- T6 aluminium alloy by using three different rotational speeds and three different welding speeds. The rotational speed of 1120 rpm with a welding speed of 40 mm/min produced welds which had the best mechanical properties compared to other speeds combinations.

Widener et al. (2006) investigated and compared the effect of higher rotational speeds towards the quality of the joint. The rotational speeds used for the welding were higher than 3000 rpm. The welding was performed through the use of two tools i.e. fixed shoulder tool and normal tool. It was discovered that the normal tool produced welds with higher hardness in the stir zone compared to the welds produces by fixed shoulder tool which have the weld higher strength.

Hema et al. (2017) investigated the effects of process parameters in the friction stir welding of dissimilar AA 2014 and 6061 aluminium alloys. The different process parameters used were three different rotational speeds, three different welding speeds and three different axial forces. The lowest rotational speed used for this analysis was 760 rpm, 1380 rpm was used as the middle rotational speed while the highest rotational speed used was 2000 rpm. The lowest rotational speed was used in combination with the welding speed of 11 mm/min under the axial force of 0.5 kN. The axial force of 0.75 kN was used for the 1380 rpm and 24 mm/min speeds combination. The maximum axial force of 1 kN was used for 2000 rpm and 37 mm/min speed combination. The welds with the highest tensile strength were produced by the speeds combination of 2000 rpm and 37 mm/min under the axial load of 1kN.

Feng et al. (2017) studied the correlation between the rotational speed and the heat input on 6061 Al alloys. The increase in rotational speed increased input temperature up to a stable point that produced finer welds. Exceeding the stable point burns the material. The effect of welding speed on friction stir welding goes hand in hand with the fixtures clamping area. At lower welding speeds, fixtures with larger clamping areas should be used in order to have low tensile residual stress, [Farajkhah & Liu, 2017].

Sedmak et al. (2016) have developed a mathematical relationship between the speeds and temperature for FSW. The equation shows that rotational speed is directly proportional to the FSW temperature and inversely proportional to the melting temperature. Therefore, as the rotational speed increases the FSW temperature increases and the melting temperature decreases; whereas increasing the welding speed causes a decrease in FSW temperature and an increase in the melting temperature. This relationship was also reported by Sakthivel et al. (2009) when investigating the effect of welding speed on microstructural and mechanical properties of friction stir welded commercial aluminium alloys by using different welding speeds (50, 75, 100, 175 mm/min) with a constant rotational speed. It was found that the lower welding speed creates enough heat for the material to be stirred together in the weld zone producing finer grains.

Rose et al. (2012) investigated the influence of welding speed towards tensile properties of friction stir welded AZ61A Magnesium alloys. The rotational speed was kept constant at 1200 rpm while the welding speed was varyied from 30 to 150 mm/min with increments of 30 mm/min. Welding speed of 90 mm/min with a rotational speed of 1200 rpm produced defect-free welds with high yield and ultimate tensile strength of 178 and 224 MPa, respectively. Producing the highest hardness value of 83 Hv.

2.2 Impact of rotational speed in dissimilar materials

In friction stir welding, rotational speeds and welding speeds are among parameters that affect the materials' mechanical properties and strength performance, [Paik, 2009]. This subchapter reports about the impact of rotational speeds on tensile properties, hardness and microstructure of dissimilar materials during friction stir welding.

2.2.1 Impact of rotational speed on tensile properties of the weld

Hao et al. (2013) investigated the effect of friction stir welding parameters on microstructure and mechanical properties of Al-Mg-Er alloy. Five samples were produced with a different pair of rotational and welding speeds. They had the following pair; 400 rpm and 100 mm/min, 800 rpm and 100 mm/min, 800 rpm and 200 mm/min, 800 rpm and 400 mm/min and 1200 rpm and

100 mm/min. The rotational speed of 400 rpm with a welding speed of 100 mm/min was found to have a finer microstructure with the highest mechanical properties of 346 MPa UTS, 218 MPa YS and a joint efficiency of 73%. A decrease of mechanical properties with an increase of rotational speed was also noticed.

Sinha et al. (2016) compared the effects of variable rotational speeds of dissimilar friction stir welding Al-Cu alloys to similar friction stir welded Cu-Cu and Al-Al alloys. Rotational speeds with increments of 150 rpm were used from 150 rpm to 900 rpm with each a welding speed of 60 mm/min. For dissimilar welds, the strength of welds increased with the increase of rotational speed until an optimum rotational speed of 600 rpm was reached and decreased for rotational speeds above 600 rpm. The properties at 600 rpm were found to be 189 MPa for ultimate tensile strength which happened to be higher than Al-Al welds, 167 MPa for yield strength and 6.92% elongation.

Jenarthanan et al. (2018) investigated the effects of friction stir welding parameters (rotational speed, welding speed and pin diameter) on the tensile strength of two friction stir welded dissimilar alloys AA2014 and AA6061. The following parameters were used, between 355 and 710 rpm rotational speeds, 28 and 56 mm/min welding speed and 5 and 7 mm pin diameters. The optimum tensile strength was found at a rotational speed of 710 rpm and a welding speed of 56 mm/min.

Kumbhar & Bhanumurthy (2012) did a study on the friction stir welding of dissimilar AA5052 and AA6061 aluminium alloys using different rotation speeds and welding speeds. Two rotational speeds were used 1120 rpm and 1400 rpm with three welding speeds 60, 80 and 100 mm/min. It was found that, as the rotational speed increased from 1120 rpm to 1400 rpm, the tensile properties of the welds improved as it provided sufficient heat input.

2.2.2 Effect of rotational speed variation on hardness

The hardness of a material is a characteristic and it is measured by the materials ability to resist the penetration of an indenter, [Yovanovich, 2006]. It is necessary to review the studies that have been performed around this property. This is done so as to establish the correlation between the welding speeds and the material's resistance to deformation (hardness).

Wang et al. (2015) investigated the effects of rotational speed on microstructure and mechanical properties on friction stir welded Al–Li alloy using a bobbin pin. Rotational speed 400, 600, 800 and 1000 rpm were used with a welding speed of 42 mm/min. It was found that the hardness in the stir zone increased with the increase in rotational speed to an optimum

value above 104 Hv but decreases in the thermo-mechanically affected zone and heat affected zone.

Ghaffarpour et al. (2013) compared a numerical analysis to experimental results performed by friction stir welding. The main purpose of this comparative analysis was to optimize the process parameters for welds of dissimilar 5083-H12 and 6061-T6 aluminium alloys. Rotational speeds used for the welding varied between 630 and 3000 rpm. The welding speed also was varied between 15 and 500 mm/min. There was not much difference between the test results of the two methods. It was found that, as the rotational speed increased, the hardness of the welds in the nugget decreased. The minimum hardness was found on the HAZ side of the 6061-T6 aluminium alloy.

2.2.3 Effect of rotational speed variation on microstructure

Heat, in Friction Stir Welding, can be caused by different parameters including rotational speed. The amount of heat the welded material goes through affects its mechanical properties and its grain size as well as orientation. This effect brings the necessity to review the works reported around this area so as to establish the trend.

Sharma & Dwivedi (2017) investigated the microstructure and mechanical properties of friction stir welded dissimilar alloys (structural steel and ferritic stainless steel). A welding speed of 20 mm/min and a rotational speed of 508 rpm were used. It was found that the weld at the stir zone is stronger compared to the thermo-mechanically affected zone and the heat affected zone because of the grain alignment found at the stir zone which has approximately the same geometry and equal sizes.

Singh & Sharma (2013) investigated the influence of rotational speed on mechanical properties of friction stir welded dissimilar alloys AA2014 and AA5083. Four different rotational speeds (1900, 2000, 2100 and 2200 rpm) were used with one welding speed of 42 mm/min. It was found that, as rotational speed was increased, large microstructural grains were formed in the process which had an adverse impact on tensile strength and hardness.

Bisadi et al. (2013), investigated the influence of rotational speeds and welding speeds of dissimilar joints in friction stir welding. Four different rotational speeds (600, 825, 1115 and 1550 rpm) with two welding speeds (15 and 32 mm/min) were used. The conclusion drawn from this work was that, joints produced at 600 and 1550 rpm rotational speeds had more defects. The joint with lesser defects were achieved at the rotational speed of 825 rpm in combination with 32 mm/min.

Ko et al. (2017) investigated the effect of rotational speed on mechanical properties and microstructure of friction stir welded Ti-6Al-4V alloy sheets. Five different rotational speeds were used against constant welding speed. The rotational speed was varied between 300 and 500 rpm with intervals of 50 rpm. The scanning electron microscopy results reveal that the increase in rotational speed yielded two alpha phases in the weld nugget. The alpha prime was found to be dominating the nugget at higher speeds and this had resulted in the increase in hardness.

Nourouzi et al. (2012) investigated the effect of rotational speed and welding speed on the friction stir welding of dissimilar material (1100 aluminium alloy and 1045 carbon steel) by using two different rotational speeds (710 and 1000 rpm) and three different welding speeds (20, 28, 40 mm/min). A weld with smaller grains of approximately the same size with no voids visible in the stir zone was achieved when the rotational and welding speeds were 710 rpm and 28 mm/mm respectively.

2.3 Impact of rotational speed in similar materials

This sub-chapter reports on found studies about the impact of rotational speeds on tensile properties, hardness and microstructure of dissimilar materials during friction stir welding.

2.3.1 Impact of rotational speed on tensile properties of the weld

Input temperature in FSW can be controlled by adjusting the welding and rotational speeds, i.e. it can be reduced by reducing the welding speed but increasing the rotational speed which in turn increases tensile properties, [Rajamanickam & Balusamy, 2008].

He et al. (2016) investigated the effects of rotational speed on the tensile properties, residual stress and microstructure of 6061-T6 aluminium alloy 16 mm thick plates. The investigated rotational speeds were, 500, 700 and 900 rpm with a constant welding speed of 120 mm/min. Both longitudinal and transverse residual stresses, were found to be increasing with the increase in rotational speed. The highest residual stress achieved was from rotational speed of 900 rpm with a value of 153 MPa. The highest ultimate tensile strength achieved was from rotational speed of 700 rpm and it had a value of 236 MPa.

Kumar et al. (2018) compared similar and dissimilar welds of 5083 and 6082 aluminium alloys. The combination of these alloys included 5083-5083, 6082-6082 and 5083-6082 aluminium alloys. The rotational speed of 1200 rpm and 63 mm/min welding speed were used constantly throughout welding. It was found that similar FSW welds had less hardness values and joint efficiency than those of dissimilar FSW welds. While on the other hand they had higher tensile strength and yield strength values.

Rao et al. (2017) investigated the effects of welding parameters, rotational speed, welding speed and pin profile on tensile properties of friction stir welded 65032 aluminium alloys. Three rotational speeds (1000, 1300 and 1600 rpm), three welding speed (60, 80 and 100 mm/min) and three pin profiles (taper cylindrical, taper triangular and taper square) were used. Regardless of other welding parameters, rotational speed of 1300 rpm gave higher tensile properties (tensile strength, yield strength, elongation and joint efficiency) while rotational speed of 1000 rpm gave lesser tensile properties. It was also noted that tensile properties increased with the increase in the rotational speed from 1000 to 1300 rpm and decreased from 1300 to 1600 rpm.

2.3.2 Effect of rotational speed variation on hardness

Higher hardness in the stir zone than in the base metal is achieved with higher grain refinement in the stir zone, [Zhang et al., 2008].

Raja et al. (2016) investigated effects of friction stir welding on the hardness of 6061-T6 aluminium alloy. Two different rotational speeds 1030 and 1500 rpm were compared using a welding speed of 20 mm/min. It was found that the stir zone for all rotational speeds had higher hardness than that of the base metal but rotational speed of 1030 rpm had the highest hardness values.

Saini et al. (2013) investigated the effect of a straight cylindrical pin on the hardness of 6061-T6 aluminium strips through friction stir welding. Three rotational speeds (1950, 3080, 4600 rpm) were used with three different welding speeds (20, 25, 30 mm/min). Two hardness evaluation methods, Brinell and Rockwell were used to evaluate the hardness values. The hardness values were found to increase and decrease with no pattern aligning to the welding and rotational speeds. The highest hardness values recorded for both Brinell and Rockwell methods were of rotational speed of 3080 rpm and welding speed of 30 mm/min.

Raja et al. (2018) investigated the effects of rotational speed and welding speed on friction stir welded AA1100 aluminium alloy. The rotational speeds of 1500, 2500 and 3500 rpm and welding speeds of 10, 30 and 50 mm/min were used in this investigation. Fracture morphology analysis under Scanning Electron Microscope was done for the fractured specimens. It was found that high rotational speeds (3500 rpm) produced brittle fractures and lower rotational speeds (1500 rpm) produced ductile fracture. The hardness in the stir zone was found to be higher than in the thermo-mechanically affected zone but lower at the heat affected zone and on the parent metal zone.

2.3.3 Effect of rotational speed variation on microstructure

Rotational speed is known to be one of the most important parameters in welding. Its importance plays a certain role in microstructural arrangement of the joint. This then brings a necessity to review the related literature.

Ugender (2018) investigated the influence of rotational speed and tool profile on formation of zones in the friction stir welding of AZ31 magnesium alloy. Three pin profiles (straight cylindrical, taper cylindrical and taper threaded), three rotational speeds (900, 1120 and 1400 rpm) and three welding speeds (24, 40 and 75 mm/min) were used for the investigation. It was found that both rotational speed and welding speed have most influence on the formation of the zones in the friction stir welding of AZ31 magnesium alloys. The optimum parameters with best microstructure and mechanical properties was found to be a rotational speed of 1120 rpm and a welding speed of 40 mm/min with a pin profile that is taper threaded.

Raja et al. (2016) investigated the creation of the advancing side, the retreating side and welding zones in the friction stir welding of 1XXX series aluminium alloy. During welding, the high temperature made the zones more thermally balanced and the retreating side had better grain refinement than the stir zone.

Liu et al. (2017) investigated the effects of rotational speed on the microstructure and mechanical properties of friction stir welded 2060-T8 aluminium alloys. The two 2mm thick 2060-T8 aluminium alloys were welded at rotational speeds of 600, 800 and 1000 rpm with a constant welding speed of 300 mm/min. All welds at different rotational speeds contained no defects. The increase in rotational speed led to the increase in the Thermo-Mechanically Affected Zone (TMAZ) of the retreating side. There was also a match increase in grain size with the rotational speed increase in the nugget zone.

Klobčar et al. (2012) investigated the effects of friction stir welding parameters on microstructure and mechanical properties of friction stir welded 5083 aluminium alloy. The following combinations of rotational speed and welding speed were used and compared; 1250 rpm with 450 mm/min, 1250 rpm with 71 mm/min, 800 rpm with 280 mm/min, 800 rpm with 450 mm/min, 200 rpm with 280 mm/min, 200 rpm with 450 mm/min, 800 rpm with 280 mm/min and 200 rpm with 71 mm/min. It was concluded that higher rotational speeds tend to create higher frictional heat which increases the grain sizes and lower rotational speeds create lesser frictional heat input which produces smaller grain sizes making the welds harder.

Prabha et al. (2018) investigated the effects of rotational speed on mechanical properties by looking at the microstructure of friction stir welded 5083 aluminium alloys. The rotational speed

used was varyied while the welding speed was kept constant. The lowest speed used was 900 rpm while the highest was 1800 rpm. The grain sizes for welds produced at these varying speeds were studied comparatively. It was discovered that the grain size for the welds produced at 1120 rpm was smaller compared to those produced from other speeds. The speeds higher than 1120 rpm produced coarser grain structure which contributed to the ultimate tensile strength (UTS) drop of the welds.

2.4 Summary

A wide range of literature on friction stir welding and the effect of rotational speed in the attempt to define, develop and support this research was reviewed. This chapter has explored the effects of different welding parameters on dissimilar and similar FSW welds. It also looked at how rotational speed affects similar and dissimilar materials tensile properties, hardness and microstructure. There is not much literature on similar friction stir welded material, specially of 6082-T6 aluminium alloys. This study will cover the gap of lesser similar friction stir welded materials and come up with the optimum welding parameter (rotational speed).

CHAPTER 3: EXPERIMENTAL SETUP AND PERFORMANCE

This chapter contains all the experimental setup and experimental performance for the entire study. It starts of by explaining equipment used for the welding. The equipment used for preparing welded plates for analysis is thoroughly explained. The preparation processes of specimens for all tests performed are also explained.

3.1 Equipment used for producing welds

The equipment used for producing the welds is listed below:

- TA Shear Master guillotine
- Semi-automated milling machine (LAGUN FA. 1-LA)/ FSW Machine

3.1.1 TA Shear Master guillotine

Guillotine is a sheet metal working machine from the TA Shear Master brand. It has a maximum cutting thickness of 10 mm and has the moving blade driven by a rotary motor. It consists of a drive system, shear table and a fixed lower and moving upper blades (see figure 3.1). When cutting, a sheet metal/ plate is placed on the bed aligning the line to be cut under and on top of the shear blades. The drive mechanism is powering all parts, moving the upper blade to come down to the fixed blade cutting the plate when the controls have been activated.

Figure 3.1: Shows the picture of a Guillotine Machine

3.1.2 Semi-automated milling machine (LAGUN FA. 1-LA)/ FSW Machine

The friction stir welding machine for this study is a converted semi-automated milling machine with an X, Y and Z movements. The milling head has been modified especially on the spindle where the tool (see figure 3.2) is installed to turn it to a FSW machine. It consists of a machine bed which has a steel backing plate, clamp mechanism and power controlling system. Instead of cutting the material, the rotating tool feeds on the material heating it enough to soften and mixing it while moving through the material.

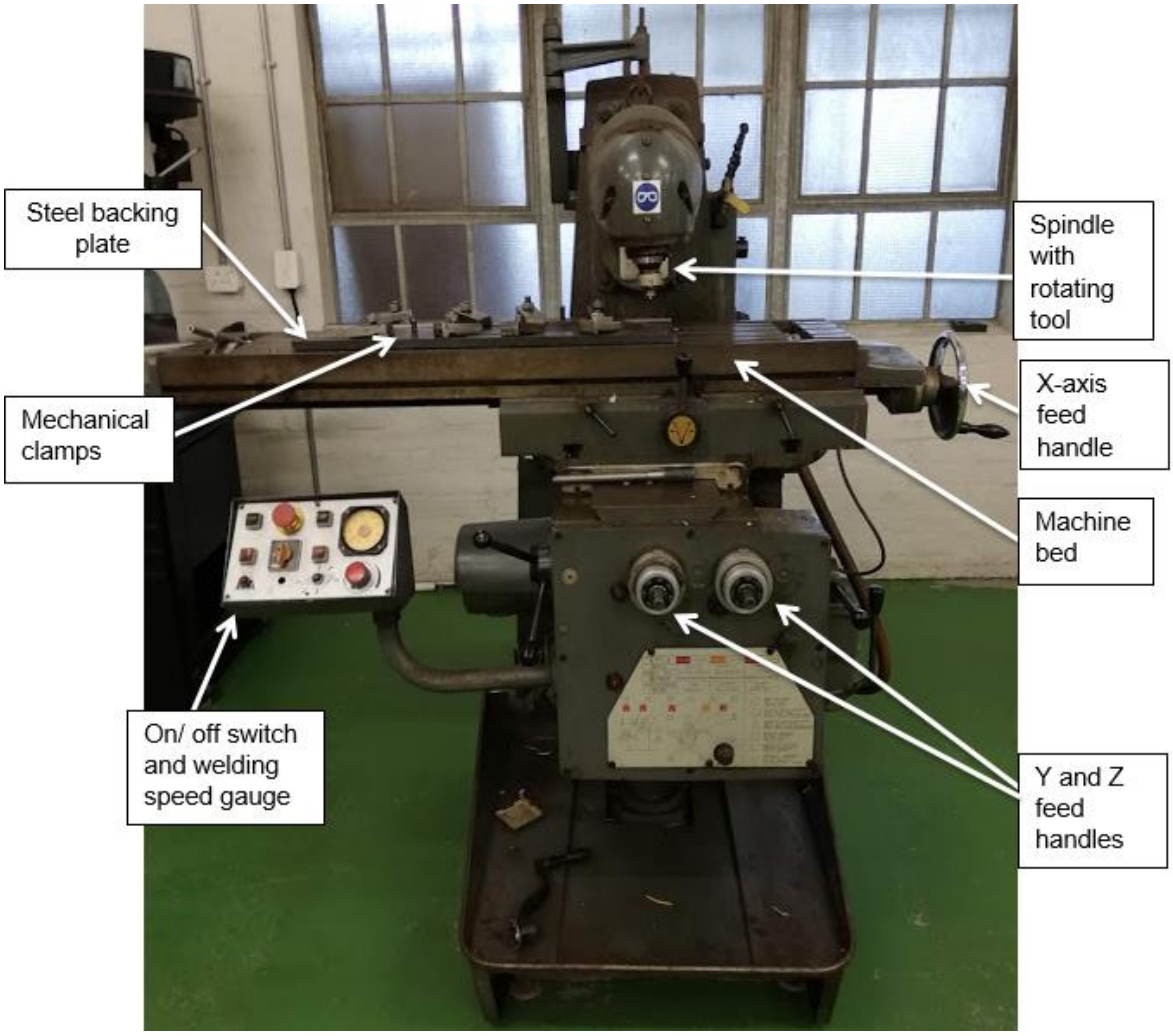

Figure 3.2: Shows the friction Stir Welding Machine used for welding

3.2 Welding performance

Twelve 6mm thick plates of 6082-T6 aluminium alloy were cut into the same size 400 mm length x 60 mm width. The TA Shear Master guillotine machine with the help of measuring tools such as a tape measure and Vernier calliper were used. A scriber was used to mark the areas to be cut and Q20 lubricant was applied to the guillotine machine. The desired plates were cut from a 1250 x 1500 x 6 mm 6082-T6 standard plate size. When the cutting was done, the plates were wiped to remove the residual from the lubricant to reduce the possibility of

smoke and burning smell when welded. Two plates were laid down together, supported on the fixture's backing plate on the FSW machine (see figure 3.4). The fixture comprised of a backing plate to cool down the work piece and steel screw clamps to hold the work piece down rigidly while welding. The machine had an H13 tool (see figure 3.3) with a shoulder diameter of 20 mm and a threaded and tapered pin with outside diameter of 6 mm and length of 5.8 mm fixed and tightened at its spindle.

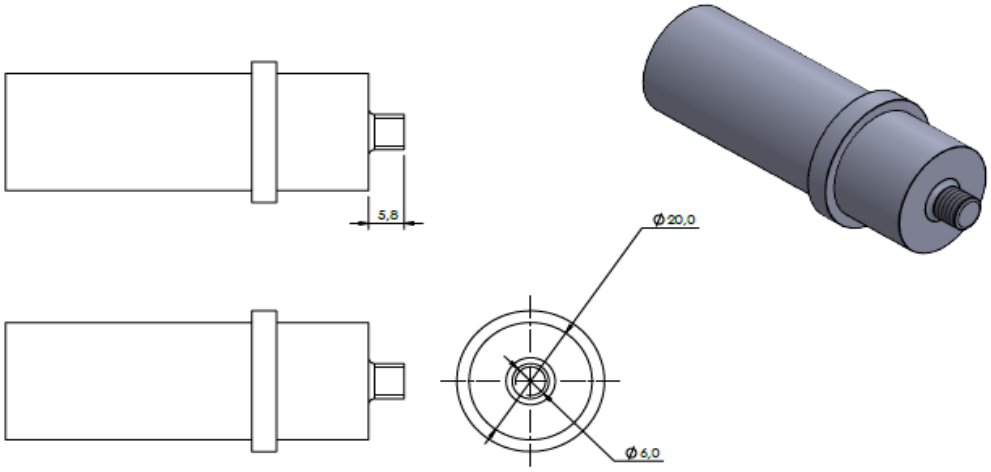

Figure 3.3: Shows the H13 Tool

3.2.1 Friction Stir Welding

The clamps were tightened enough to keep the plates down using a ratchet. The machine was set such that the tool was tilted at an angle of 3° and centrally positioned with the plates to be welded. The first set of welding parameters (shown in Table 3.1) were set to the machine prior welding. The rotating tool was plunged into the pieces to be welded and the plunged depth was 5.8mm. The plunged rotating tool was kept in the same position for twenty seconds for heat input stabilization. The traverse speed was then activated to start welding (see figure 3.4). When the rotating tool reached the end of the plates it was slowly drawn out. The machine was switched off.

The work piece in figure 3.5 was gently unclamped and excess material from welding was removed. The same procedure was repeated for all rotational speeds after every hour (cooling period for machine).

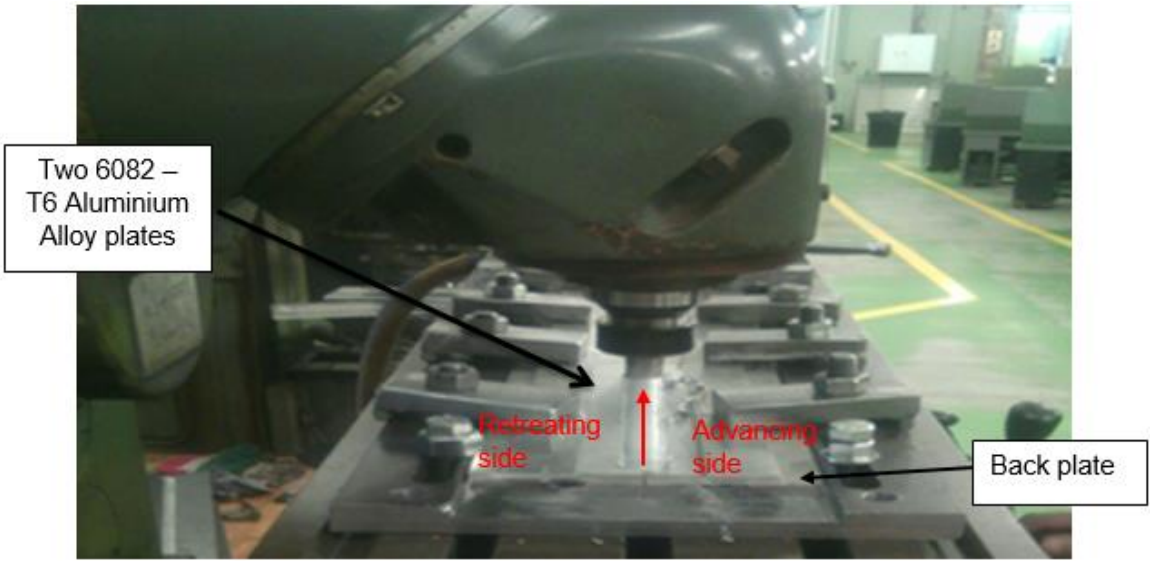

Figure 3.4: FSW setup of two 6082-T6 Al alloy plates

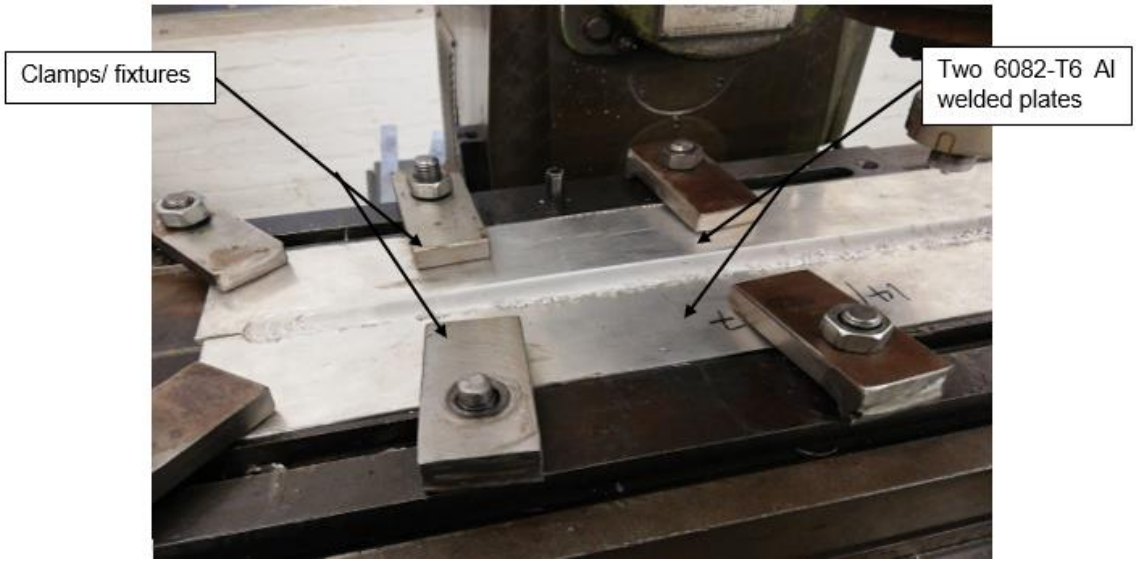

Figure 3.5: Shows two welded plates

Table 3.1: Tool process parameters

Rotational speed (rpm)	Welding speed (mm/min)
600	80
700	
800	
900	
1000	
1200	

3.3 Weld preparation for analysis

This section list all the equipment used in preparing welds for different analysis. The listed equipment is later explained. Equipment used for the preparation of weld analysis are listed below:

- Accutex AU-500iA EDM wire cutter
- Metallurgy Specimen Mounting equipment
- Grinding and Polishing equipment for Metallurgical specimens

3.3.1 Accutex AU-500iA EDM wire cutter

A Computer Numerical Control (CNC) machine known as the Accutex AU-500iA EDM wire cutter in figure 3.6 is used for precision cutting. It's an automatic machine that uses an efficient high speed threading system. It contains a T-base moving column with direct transmission and 3D laser measuring technique moving on the x, z and y-axis.

Figure 3.6: The Accutex AU-500iA EDM Wire Cutter

3.3.2 Mounting equipment

The mounting equipment include a Bakelite black hot mounting powder epoxy resin and the Struers LaboPress-3 mounting machine in figure 3.7. It has a housing that heats and cools which ever specimen that's on the ram inside it. This mounting material has resistance to physical distortion and it is chemically inactive to etchants.

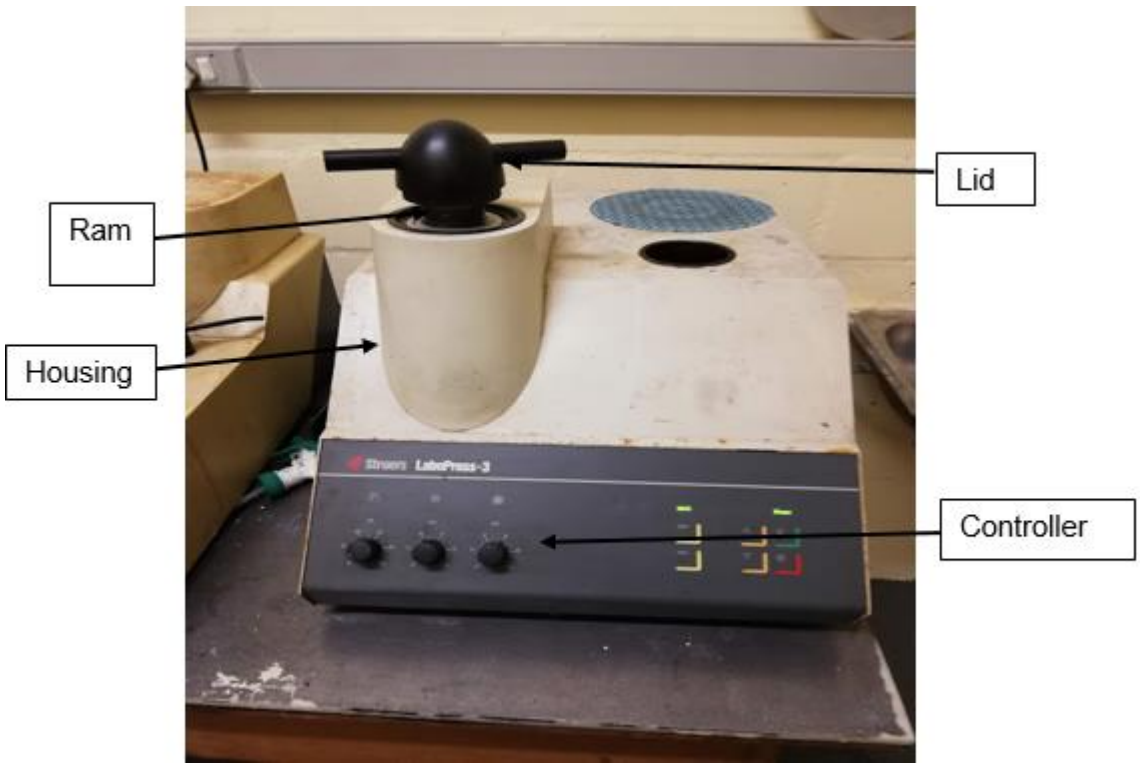

Figure 3.7: The Struers LaboPress-3 mounting machine with specimen after mounting

3.3.3 Grinding and polishing equipment for metallurgical specimens

Grinding and polishing equipment is shown in figure 3.8. It contains a polishing and grinding machine with a rotation round flat face plate where disks are placed, named the Struers LaboPol5 machine. The disks and lubricants used on the machine can be for grinding or polishing. Rhaco Grit P320 grade disk is used for grinding with distilled water as a lubricant. The Largan 9 grade disk is used for polishing with the DiaMaxx Poly 6 μm solvent. The Moran-U grade disk is used for fine polishing with a DiaMaxx Poly 3 μm solvent. The Chemal grade disk is used for finer polishing with a fumed Silica 0.2 μm lubricant. The Struers DP- Lubricant Blue can also be used on the chemal grade disk.

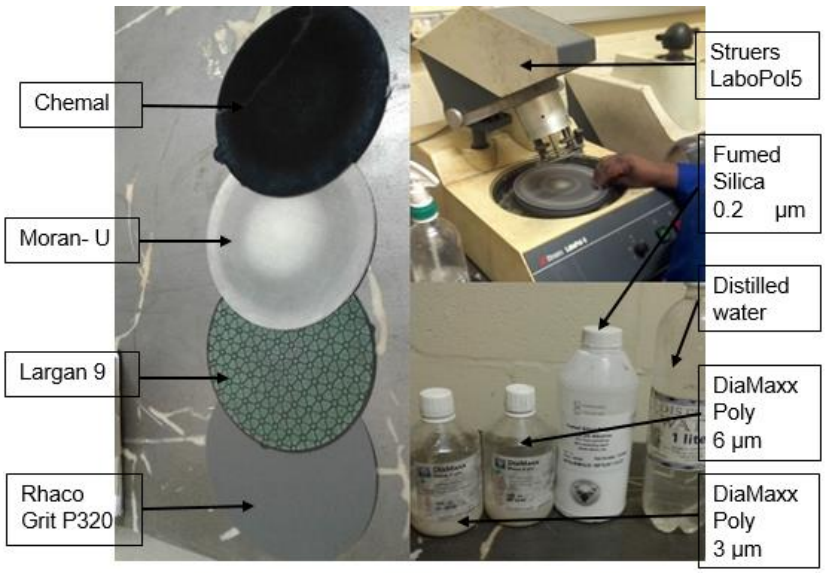

Figure 3.8: Shows grinding and polishing tools

3.4 Performance of specimen preparation

This sub-section contains procedures for preparation of specimens for all tests conducted that needed specimens to be prepared.

3.4.1 Tensile tests specimens

The ASTM E8M-04 standards indicate that for tensile testing, plates with a maximum thickness of 6 mm should use specimen dimensions with a nominal width of 6 mm. Figure 3.9 shows the tensile test specimen designed through ASTM E8M-04 standard.

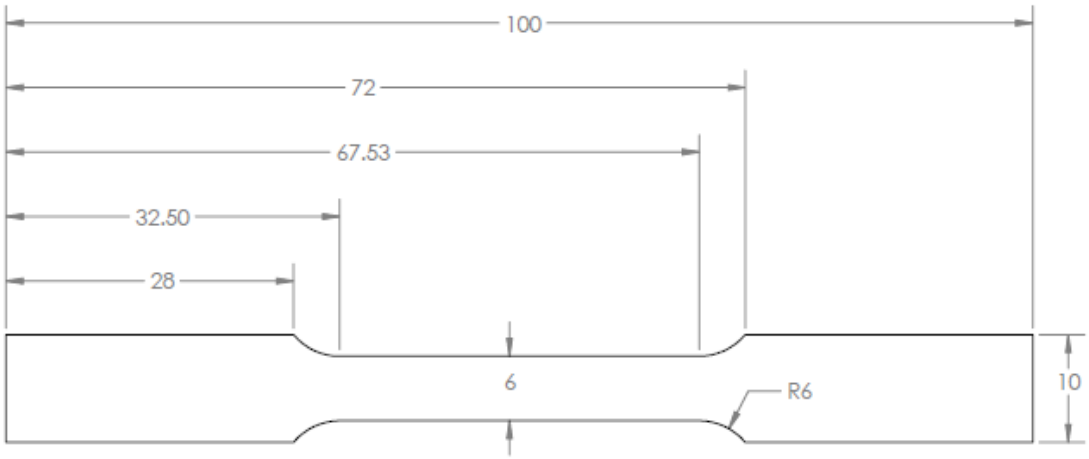

Figure 3.9: Dimensioned Tensile testing specimen according to the ASTM E8M-04 standards without weld

3.4.1.1 Cutting of specimens

The workpieces were marked out using a steel ruler and a scriber (see figure 3.11). It was then cut using the wire cutter machine (see figure 3.10) and this cutting technique was chosen since it does not induce temperature to the workpiece during cutting. The specimens for each welded plate were cut from different location of the plate i.e. beginning of the weld, middle and the end of the weld. The cut out specimens are shown in figure 3.12. The following shows the naming of the specimens per location as shown in figure 3.11:

- 600 rpm: S1 (start of weld), M1 (middle of weld) and E1 (end of weld)
- 700 rpm: S2, M2 and E2
- 800 rpm: S3, M3 and E3
- 900 rpm: S4, M4 and E4
- 1000 rpm: S5, M5 and E5
- 1200 rpm: S6, M6 and E6
- Parent material: PM

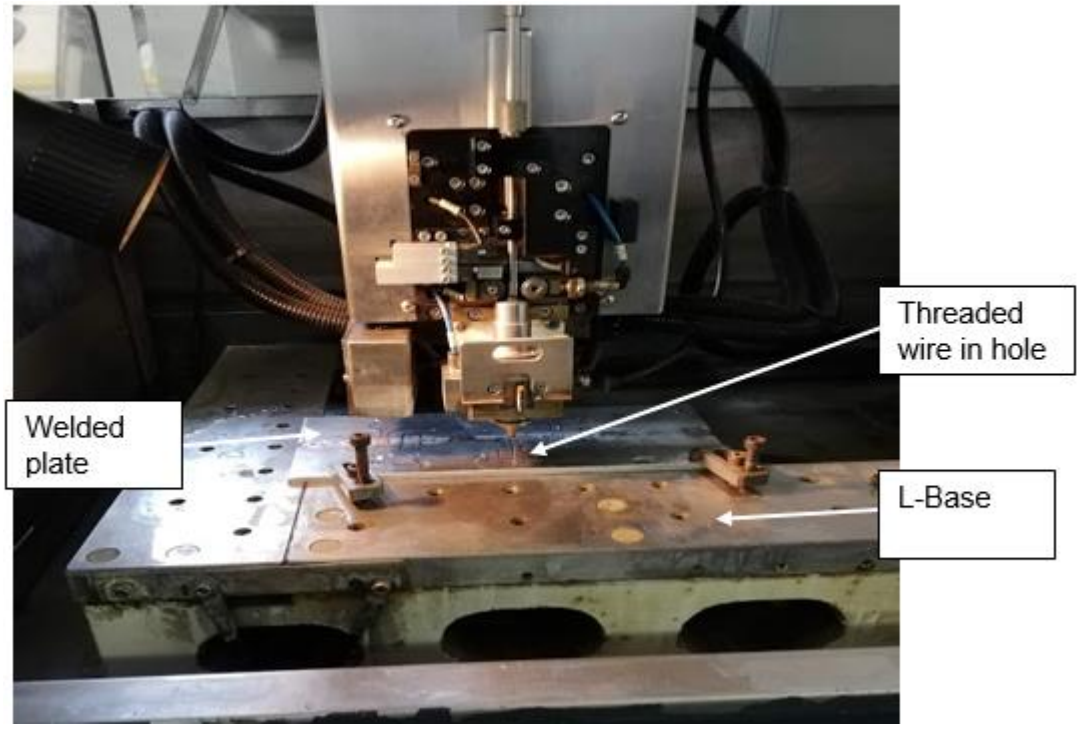

Figure 3.10: Shows two welded plates placed and clamped in the wire cutter.

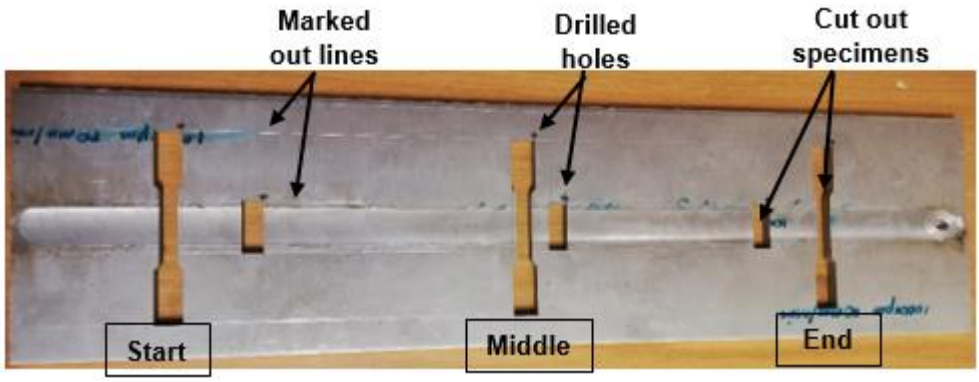

Figure 3.11: Shows marked and cut 1000 rpm work piece

Figure 3.12: Cut out tensile specimens of 600 rpm from start and middle

3.4.2 Microstructure and macro-structure specimens

The microstructure and macro-structure specimens were also designed using SolidWorks. They were made out to have the dimensions, 8 mm width, 6 mm thickness and a length of 26 mm as shown in figure 3.13.

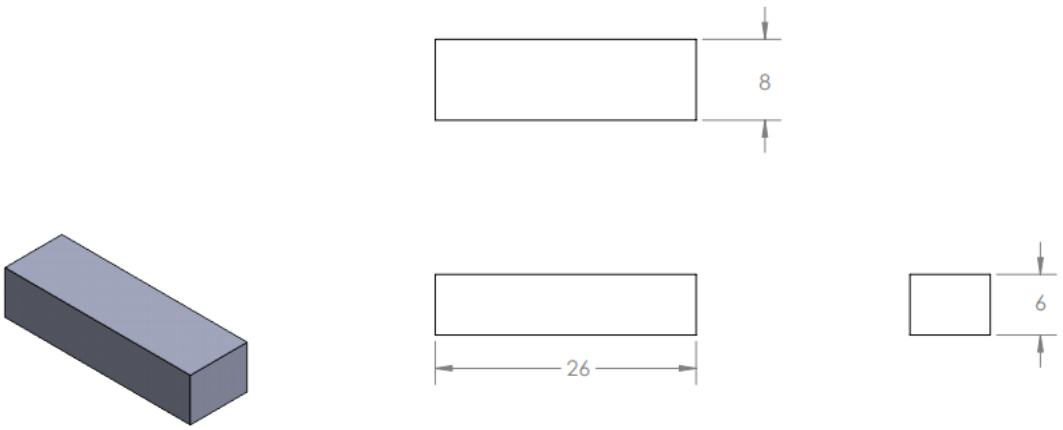

Figure 3.13: Dimensioned microstructure and micro-hardness testing specimen without weld

For the microstructure specimens, two lines were drawn perpendicular to the weld edge and at the beginning of the weld. These two lines were 15 mm away from the tensile specimen drawn lines and they were 10 mm away from each other. These microstructure specimens and the welded plated were done the same way at the middle and at the end of the weld.

Figure 3.6 shows the wire cutter machine that was used to cut out the microstructure specimens diplited in figure 3.14.

Figure 3.14: Shows cut-out microstructure specimen welded at 1200 rpm.

3.4.2.1 Mounting of specimens

Figure 3.7 shows the Struers Labo Press-3 mounting machine that was used together with the Bakelite black hot mounting powder epoxy resin to mount the microstructure specimens. The mounting machine was turned on and the upper ram was elevated to the top. The specimens were placed on the upper ram and it was lowered to a distance of 30 mm in the housing with heating and cooling. The mounting resin was poured on top of the ram and specimens until the 30 mm space was totally covered. The lid was closed and 180 ºC temperature was applied at a pressure of 120 KN. The heating process took 6 minutes and the process started curing which took 9 minutes. When done, the ram is moved up and the specimens were hot and mounted as seen in figure 3.15.

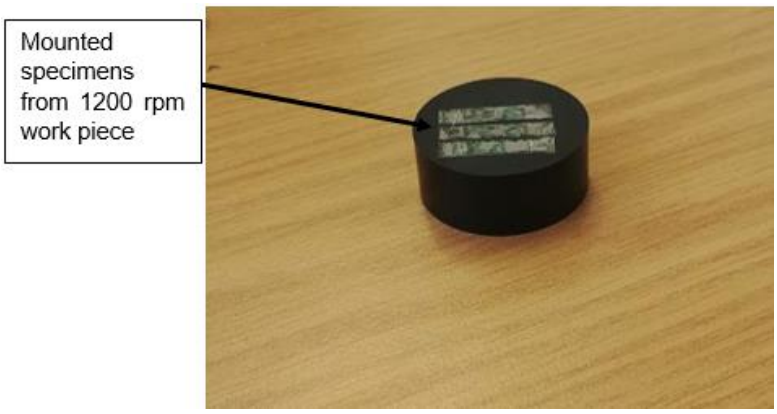

Figure 3.15: Shows three mounted specimens extracted from the start, middle and end of 1200 rpm workpiece.

3.4.2.2 Grinding and polishing of specimens

The microstructure specimens had to be grinded, polished and etched in order to identify phases of the weld and the general grain structure. The machine used for grinding and polishing was the Struers LaboPol-5 metallurgical grinder/polisher in figure 3.8 with its accessories. Table 3.2 presents the four-step procedure followed, which was adapted from AKASEL's polishing procedure for aluminium alloys.

The specimens were grinded until they were plane using the Rhaco grit and distilled water. Their direction was changed from previous position by 90º and grinded using the Largan 9 disk with a 6 µm lubricant. At a different direction, changing it by 90º they were polished using the Moran-U disk and the 3 µm lubricant. For a finer and clean finish, they were polished with the Chemil disk and a 0.2 µm alkaline lubricant. Between each grinding and polishing steps, Struers DP- Lubricant Blue was used to flush off any debris and grit left from the Bakelite, and weld joint specimens.

Table 3.2: The AKASEL four polishing steps for preparing aluminium specimens

	1st Step	**2nd Step**	**3rd Step**	**4th Step**
Disk grade	**Rhaco Grit P320**	**Largan 9**	**Moran- U**	**Chemal**
Lubricant	Distilled water	DiaMaxx Poly 6µm	DiaMaxx Poly 3µm	Fumed Silica 0.2 µm Alkaline
Speed	300 rpm	150 rpm	150 rpm	150rpm
Duration	Until plane	5 min	4 min	2 min

3.4.2.3 Etching of specimens

The specimens in figure 3.16(b) were first etched using the Keller's reagents that was made out of (see table 3.4) 190 ml distilled water, 5 ml hydrochloric acid, 3 ml hydrofluoric acid and 2 ml of nitric acid. The ASTM E 407-99 standards for micro-etching metals and alloys was followed in the etching of 6082-T6 friction stir welded specimens. After etching ethanol was poured over the specimens and they were dried with warm air. The etchants effectiveness was checked under a light microscope; of which it wasn't effective enough.

As the Keller's reagent did not bring out the grains on the specimens, making it harder to view them and the different stages under a light microscope. It was then that the decision was taken to use the Weck's reagent and applying pre-etch before applying the Weck's reagent. The specimens were prepared again to remove the Keller's etchant by grinding and polishing using the Akasel steps in table 3.2. They were rinsed thoroughly with distilled water to completely remove any residue that might have been left from the polishing and they were dried again with hot air. Ethanol was poured on the the dried specimens surface and dried with hot air to clean them. The pre-etch was applied followed by the Weck's etchant. Specimens etched with the Weck's reagent are found in figure 3.16(a) having colour tinted surface. All specimens were etched immediately after the last stage of polishing and gloves were worn at all times.

Table 3.3: NaOH Pre-Etch and Weck's Etchant concentration

Etchant	**Pre-Etch**		**Weck's Reagent**		
Solution	NaHO	Distilled water	NaHO	Distilled Water	$KMnO_4$
Quantity	2 g	100 ml	1 g	100 ml	4 g

Table 3.4: Keller's reagent concentration

Solution	Distilled water	Hydrochloric acid	Hydrofluoric acid	Nitric acid
Quantity	190 ml	5 ml	3 ml	2 ml

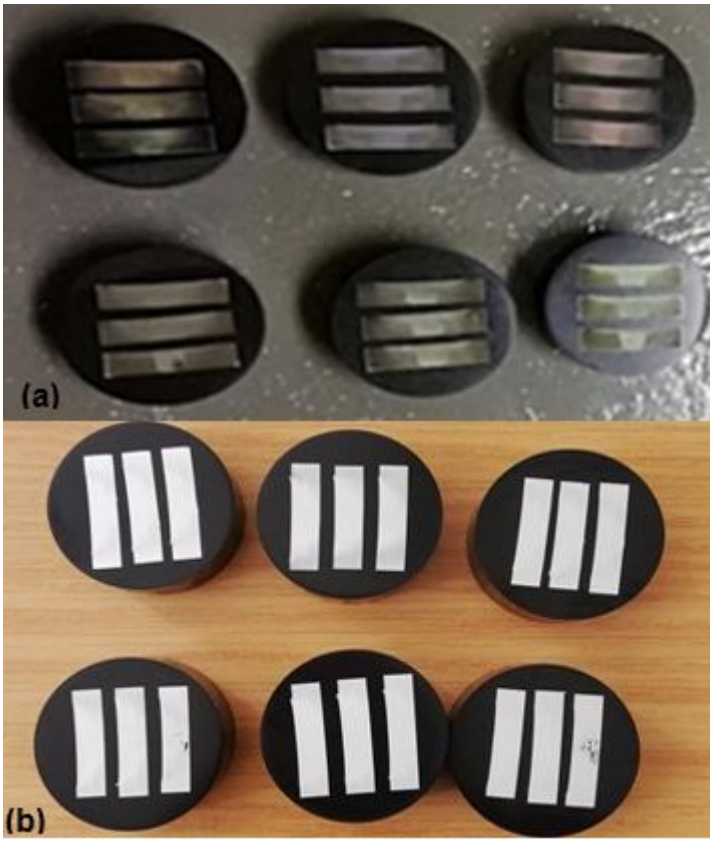

Figure 3.16: Mounted and etched specimens with (a) Weck's reagent and (b) Keller's reagent

3.5 List of Tests performed

This subsection entails the analysis for the friction stir welding joints of 6082-T6 aluminium alloys. The tests that were done are listed below:

- Tensile Tests
- Rockwell Hardness tests
- Fractography Analysis (SEM)
- Microstructure Analysis
- Macrostructure Analysis

3.6 Mechanical Tests

There are two mechanical tests conducted in this study i.e. tensile test and hardness test. The performance of these test is explained in the following sections.

3.6.1 Tensile tests

This test was done to compare the effects of different rotational speeds on tensile properties of 6082-T6 friction stir welded aluminium alloys to those of parent material.

The bench top Hounsfield testing machine in figure 3.17 with upper and lower jaws for holding test specimens was used for tensile tests with a QMAT software. This machine has vertical movement, with the upper jaw moving up during testing and a desktop connected to it, collecting the data.

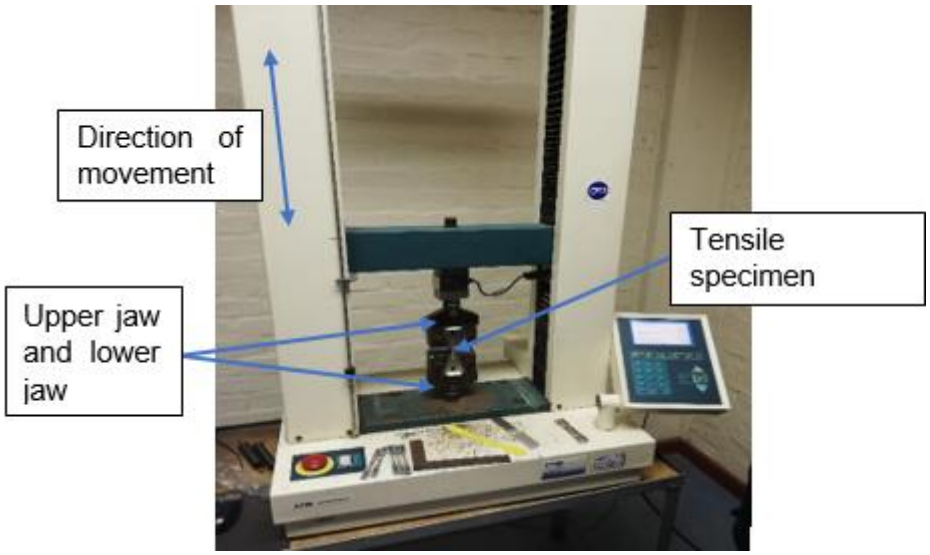

Figure 3.17: Bench top Hounsfield tensile tester

One specimen at a time was clamped on the machine and the clamps were zeroed. The following parameters found in table 3.5 were used, then auto return was set off. The test specimen button was pressed and the machine pulled the specimen until fracture/ failure. The data was recorded as raw data and the broken specimen was unclamped and its extension was measured using a Vernier Calliper just to see if it corresponds with that of the recorded data. This procedure was repeated for all remaining 18 specimens with the same test settings.

Table 3.5: Parameters applied to tensile test machine

Load range (N)	Extension range (mm)	Speed (mm/min)	Preload (N)
1500	20	3	0

The data in appendices on Microsoft Excel spreadsheet was divided into the following manner with each speed having three specimens based on the lay of the weld on the work piece. 600 rpm specimens are in appendix A, 700 rpm in appendix B, 800 rpm in appendix C, 900 rpm in

D, 1000 rpm in E, 1200 rpm data in appendix F and the parent material data in G. For each specimen the tensile strength was calculated. The strain which is the change in length over the original length was then calculated.

Stress-Strain graphs were then drawn for each specimen. The ultimate tensile strength for each specimen was computed as the maximum value reached stress. To make the data in the graph less ambiguous, the unit for stress was converted to Mega Pascal's (MPa). Three bar graphs were drawn for ultimate tensile strength in the y-axis and rotational speed in the x-axis. The first graph was for the start of the weld, the second graph was for the middle of the weld and the third and last was for the end of lay. Percentage Elongation was calculated and plotted on the UTS graph. The strain that was at high tensile strength was the one taken to calculate the percentage elongation because that is the fracture point.

3.6.2 Rockwell Hardness tests

The Future-Tech Rockwell tester in figure 3.18 was used for the hardness test. The machine was manually operated with a ball indenter having a diameter of 1/16" and loading of 100 kilograms. The Rockwell hardness HRB which was used applies a preload 98.07 N to the tested specimen. It is operated manually by turning the rotary wheel to raise the test anvil to apply the minor load to the specimen. It also contains a notification sound for when a minor load has been reached.

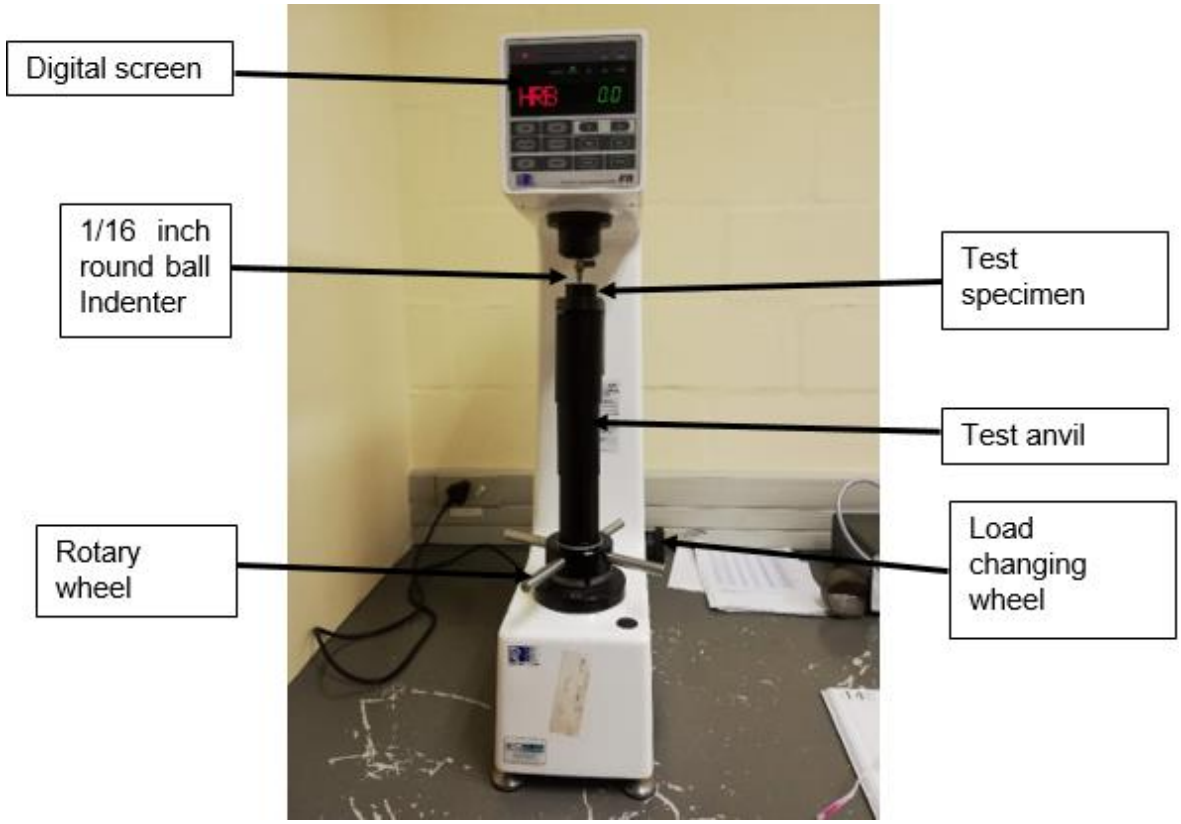

Figure 3.18: The Future-Tech Rockwell hardness tester

The test was carried out by inserting the 1/16 inch round ball indenter into the machine in figure 3.18 and the fastening screw was fastened so the indenter would not fall. A loading of 100 kilograms was set using the load changing wheel and the testing specimen was placed on the test anvil. The anvil was lifted using the rotary wheel up until there was a millimetre between the specimen and the edge of the indenter. The specimen was adjusted in order to position the point where the indenter was going to be inserted under it. The machine was set to auto and zeroed. The rotary wheel was turned around to gradually raise the anvil for the indenter to touch the specimen and apply the preload of approximately 98.07N, once it got to the preload the start button was pressed and the tester applied an additional load. The indents on all of the specimens are shown is figure 3.19 having approximately 3 mm distance apart from each centres.

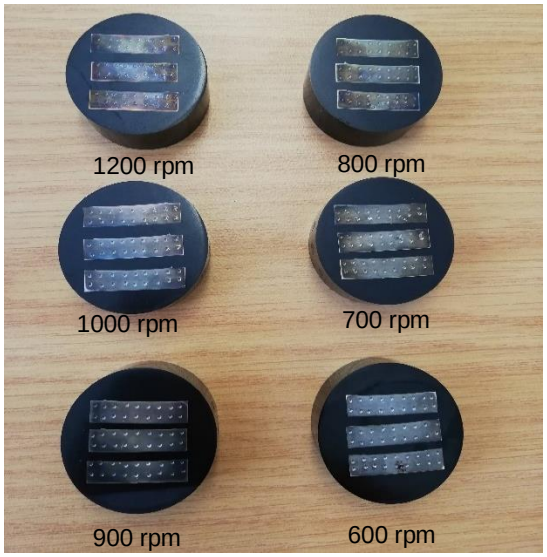

Figure 3.19: Indented macro hardness specimens

The machine calculated and gave the hardness value after the beep sound. This procedure was repeated for all indents in all specimens.

3.7 Microstructure and Macrostructure Tests

Materials contains unique and different microstructure. The microstructure of a non-welded material is different from the welded one. In this sub chapter, the microstructure of base specimens, friction stir welded specimens and fractured specimens are compared using fractography analysis, microscopic analysis and macroscopic analysis.

3.7.1 Fractography Analysis

A similar desktop Phantom Pro SEM machine shown in figure 3.20 was used to take images of fractured specimens at higher magnifications. It contains the main instrument with a vacuum

chamber which has a door and inside that door is where the standard specimen holder goes in. To ensure that the sample was fixed on the sample holder, a stub was used with a conductive graphite attaching the specimens. The two monitors were used for viewing.

Figure 3.20: Desktop Phanom Pro SEM (Kaplonek & Nadolny, 2013)

Fractured specimens that went through tensile testing were taken to be cut to small specimens to fit in a SEM tester. Out of the two fractured halves for all specimens, the half with less damage should be the one taken for fracture morphology, [Zipp et al., 1987]. The specimens in figure 4.1 were cut on the half containing the weld zone using a hack saw and grinding abrasives to create a parallel platform to that of the fracture (see figure 3.21). The Phenom Pro tester in figure 3.20 was used to capture photographs of the fracture at bigger magnifications.

Figure 3.21: Cut off fractured tensile specimens

3.7.2 Microstructure analysis

The Nikon Eclipse L150 microscope with a camera attached at the camera port connected to a computer with the Carl Zeiss AxioVision se64 software was used (see figure 3.22). One specimen a time was placed on the mechanical stage. Most settings were already set. The correct objective was adjusted and placed correctly. The mechanical stage was moved around using the X-Y translation mechanism until the best requisition picture of microstructure was found. The picture was captured and opened to be measured. For measuring of grain sizes,

the following was done. On the Axiovision, measure was opened on the tool bar, Interactive Measurement was selected followed by start measurement. The required measurements were taken and saved in a table form for all microstructure specimens taken.

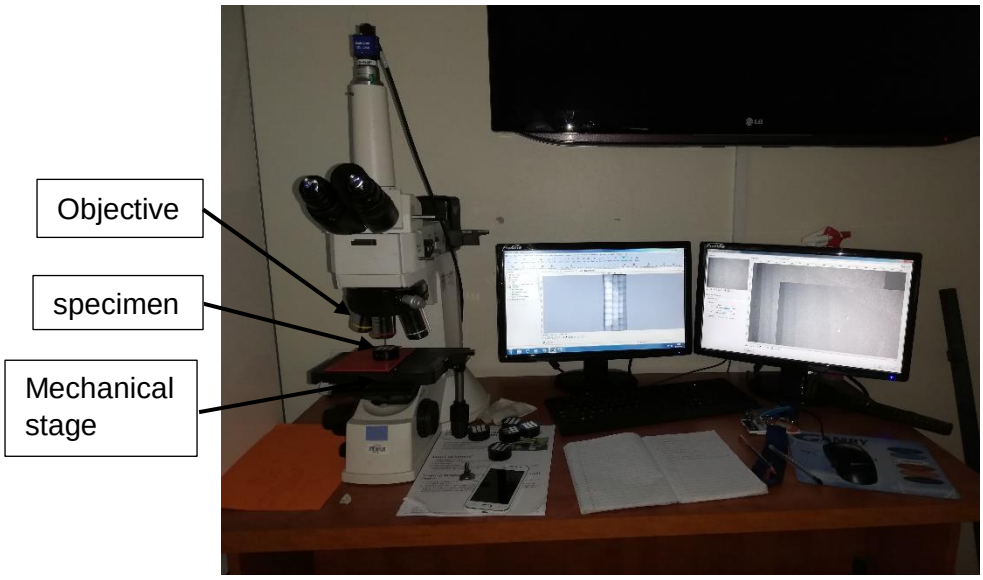

Figure 3.22: The Nikon Eclipse L150 microscope with working desktop

3.7.3 Macro-structure analysis

The Olympus stereo zoom 7x to 70x microscope with a ring light illuminator in figure 3.23 was used to take the specimens' macro-structure.

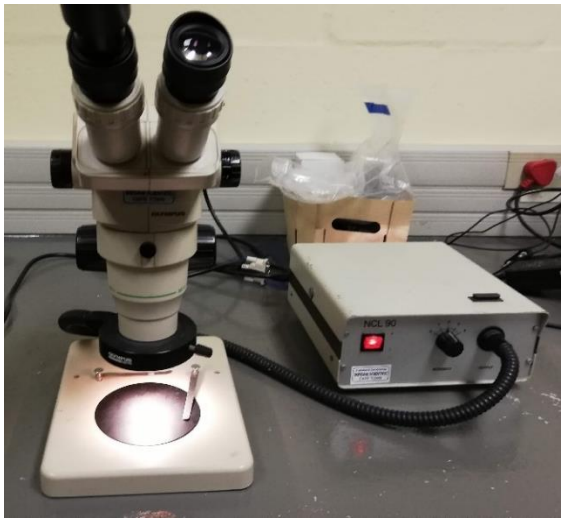

Figure 3.23: The Olympus microscope for macrostructure

A specimen was placed under the microscope and positioned correctly. The microscope was focused and a picture of the macrostructure was taken for each specimen. The captured pictures are presented and discussed in chapter 4.

CHAPTER 4: RESULTS AND DISCUSSIONS

In this chapter, tests and analysis results are analysed and discussed. It was mentioned from the previous chapter that each plate produced three specimens that were cut from different locations of the plate. The presentation of the results in this chapter follows that fashion.

4.1 Tensile Tests

The tensile tests analysis are presented in Figure 4.1 shows all tensile specimens failed during tensile testing, with the Advancing Side (AS) and the Retreating Side (RS) marked. Specimen S1 and S2 fractured at the centre of the weld, this could mean that the weld wasn't strong enough or there were defects (wormholes/ voids), with the fracture point shown by the blue circle. Specimen M1, M4, E4, M5 and S6 fractured outside the weld line on the heat affected zone (HAZ) of the advancing side. This means that the material on the advancing side was not strong enough, but the weld was strong. Specimen E1, M2, E2, S3, M3, E3, S5, E5, M6 and E6 fractured outside the weld line on the HAZ of the retreating side, meaning the material reached a maximum solid state on the advancing side and it plasticized well.

All specimens tested were compared to that of the parents' material which had a UTS value of 323 MPa and a percentage elongation of 24%. The ultimate tensile strength of all welded specimens are all falling within 60% of the parent materials UTS. Specimens of different rotational speeds with same weld location were compared to find which had values closest to those of the parent material.

For specimens extracted from the beginning of the weld, it can be seen from table 4.1 that the specimen with the closest properties to that of the parent material is from 600 rpm rotational speed with a UTS value of 187 MPa and percentage elongation value of 18%. The lowest values were seen in 700 rpm with 149 MPa and 8% UTS and percentage elongation respectively.

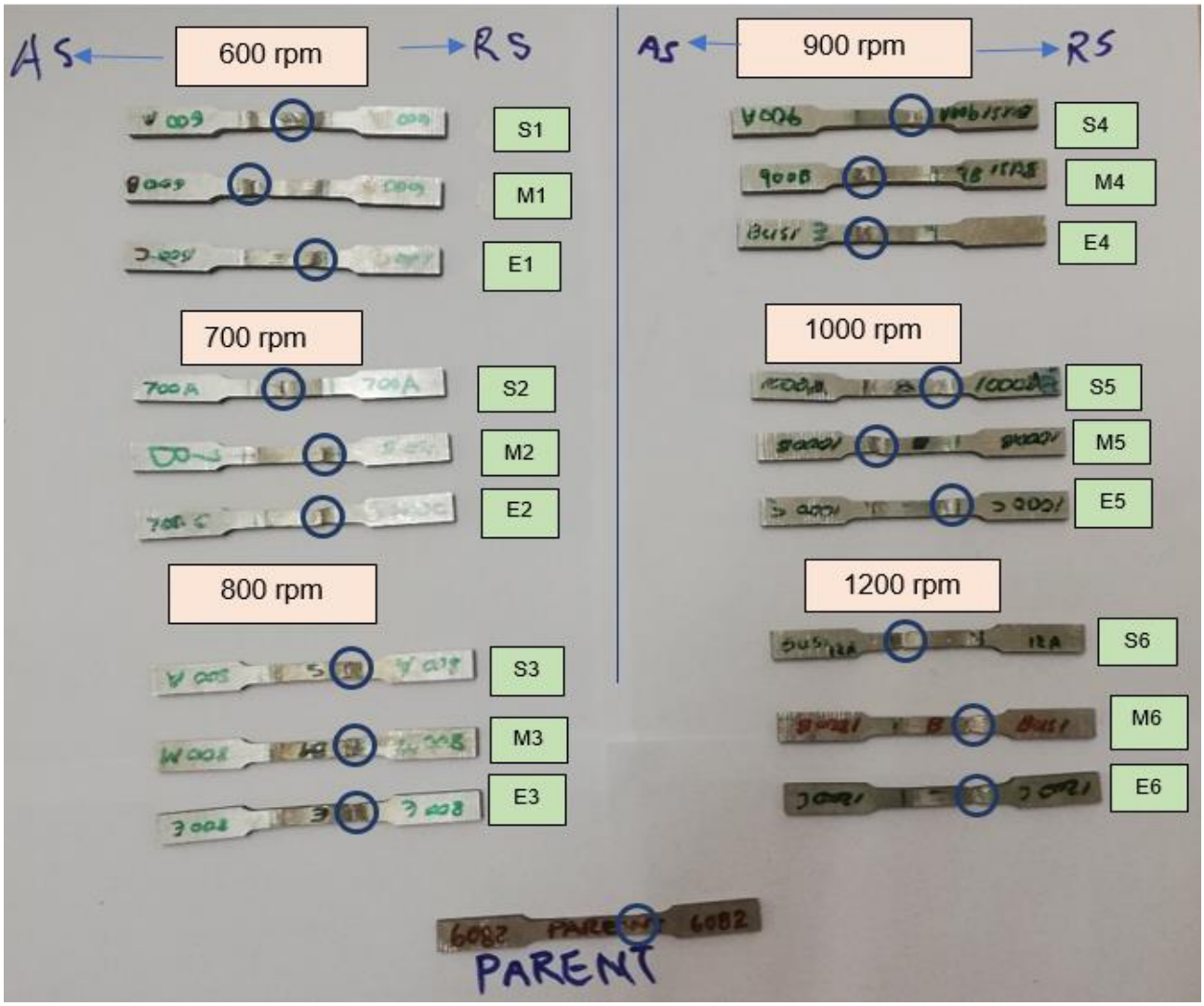

Figure 4.1: Shows fractured tensile specimens for all rotational speeds and parent material

Table 4.1: FSW tensile property results for 6082-T6 Al alloys at the beginning of weld

Specimen	Rotational Speed (rpm)	UTS (MPa)	% Elongation
Parent	-	323	24
S1	600	187	18
S2	700	149	8
S3	800	178	16
S4	900	183	18
S5	1000	176	16
S6	1200	175	15

For specimens taken from the middle of the weld (see table 4.2), the specimen with property values closest to that of the parent specimen is from the rotational speed of 600 rpm specimen

with the highest value of 189 MPa and 18% for both UTS and percentage elongation, respectively. The lowest properties are observed at 700 rpm specimen for UTS with a value of 161 MPa and from the 900 rpm specimen for percentage elongation value of 14%.

Table 4.2: FSW tensile property results for 6082-T6 Al alloys at the middle of the weld

Specimen	Rotational Speed (rpm)	UTS (MPa)	% Elongation
Parent	-	323	24
M1	600	189	18
M2	700	161	15
M3	800	173	15
M4	900	172	14
M5	1000	171	15
M6	1200	171	15

Tensile property results for specimens extracted at the end of the weld are presented in table 4.3. The closest UTS value to that of parent specimen obtained has a value of 186 MPa from 1200 rpm specimen and the highest percentage elongation obtained was 19% from 600 rpm specimen. The lowest percentage elongation and UTS are found on the 800 rpm specimen with the values 16% and 174 MPa respectively.

Table 4.3: FSW tensile property results for 6082-T6 Al alloys at the end of the weld

Specimen	Rotational Speed (rpm)	UTS (MPa)	% Elongation
Parent	-	323	24
E1	600	185	19
E2	700	183	16
E3	800	174	16
E4	900	182	17
E5	1000	177	16
E6	1200	186	16

Specimens from rotational speed 600 rpm show high tensile properties from start to middle and end. While the tensile properties of 1200 rpm has shown an increase from start to end.

The tensile properties results suggest that 600 rpm at a welding speed of 80 mm/min is a good rotational speed for welding similar 6082-T6 aluminium alloys as it has an ultimate tensile strength and a percentage elongation closest to that of the parent material 323 MPa and 24%

respectively.

4.1.1 Micro-fractography analysis

Fractured tensile specimens were tested under a SEM for failure analysis and provided low magnification images (fractographs) of the fractured part. Fractographs for different rotational speeds were compared by the position of where their specimens were extracted from the weld, start, middle and end. Wen et al. (2016) found that fractures with dimples are that of a ductile fracture, those with shallow and smaller dimples have lower elongation and those with larger and deeper dimples have higher elongation. The parent fractograph in figure 4.2 revealed failure features similar to that of a ductile fracture as it contains large and deep sheared dimpled structures with risen cavities.

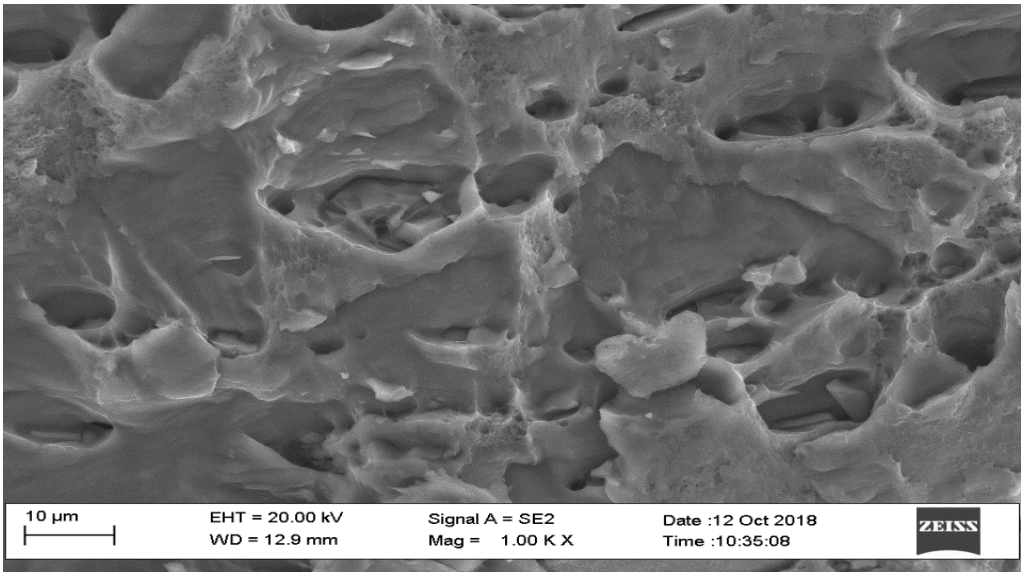

Figure 4.2: SEM fractograph for parent material

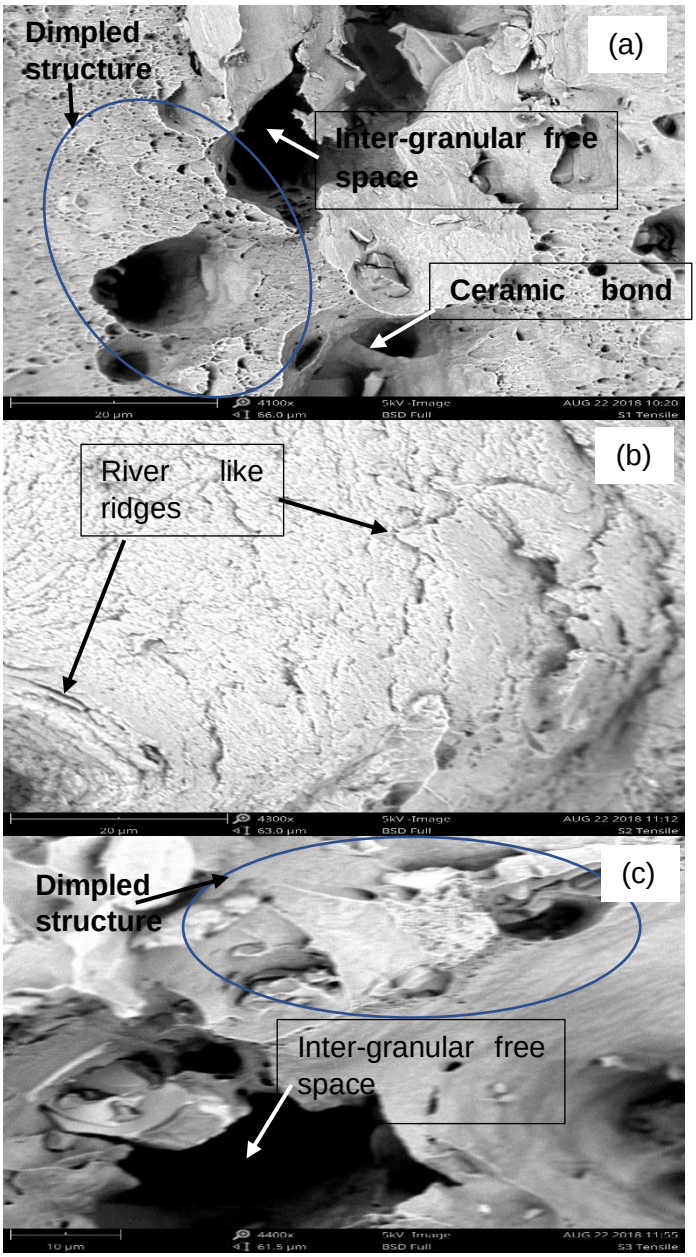

Figure 4.3: Fractured SEM photographs at the start of the weld for specimens (a) S1, (b) S2 and (C) S3

Figure 4.3 shows the fractographs for specimens at the start of the weld, for rotational speeds 600, 700 and 800 rpm. In figure 4.3 (a) is a fractured surface for specimen S1 having wide and deeper sheared dimples with risen cavities which suggest the ductile fracture with ceramic bond bridges and inter-granular free spaces, [Kaplonek & Nadolny, 2013]. In figure 4.3 (b) is a fractured surface for specimen S2 which is categorised as a brittle fracture because it has insufficient plastic deformation and has river like ridges with facet formation, [Sun et al., 2017]. Whereas in figure 4.3 (c) is a fractured surface for specimen S3 showing inter-granular brittle fracture features like peeling-off grain boundary shells.

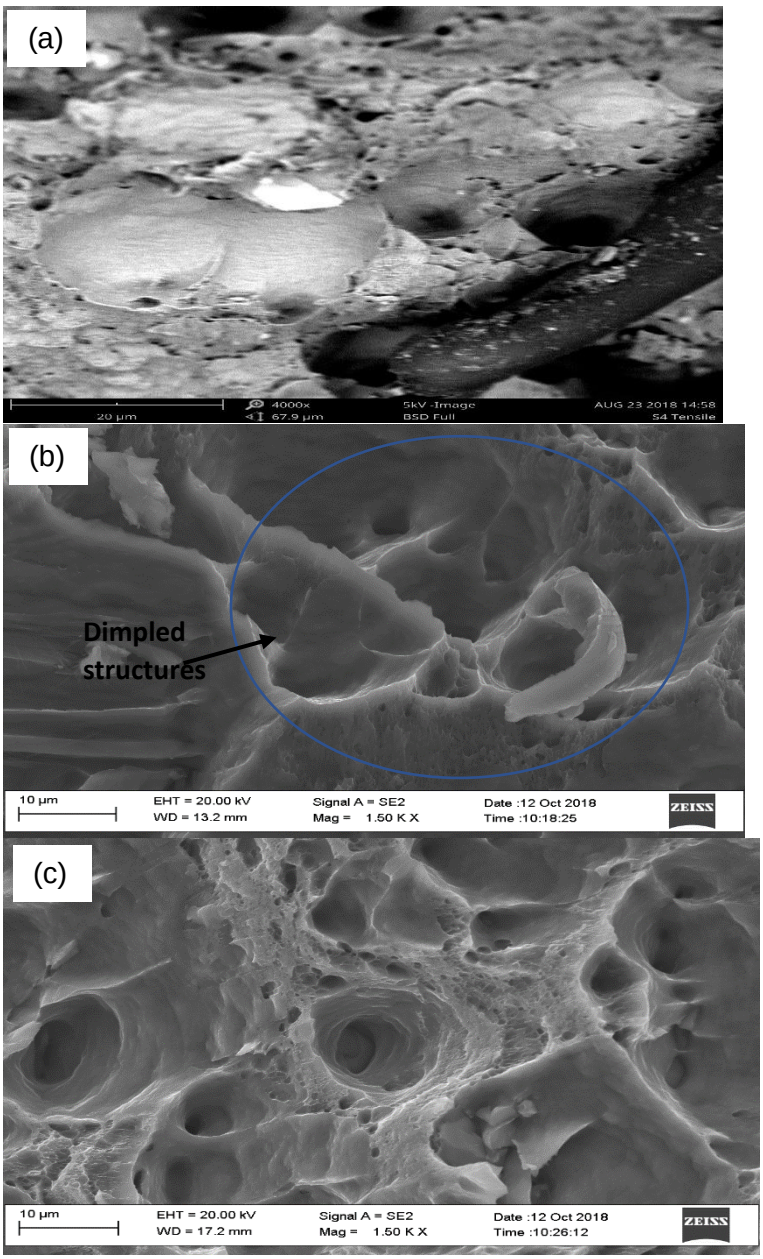

Figure 4.4: SEM fractographs at the start of the weld for specimens (a) S4, (b) S5 and (c) S6

Figure 4.4 contains SEM fractured surfaces which were extracted at the start of the weld for rotational speeds, 900, 1000 and 1200 rpm. They all show ductile fracture features such as sheared dimpled structures with risen cavities. Specimen S4 has smaller and shallow dimples. S5 has large but shallow dimples and S6 has deep and large dimples.

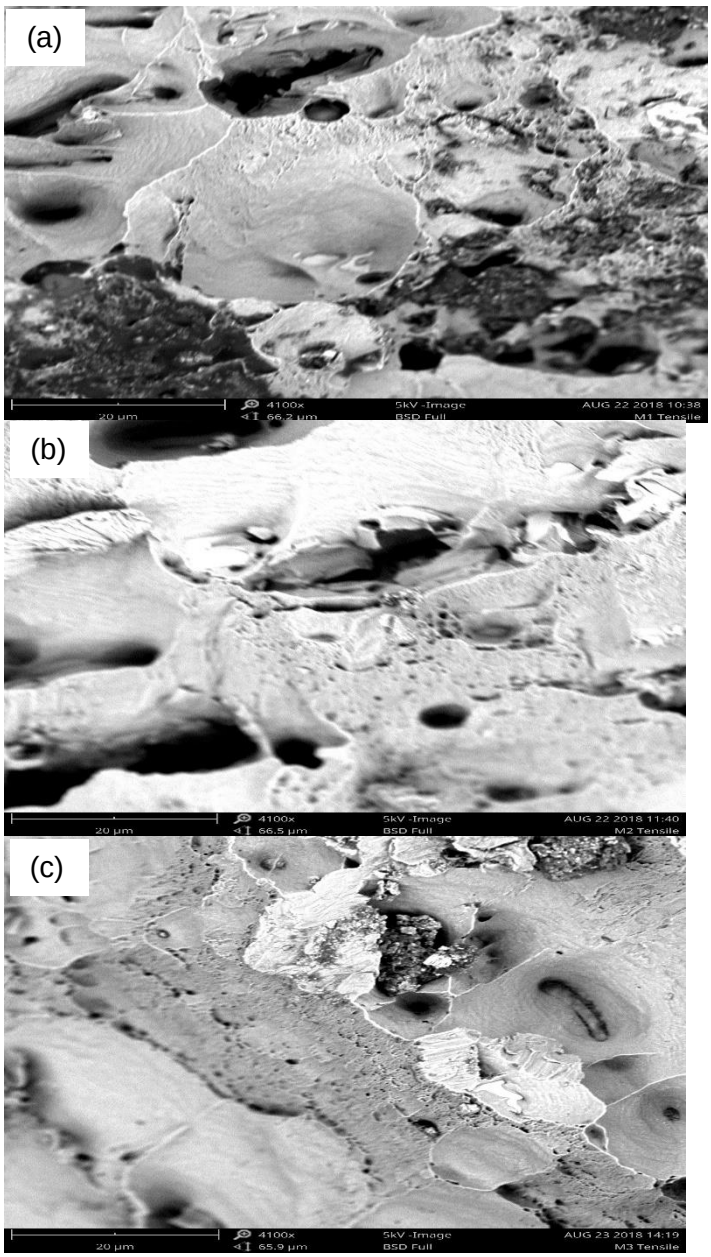

Figure 4.5: Presents SEM fractographs at the middle of the weld for specimens (a) M1, (b) M2 and (c) M3

Figure 4.5 presents SEM fractured surfaces of specimens extracted from the middle of the weld for rotational speeds, 600, 700 and 800 rpm. Figures 4.8 (a), (b) and (c) show ductile fracture features such as necked and sheared dimpled structures with risen cavities. These specimens have large and shallow dimples.

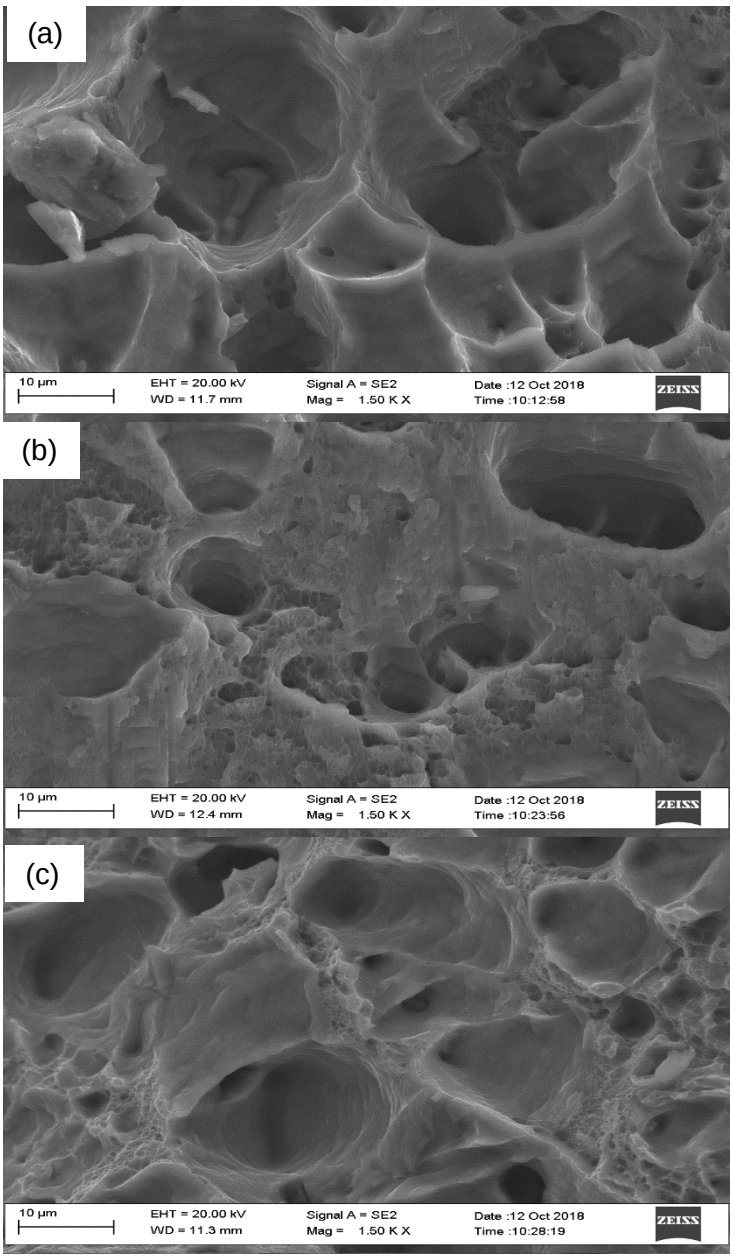

Figure 4.6: SEM fractographs at the middle of the weld for specimens (a) M4, (b) M5 and (c) M6

Figure 4.6 shows SEM fractured surfaces for specimens extracted from the middle of the weld for rotational speeds, 900, 1000 and 1200 rpm. They all show ductile fracture features such as necked /sheared dimpled structures with risen cavities. All specimens contain large but shallow dimples.

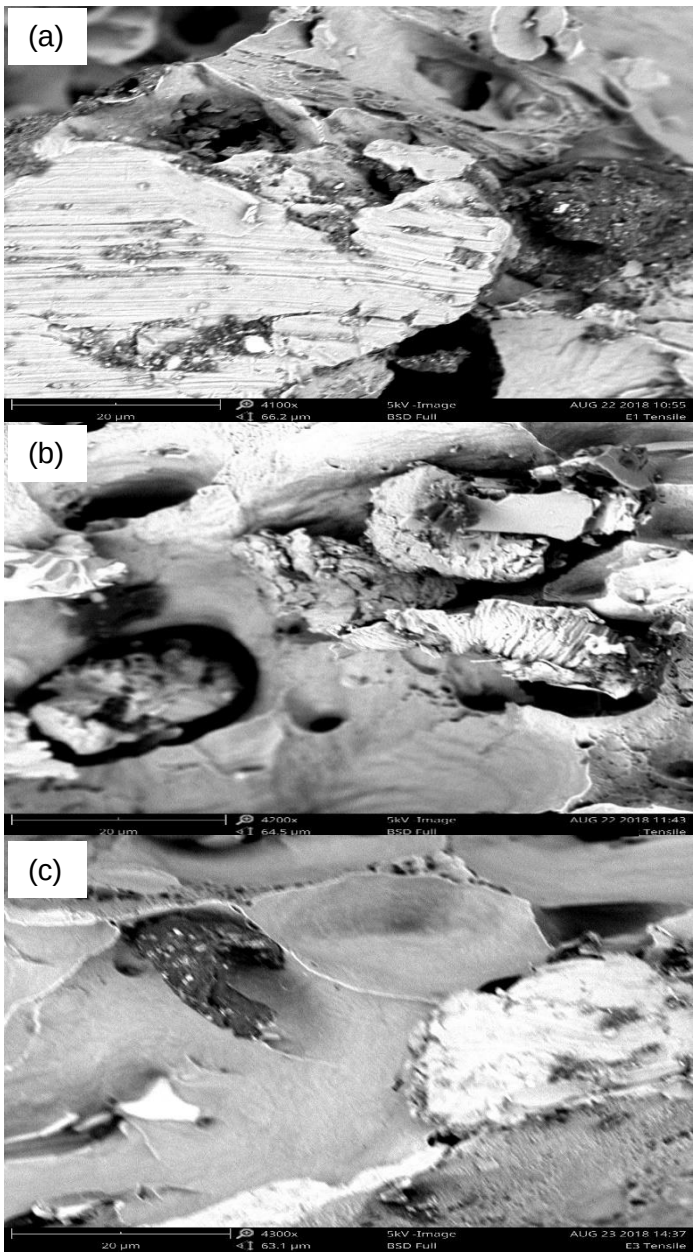

Figure 4.7: SEM fractographs at the end of the weld for specimens (a) E1, (b) E2 and (c) E3

Figure 4.7 contains SEM fractured surfaces for specimens extracted from the end of the weld welded at rotational speeds, 600, 700 and 800 rpm. They all show ductile fracture features such as necked and sheared shallow dimples. With specimen E1 and E3 showing extra coarse slip bands.

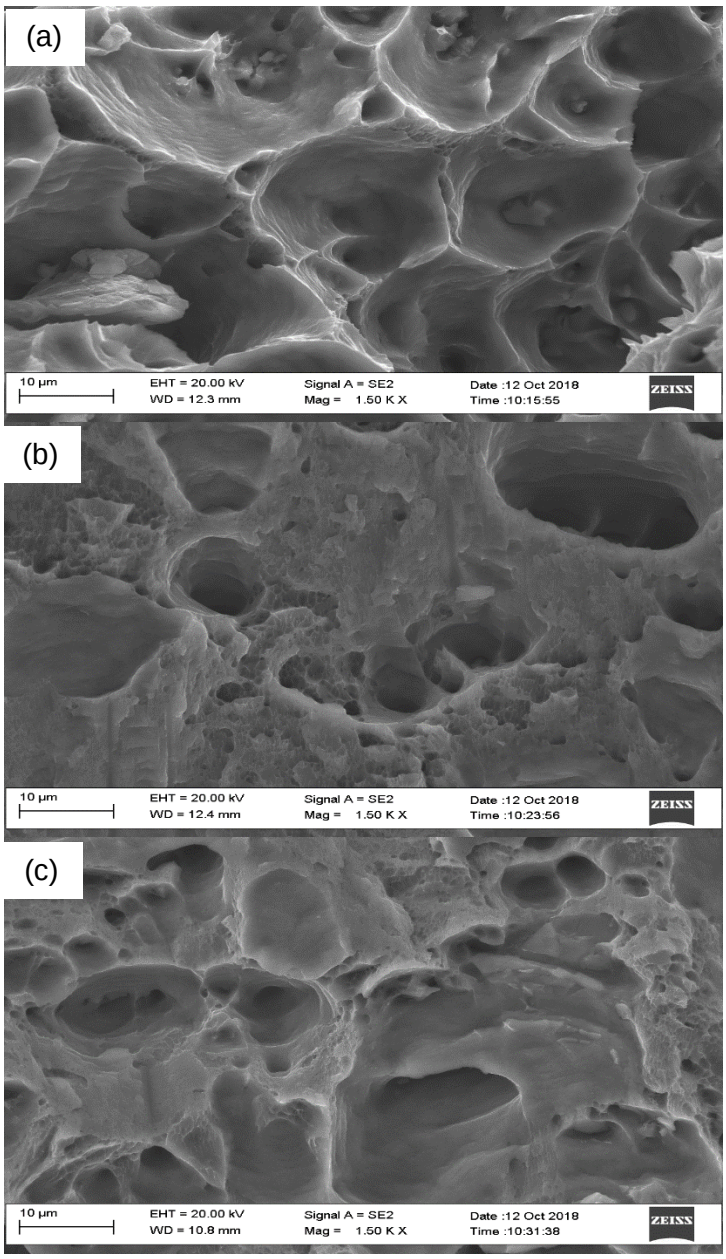

Figure 4.8: SEM fractographs at the end of the weld for specimens (a) E4, (b) E5 and (c) E6

Figure 4.11 shows the SEM fractured surfaces for specimens extracted from the end of the weld for rotational speeds 900, 1000, and 1200 rpm. Figures 4.11 (a) show ductile fracture features such as necked larger and shallow dimpled structures, whereas figure 4.11 (b) and (c) show ductile fracture features such as sheared deep and larger dimple structures.

In order for structures to withheld forces of failure, they should be strong and ductile, (Möser, 1987). In this study, fractured tensile specimens under SEM evaluation, were found to be brittle for specimen S2, intergranular brittle fracture for specimen S3 while all other specimens shown ductile fracture just like the parent material specimen. These results are showing that all other specimens were strong to withhold forces of failure during tensile testing except specimen S2

and S3 which should shown lower tensile properties. Specimen S1, S5, S6, M5, M6, E5 and E6, should have higher elongation.

4.2 Microstructure

Each specimen comprises of the stir zone, the advancing side (AS) and retreating sides (RS) have both the thermo-mechanically affected zone (TMAZ) and the heat affected zone (HAZ). The specimens average grain sizes are compared with the assistance of microscope images taken at a magnification of 100 mm for each zone to evaluate the strongest. The smaller the grain sizes, the stronger is the material, [Ahmadi et al., 2012]. Fractogrphic images are also presented for all specimens at different rotational speed, at all zones and positions, as seen from figure 4.12 to figure 4.29. These figures show the grains found and voids (circled in white) that were present.

The grain sizes for all rotational speeds in the stir zone are presented in figure 4.9, figure 4.10 for thermo-mechanically affected zones and figure 4.11 for heat affected zones. The average grain sizes in the stir zone had the same trend as tensile properties in tensile tests, see figure 4.9. At the start and middle of the weld, 600 rpm had the smallest grain sizes, 3.41 and 6.16 μm respectively. While at the end, 1200 rpm had the smallest average grain size of 6.43 μm. Therefore, looking at the average grain sizes in the stir zone, 600 rpm specimens are the strongest at the beginning and middle of the weld while 1200 rpm specimen is the strongest at the end of the weld.

The thermo-mechanically affected zone average grain sizes are found in figure 4.10. It comprises of three positions, start, middle and end. Each position was divided into two, the retreating side and the advancing side. At the start of the weld in the retreating side and the advancing side, 600 rpm had the lowest average grain sizes of 6.08 and 6.49 μm respectively. In the middle of the weld on the retreating side, rotational speed of 600 rpm had the smallest average value of 8.46 rpm. In the advancing side rotational speed of 900 rpm had the lowest average value of 7.76 μm. At the end of the weld, in the retreating side rotational speed of 700 rpm had the lowest average value of 8.81 μm and in the advancing side, rotational speed of 1200 rpm had the lowest average value of 9.75 μm.

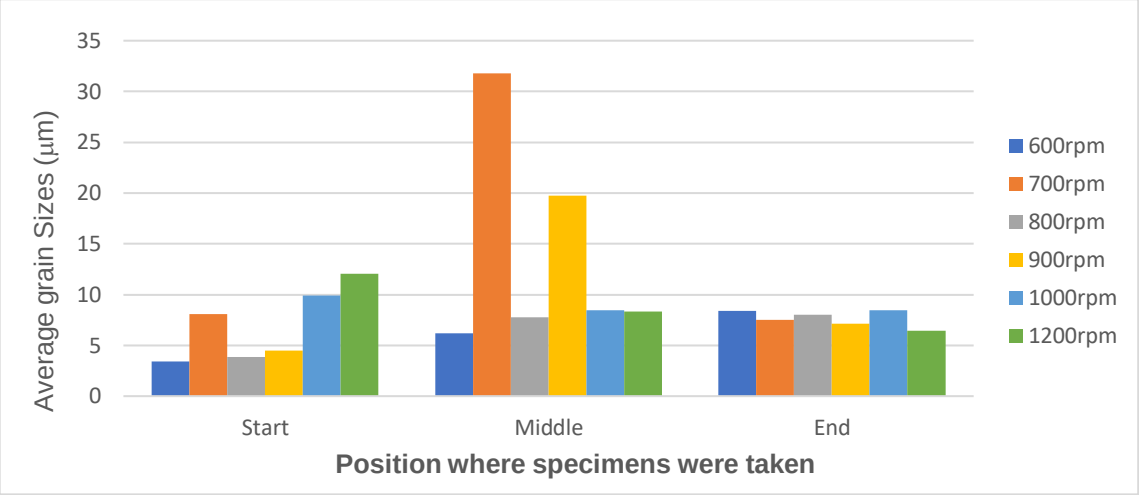

Figure 4.9: Comparison of grain sizes in the stir zone

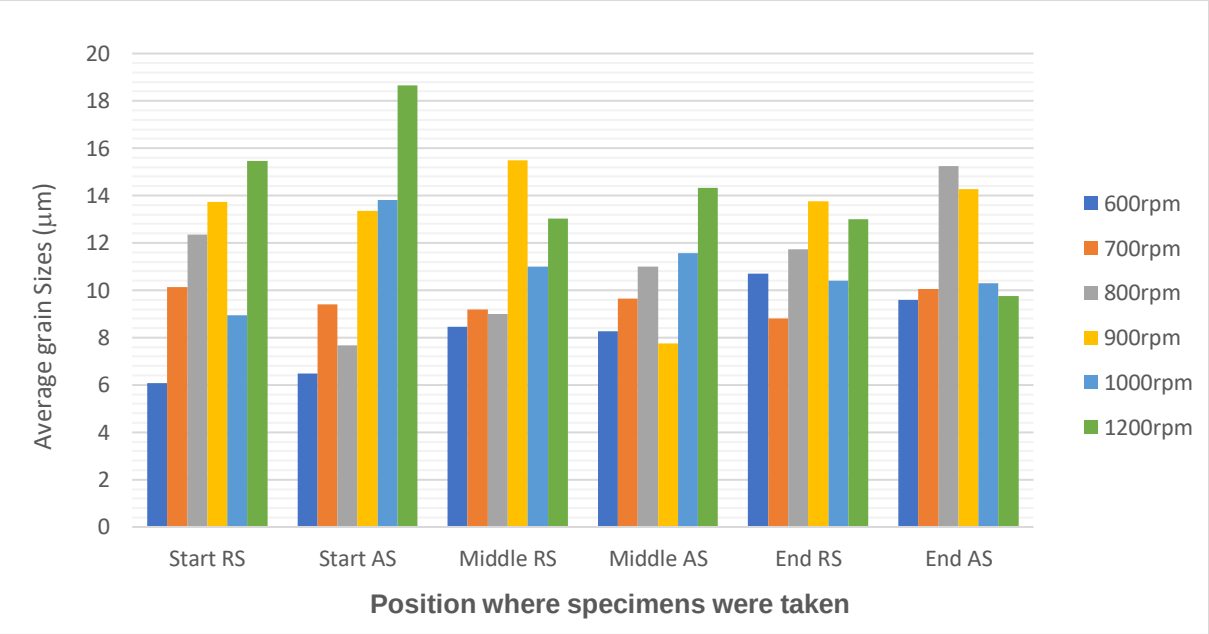

Figure 4.10: Comparison of grain sizes in the thermo-mechanically affected zone

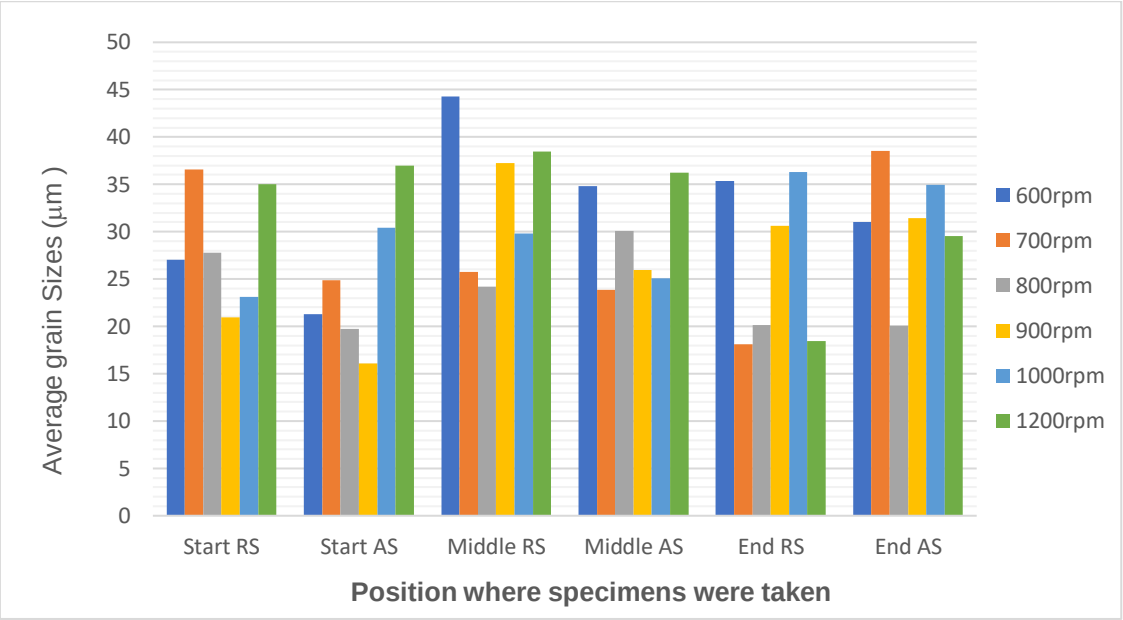

Figure 4.11: Comparison of grain sizes in the heat affected zone

The heat affected zones average grain sizes are shown in figure 4.11. At the beginning of the weld, the rotational speed of 900 rpm has the lowest average grain size values in the retreating side and the advancing sides of 20.94 and 16.07 μm respectively. In the middle of the weld, the retreating side has a lowest average value of 8.99 μm from 800 rpm rotational speed. In the advancing side rotational speed of 700 rpm has the lowest average grain size value of 9.64 μm. At the end of the weld in the retreating side, rotational speed of 700 rpm has the lowest average grain size value of 18.1 μm. While at the advancing side, rotational speed of 800 rpm has the lowest average grain size of 20.08 μm.

4.2.1 Grains at rotational speed of 600 rpm

Microstructural grains for the 600 rpm specimens were captured in the stir zone (see figure 4.12) and the advancing and retreating sides of the thermo-mechanically affected zone (see figure 4.13) and heat affected zone (see figure 4.14).

4.2.1.1 Stir Zone (SZ)

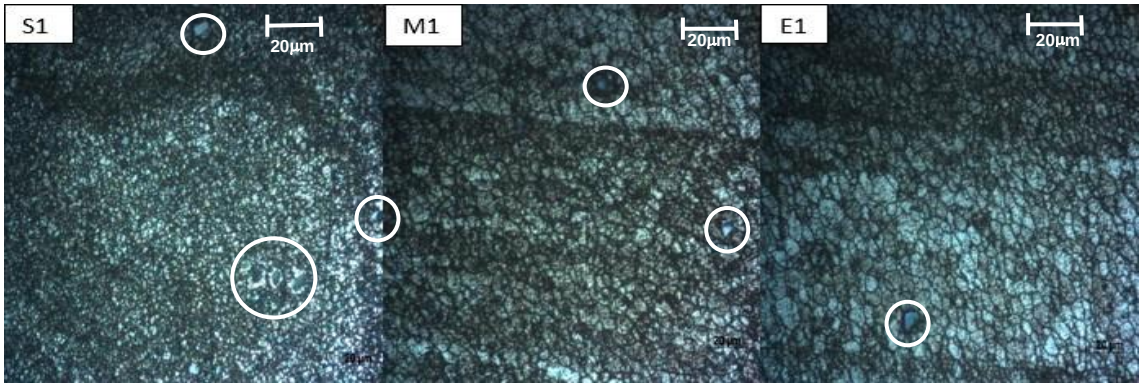

Figure 4.12: Microstructural grains in the centre of the Stir Zone, from the start (S1), middle (M1) and end (E1) of weld at 600 rpm

In the stir zone of the 600 rpm specimens (see figure 4.12) it can be noticed that specimen S1 has the smallest grains visible with an average size of 3.41 µm followed by specimen M1 with 6.16 µm. Even though specimen S1 has the smallest grain sizes, it also has the most voids (circled white) visible, this cooled be caused by rapid cooling from air, (Tamadon et al., 2018).

4.2.1.2 Thermo-Mechanically Affected Zone (TMAZ)

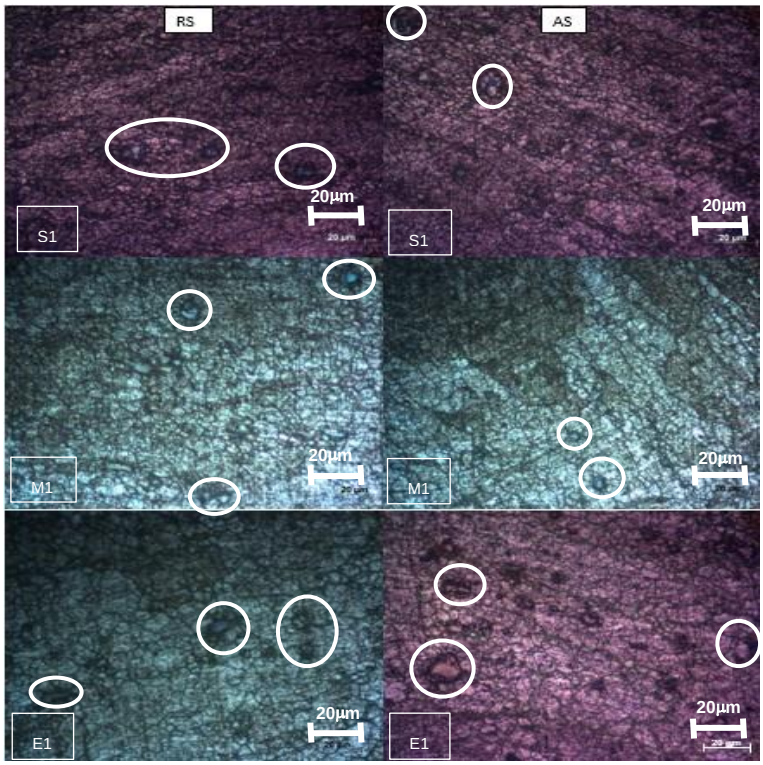

Figure 4.13: Microstructural grains at the retreating and advancing sides of the Thermo-Mechanically Affected Zone, taken from the start (S1), middle (M1) and end (E1) of weld at 600 rpm

Grains at the TMAZ for rotational speed 600 rpm are shown in figure 4.13 for the advancing side and the retreating side. In the advancing side, it can be noticed that the grains are all flowing in the same direction. This is caused by plastic deformation taking place at high temperatures which increases grain boundary creating such flow, [Zhang & Wang, 2018] Specimen S1 for both the advancing and retreating sides has more visible small and big voids than specimens M1 and E1.

4.2.1.3 Heat Affected Zone (HAZ)

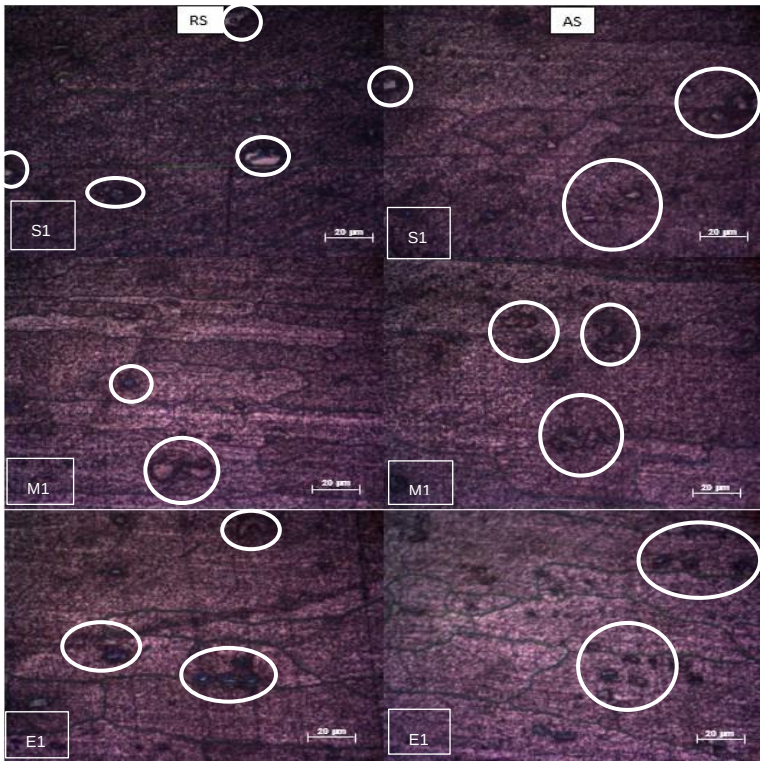

Figure 4.14: **Microstructural grains at the retreating and advancing sides of the Heat Affected Zone, taken from the start (S1), middle (M1) and end (E1) of weld at 600 rpm**

In the HAZ of 600 rpm specimens, the grain sizes are bigger than those in the SZ and TMAZ. Observing in figure 4.14 it can be seen that specimens S1 and E1 on both the advancing and retreating sides have a number of visible voids small and big whereas in specimens M1 there is hardly any.

4.2.2 Grains at rotational speed of 700 rpm

For specimens welded at a rotational speed of 700 rpm, captured images of their microstructural grains are found from figure 4.15 to 4.17. These figures contain grains at the stir zone, the advancing and retreating sides of the thermo-mechanically affected zone and the heat affected zone.

4.2.2.1 Stir Zone (SZ)

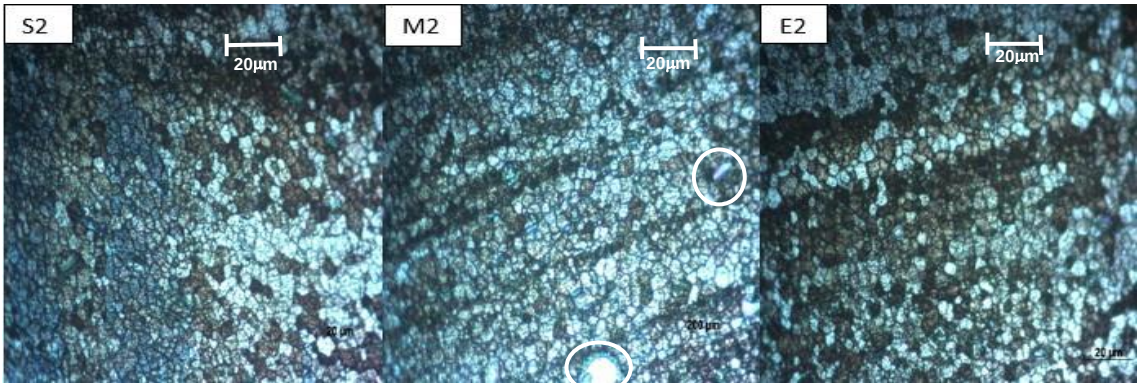

Figure 4.15: Microstructural grains in the centre of the Stir Zone, from the start (S2), middle (M2) and end (E2) of weld at 700rpm

As seen in figure 4.15, the grain sizes of specimen M2 appear to be smaller in size than those of specimens S2 and E2. Specimens S2 and E2 have no voids visible whereas specimen M2 has a few of these voids visible which could cause the materials strength to weaken.

4.2.2.2 Thermo-Mechanically Affected Zone (TMAZ)

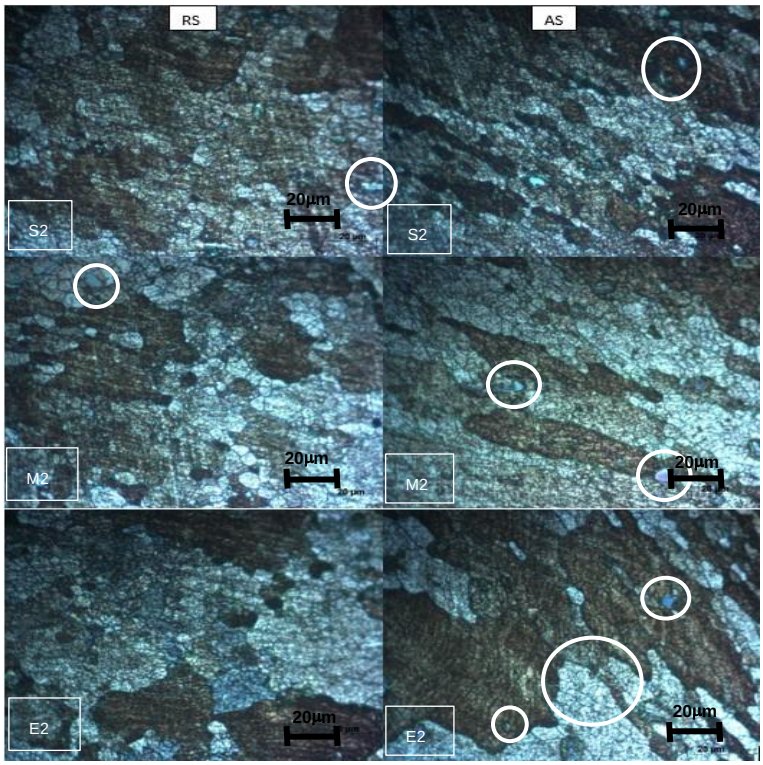

Figure 4.16: Microstructural grains at the retreating and advancing sides of the Thermo-Mechanically Affected Zone, taken from the start (S2), middle (M2) and end (E2) of weld at 700 rpm

Grain images for both the retreating and advancing sides of the thermo-mechanically affected zone for specimens welded at a rotational speed of 700 rpm are found in figure 4.16. There

are voids visible in both the advancing and retreating side of S2 and on the advancing side of specimens M2 and E2.

4.2.2.3 Heat Affected Zone (HAZ)

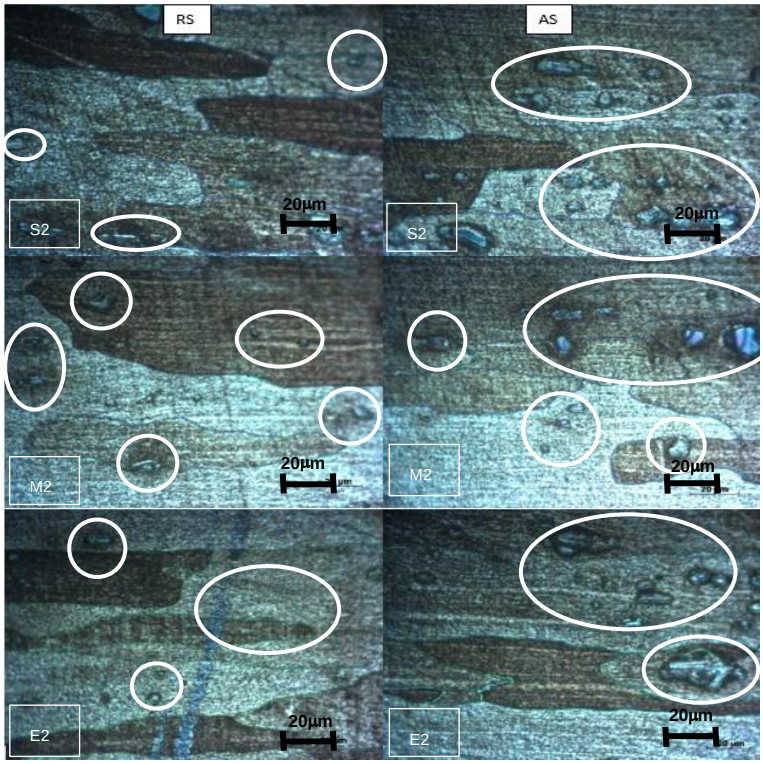

Figure 4.17: Microstructural grains at the retreating and advancing sides of the Heat Affected Zone, taken from the start (S2), middle (M2) and end (E2) of weld at 700 rpm

The HAZ of specimens welded at 700 rpm has the biggest grain sizes and appears (see figure 4.17) to have small and big voids on both the advancing and retreating sides with S2 on the retreating side appearing to have lesser voids followed by E2 on the retreating side.

4.2.3 Grains at rotational speed of 800 rpm

The microstructural grains for specimens welded at a rotational speed of 800 rpm are found in figure 4.18 to 4.20. These figures comprise grains at the stir zone and on both the retreating and advancing sides of the thermo-mechanically affected zone and heat affected zone.

4.2.3.1 Stir Zone (SZ)

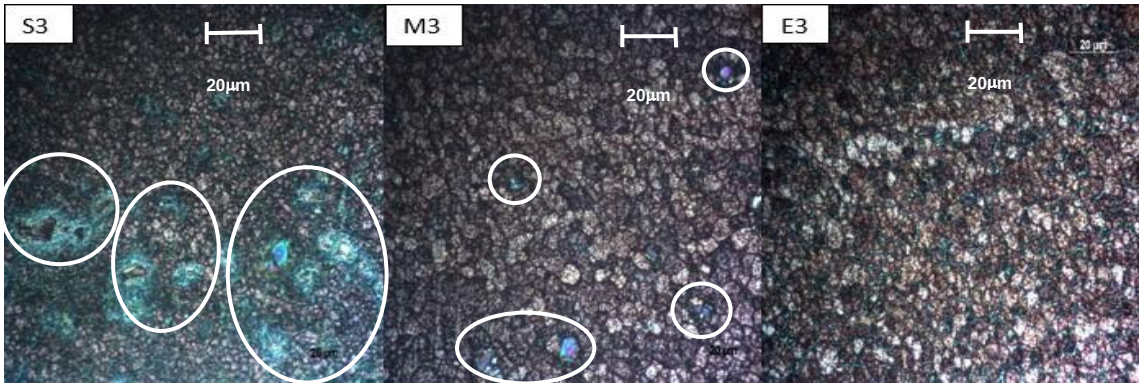

Figure 4.18: Microstructural grains in the centre of the Stir Zone, from the start (S3), middle (M3) and end (E3) of weld at 800 rpm

At the stir zone of the 800 rpm welded workpiece, the S3 specimen shows smaller grain sizes followed by specimen E3 then M3 (see figure 4.18). Not only does specimen S3 showing smaller grain sizes, but it also has a number of big voids visible. There are no voids visible in specimen E3 but specimen M3 has a few smaller voids visible.

4.2.3.2 Thermo-Mechanically Affected Zone (TMAZ)

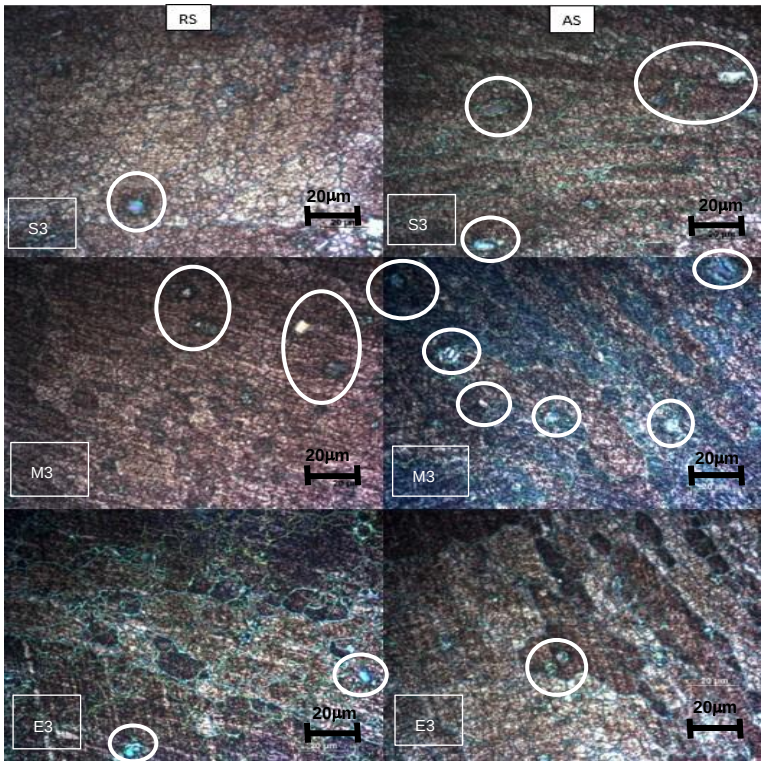

Figure 4.19: Microstructural grains at the retreating and advancing sides of the Thermo-Mechanically Affected Zone, taken from the start (S3), middle (M3) and end (E3) of weld at 800rpm

Figure 4.19 has photographs of microstructural grains on the retreating and advancing sides for the thermo-mechanically affected zones of the 800 rpm welded workpiece at start, middle and end. Looking at the advancing side, grains can be seen. A number of voids is observed in specimens S3 and M3.

4.2.3.3 Heat Affected Zone (HAZ)

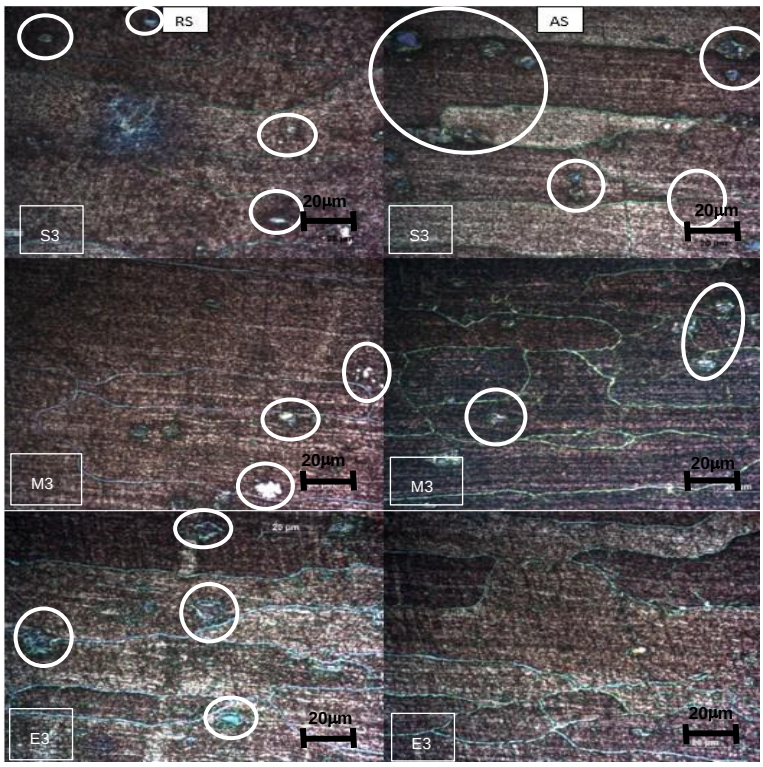

Figure 4.20: Microstructural grains at the retreating and advancing sides of the Heat Affected Zone, taken from the start (S3), middle (M3) and end (E3) of weld at 800rpm

The microstructural grains at the heat affected zone for rotational speed of 800 rpm are found in figure 4.20. This zone has bigger grain sizes than other zones. All specimens have small voids visible in both the retreating and advancing sides.

4.2.4 Grains at rotational speed of 900 rpm

Grain photographs at the stir zone, thermo-mechanically affected zone and heat affected zone for specimens welded at a rotational speed of 900 rpm are found in figures 4.21, 2.22 and 2.23 respectively.

4.2.4.1 Stir Zone (SZ)

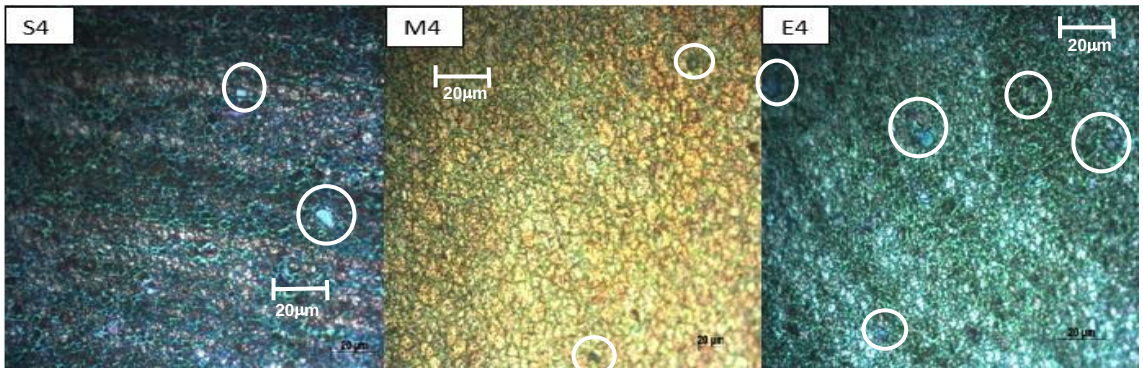

Figure 4.21: Microstructural grains in the centre of the Stir Zone, from the start (S4), middle (M4) and end (E4) of weld at 900rpm

At the stir zone of the 900 rpm specimens it can be seen in figure 4.21 that all grains in each specimen have approximately the same grain sizes. They all appear to have small voids visible.

4.2.4.2 Thermo-Mechanically Affected Zone (TMAZ)

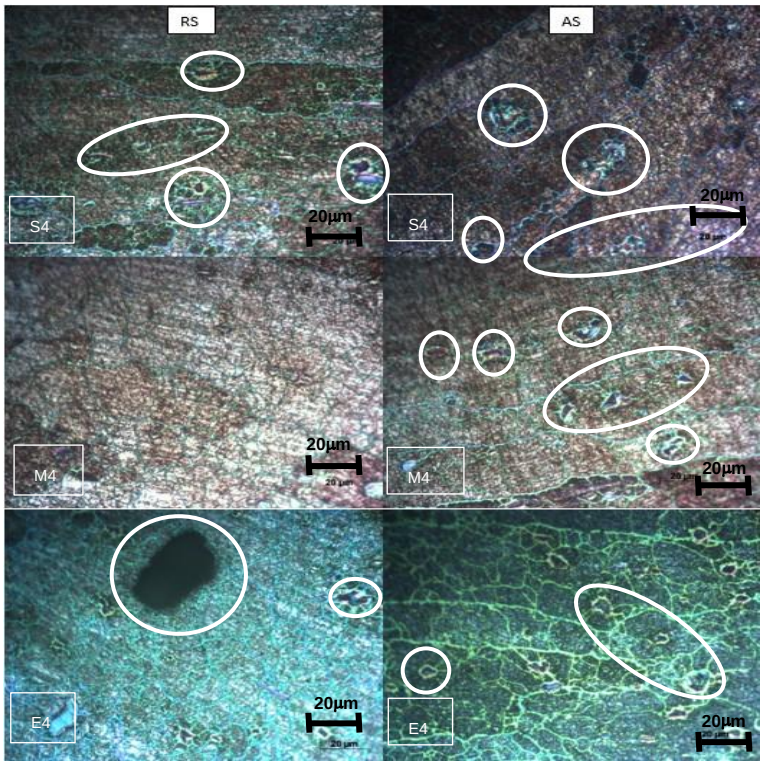

Figure 4.22: Microstructural grains at the retreating and advancing sides of the Thermo-Mechanically Affected Zone, taken from the start (S4), middle (M4) and end (E4) of weld at 900 rpm

In the thermo-mechanically affected zones in figure 4.22 it can be seen that specimen E4 in the retreating side has a very big void/ wormhole while other specimens have smaller voids.

4.2.4.3 Heat Affected Zone (HAZ)

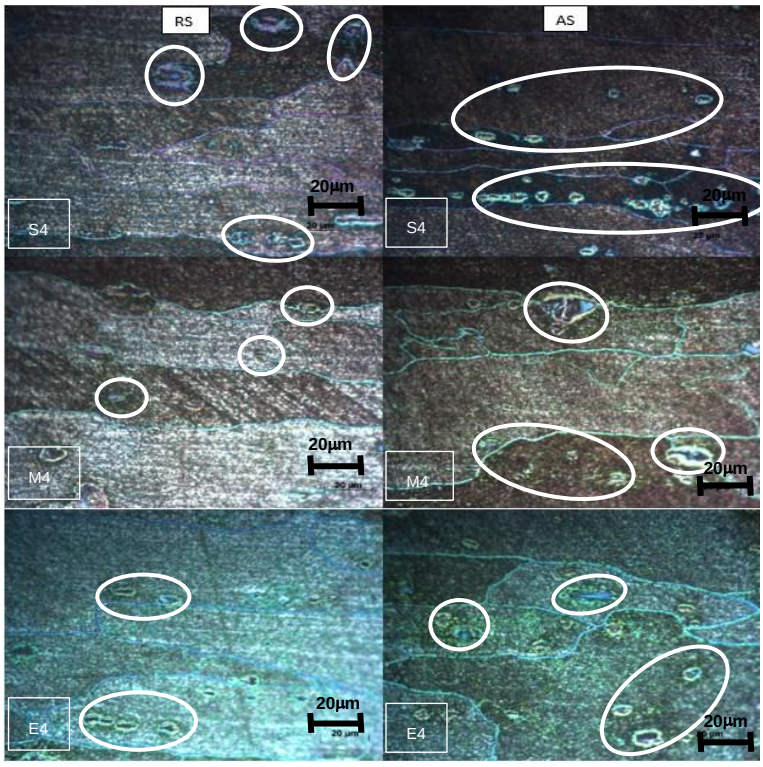

Figure 4.23: Microstructural grains at the retreating and advancing sides of the Heat Affected Zone, taken from the start (S4), middle (M4) and end (E4) of weld at 900 rpm

At the heat affected zone of the welded specimen at a rotational speed of 900 rpm, the microstructure appears to have voids on both sides (advancing and retreating) at the start, middle and end (see figure 2.23). The advancing side for all specimens has more voids available.

4.2.5 Grains at rotational speed of 1000 rpm

Grain photographs at the stir zone, thermo-mechanically affected zone and heat affected zone for specimens welded at a rotational speed of 1000 rpm are found in figures 4.24, 2.25 and 2.26 respectively.

4.2.5.1 Stir Zone (SZ)

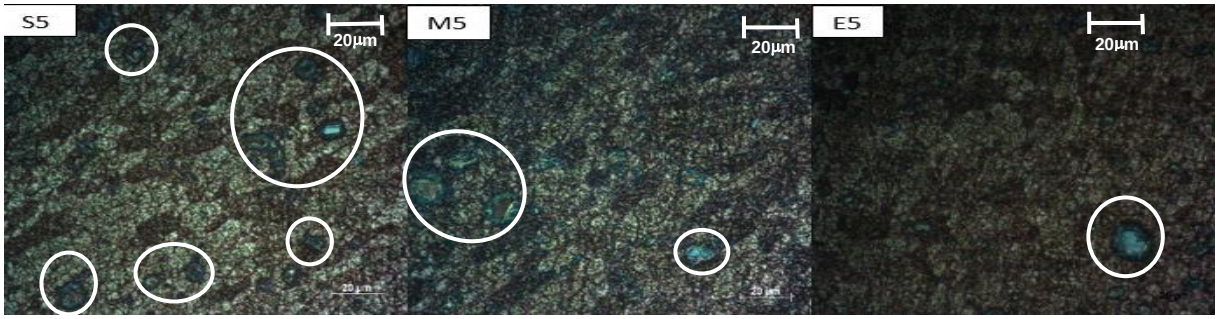

Figure 4.24: Microstructural grains in the centre of the Stir Zone, from the start (S5), middle (M5) and end (E5) of weld at 1000rpm

At the stir zone (see figure 4.24) specimen M5 appears to have voids visible than specimen S5 and E5. Specimen M5 has the smallest grain sizes.

4.2.5.2 Thermo-Mechanically Affected Zone (TMAZ)

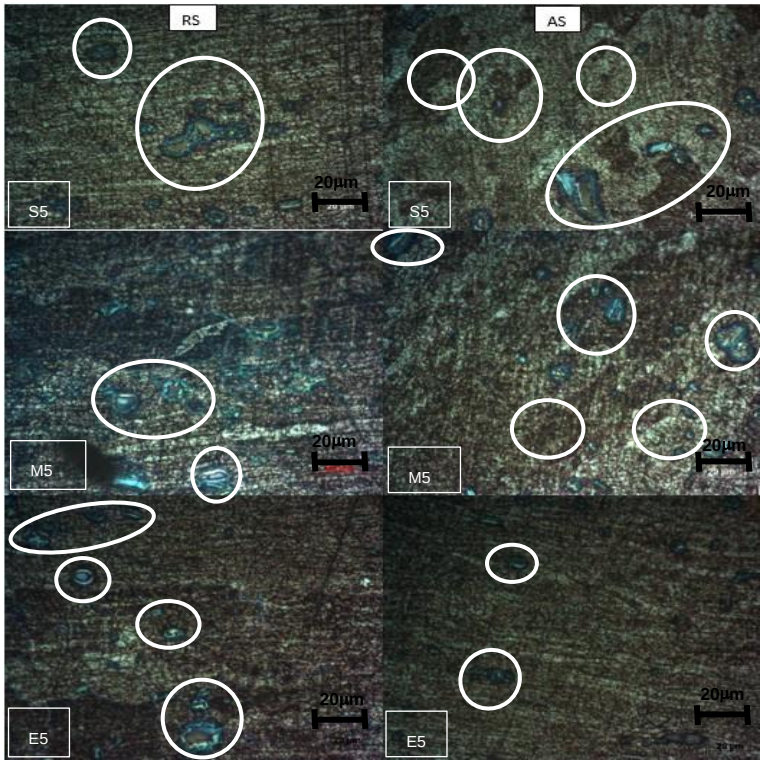

Figure 4.25: Microstructural grains at the retreating and advancing sides of the Thermo-Mechanically Affected Zone, taken from the start (S5), middle (M5) and end (E5) of weld at 1000 rpm

The microstructural grains at the thermo-mechanically affected zone of specimens welded at a rotational speed of 1000 rpm are not observable without zooming into the photographs (see figure 4.25). Specimen M5 appears to be having more number of voids followed by specimen S5 then E5.

4.2.5.3 Heat Affected Zone (HAZ)

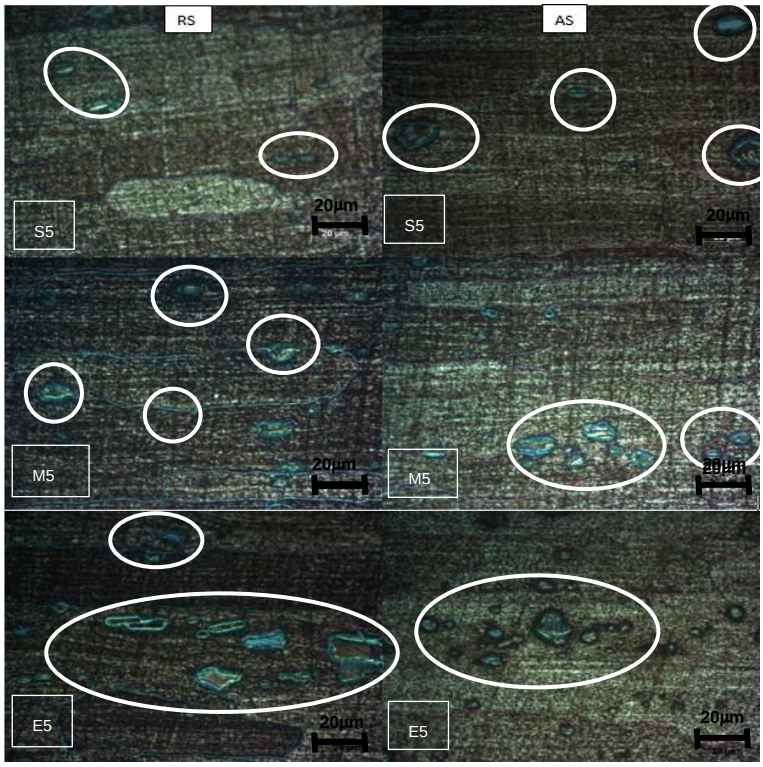

Figure 4.26: Microstructural grains at the retreating and advancing sides of the Heat Affected Zone, taken from the start (S5), middle (M5) and end (E5) of weld at 1000rpm

The microstructure photographs of the heat affected zone for specimens welded at a rotational speed of 1000 rpm in figure 4.26 shows lots of voids in all positions, at the start, middle and end.

4.2.6 Grains at rotational speed of 1200 rpm

Grain photographs at the stir zone, thermo-mechanically affected zone and heat affected zone for specimens welded at a rotational speed of 1200 rpm are shown in figures 4.27, 2.28 and 2.29 respectively.

4.2.6.1 Stir Zone (SZ)

Figure 4.27 has photographs for microstructural grains at the stir zone for specimens welded at a rotational speed of 1200 rpm. It shows specimen E6 with smaller grain sizes. All specimens (S6, M6 and E6) have few little voids visible.

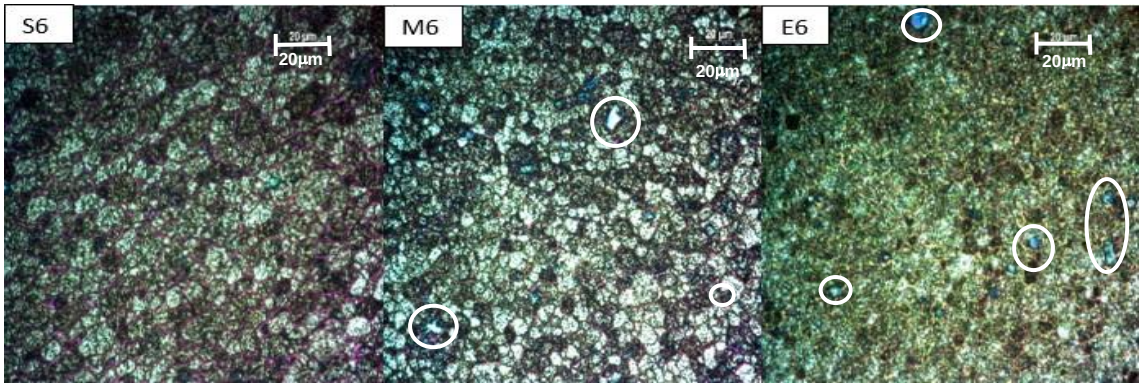

Figure 4.27: Microstructural grains in the centre of the Stir Zone, from the start (S6), middle (M6) and end (E6) of weld at 1200rpm

4.2.6.2 Thermo-Mechanically Affected Zone (TMAZ)

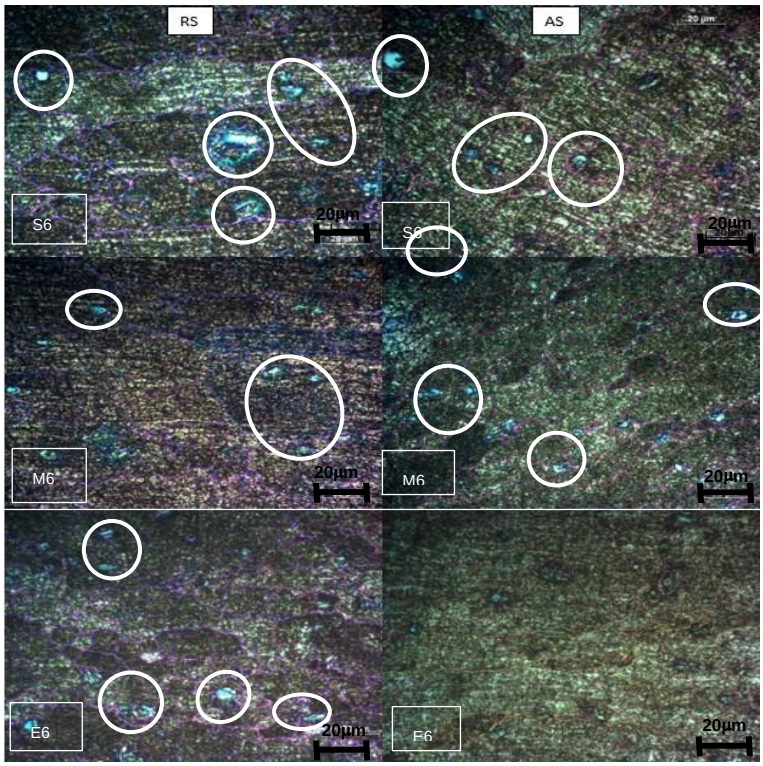

Figure 4.28: Microstructural grains at the retreating and advancing sides of the Thermo-Mechanically Affected Zone, taken from the start (S6), middle (M6) and end (E6) of weld at 1200 rpm

From figure 4.28 the microstructural grains in the thermo-mechanically affected zones of specimens welded at a rotational speed of 1200 rpm are shown. It can be seen that the grains on the advancing side are smaller than these in the retreating side for all specimens and minor voids are visible for all specimens.

4.2.6.3 Heat Affected Zone (HAZ)

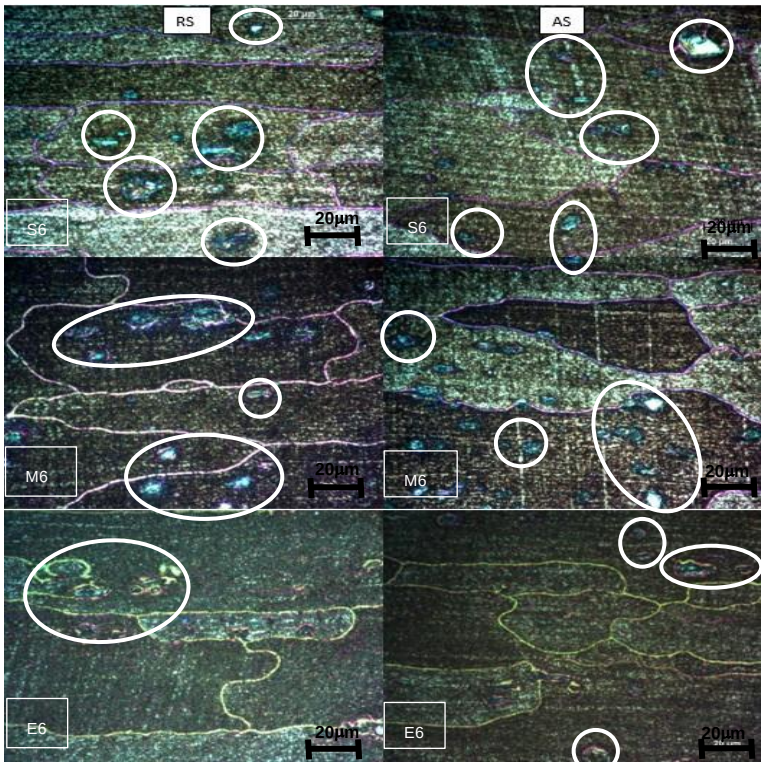

Figure 4.29: Microstructural grains at the retreating and advancing sides of the Heat Affected Zone, taken from the start (S6), middle (M6) and end (E6) of weld at 1200 rpm

Figure 4.29 shows the heat affected zone of specimens welded at a rotational speed of 1200 rpm. Big grain sizes are observed with a number of voids in all specimens (S6, M6 and E6).

4.3 Macrostructure

In order to get better understanding of the influence of high rotational speeds using a constant welding speed, the macrostructure of the specimens needed to be assessed under a polarized light microscope. Results obtained from all specimens of different rotational speeds are presented. Figure 4.31 has macrostructures of welds at start, for all rotational speeds. Figure 4.32 has macrostructures at the middle of the weld for all rotational speeds. Figure 4.33 has macrostructures for all rotational speeds at the end of the weld. The three zones can be seen; stir zone, thermo-mechanically affected zone and the heat affected zone with the defects that were observed.

The macrostructure for welds at start for all rotational speeds is found in figure 4.32. For all of the rotational speeds, it can be observed that the nugget doesn't only have one set of onion rings but a number of them except for specimen S1. These onion rings are caused by the stirring of the FSW tool and their duplication means there was sufficient mixing in the stir zone, [Leitão et al., 2008]. The specimens S1 and S3 shows wormholes and voids which are indication of poor material mixing mostly caused by either insufficient heat input or excess heat

input at the beginning of weld, [Taheri et al., 2019]. Material can be observed flowing to the advancing side; on specimen S3 having the material flow from the retreating side to the stir zone and to the advancing side.

Specimens S2, E1, M2, M4, E4, S5, M5, E5, S6, E6 and M6 have a material called flash coming out at the surface/ outside of the weld. This is caused by having too much-plasticised material escaping from under the pin shoulder during welding because of excess heat and also caused by the bending of material at the stir zone as it is welded, Soni et al., 2017].

Figure 4.30 shows surface grooves at the beginning of 600 and 800 rpm welds and at the end of 1200 rpm weld. This type of defect is caused by the lack of fill during welding because of heat input, [Safeen & Spena, 2019]. Some plasticised material sticking out at the weld surface was also observed at the beginning of weld at 600 rpm.

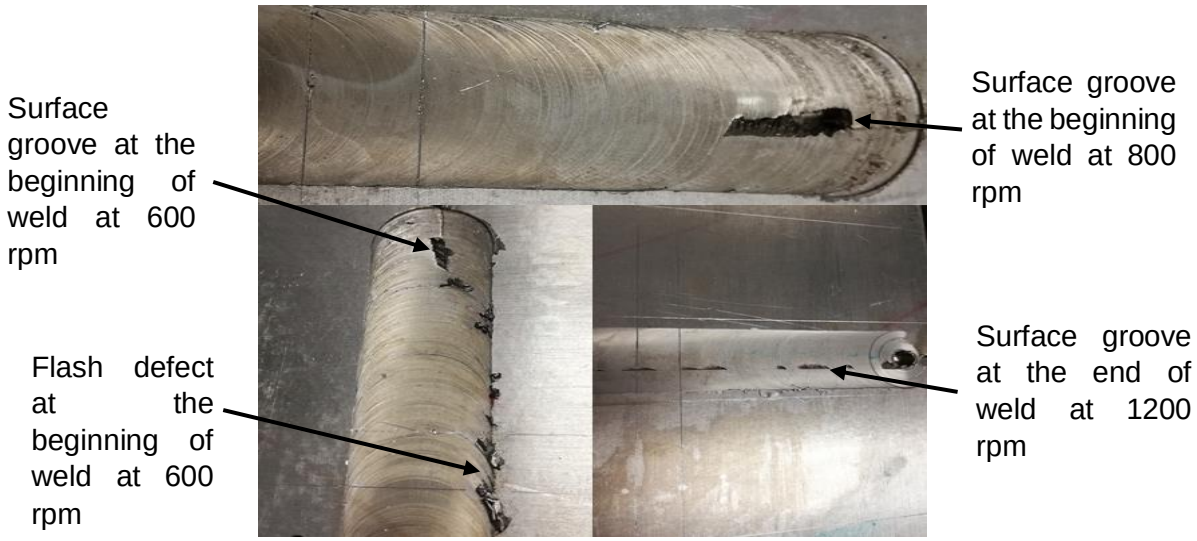

Figure 4.30: Shows the lack of fill on 600, 800 and 1200 rpm welds

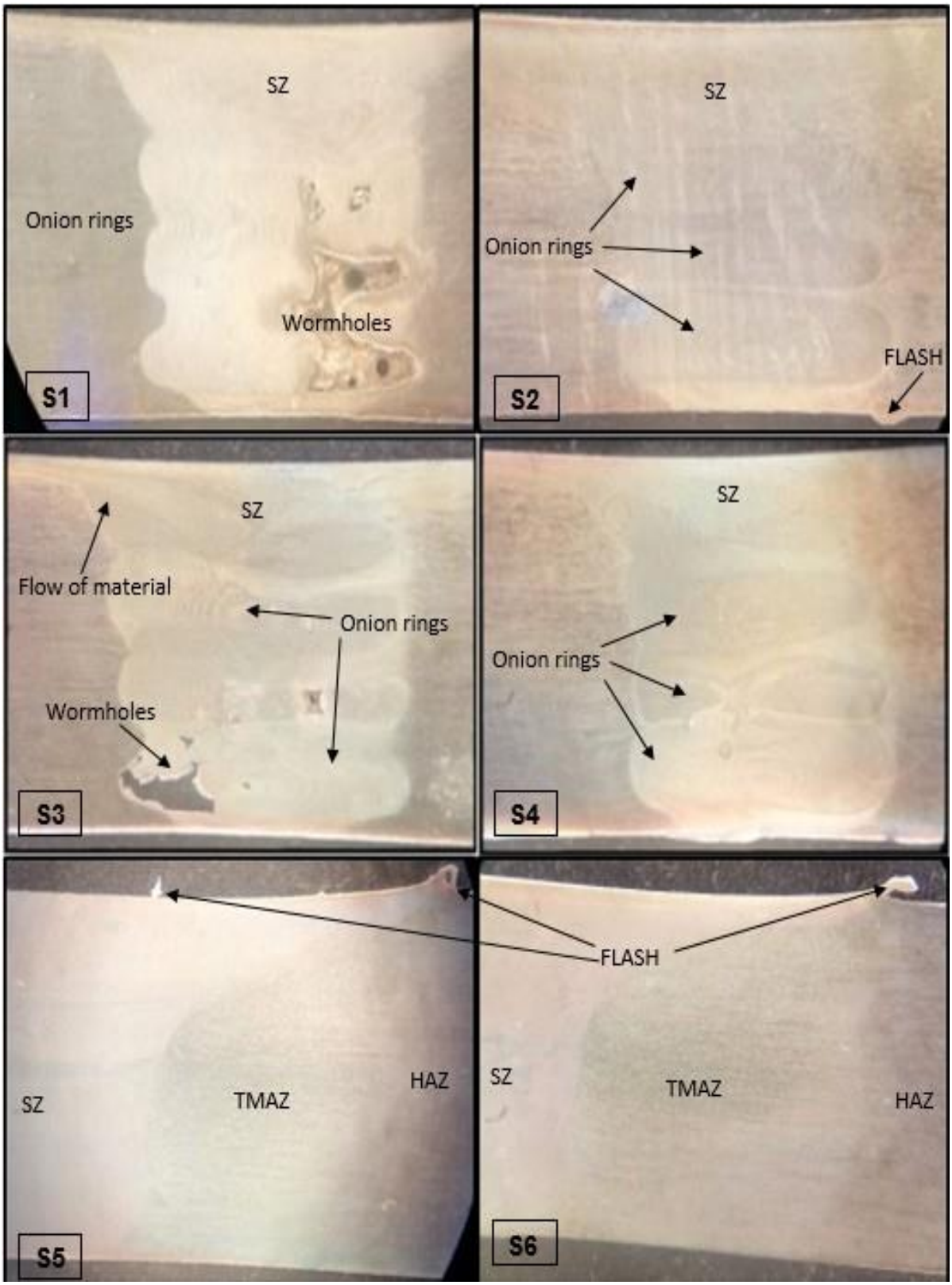

Figure 4.31: Shows the macrostructure of FSW specimens taken from the start of the weld, welded at six different rotational speeds

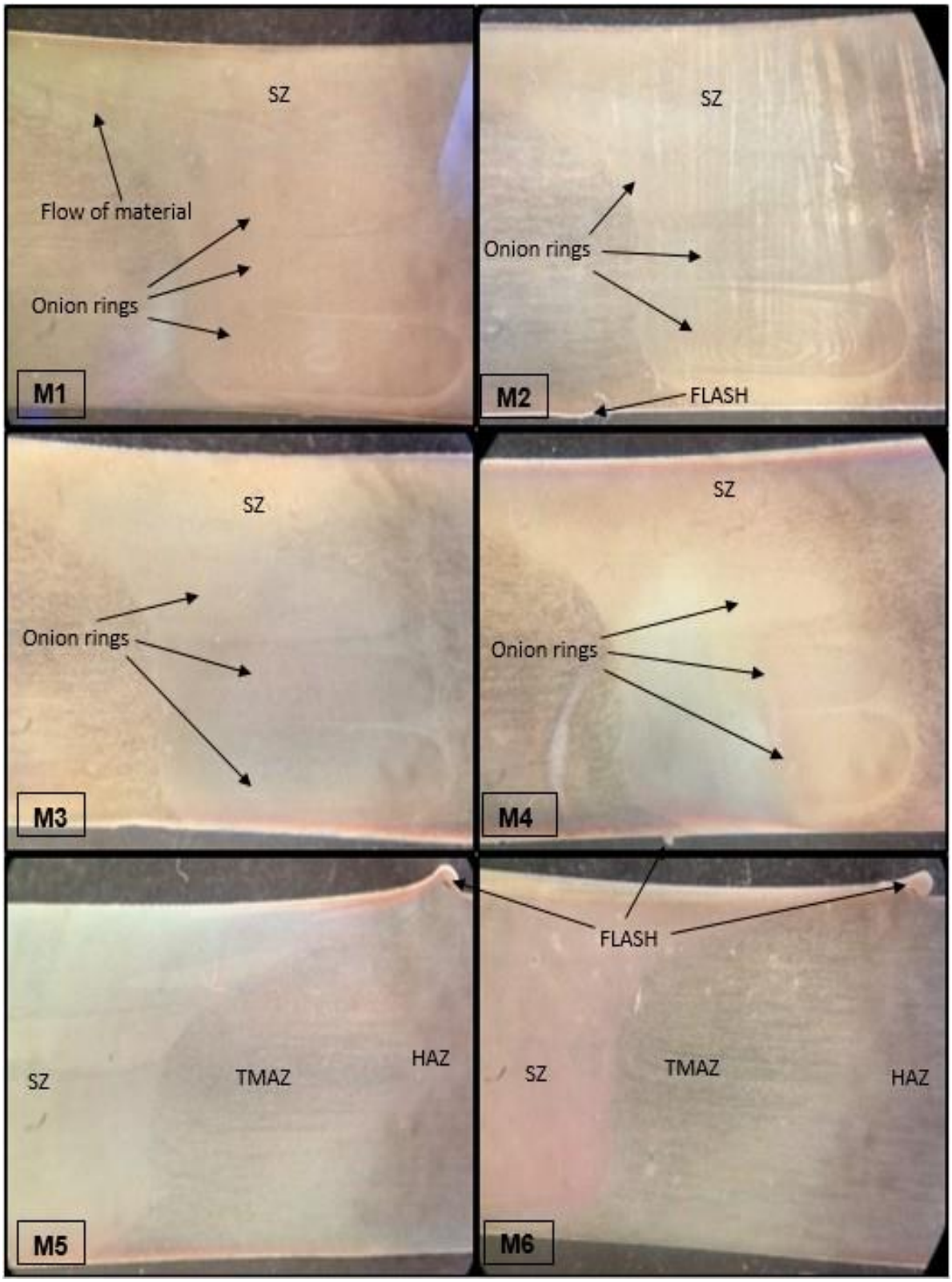

Figure 4.32: Shows the macrostructure of FSW specimens taken from the middle of the weld, welded at six different rotational speeds

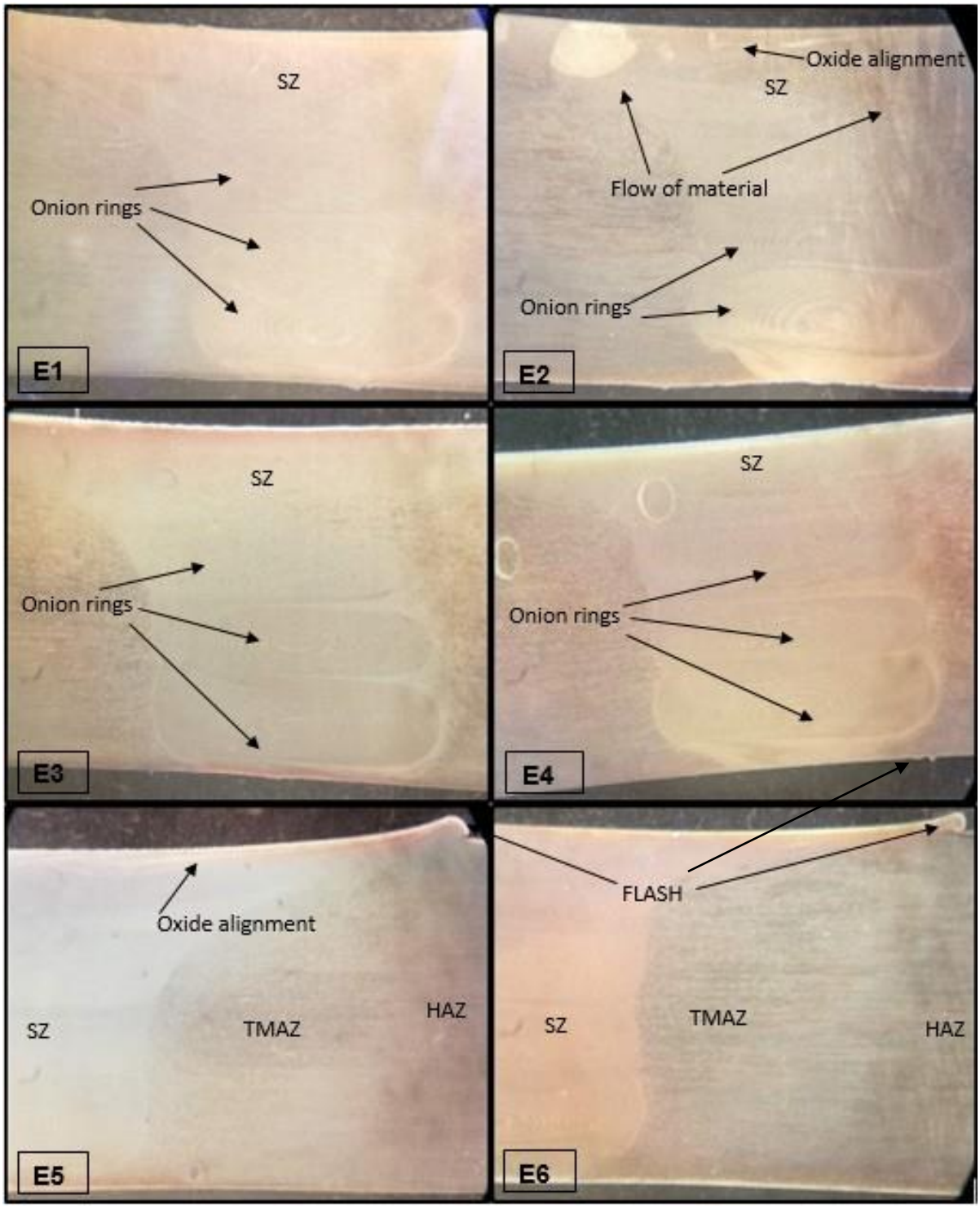

Figure 4.33: Shows the macrostructure of FSW specimens taken from the end of the weld, welded at six different rotational speeds

The specimens M1 and E1 have no visible defects even though they were produced at a low speed. The visible defects are noticed on the specimens produced from higher speeds except specimens produced at 900 rpm.

4.4 Rockwell Hardness

The hardness test was measured from the centre of the weld to either left or right of the weld with an increment of 3mm. The welds specimens were studied comparatively with the parent material of a hardness average value of 70.9HRB. Figure 4.34 shows the graphs for all the samples extracted in the start of the plate for all the speeds used in this study against the hardness of the parent material. All the hardness values were found to be lower than the parent material.

The specimen produced from 1000 rpm rotational speed has the hardness higher than all the specimens in the stir zone even though it has the second biggest average grain size and lower tensile properties. At this point, there seems to be no correlations between hardness, grain size and tensile properties.

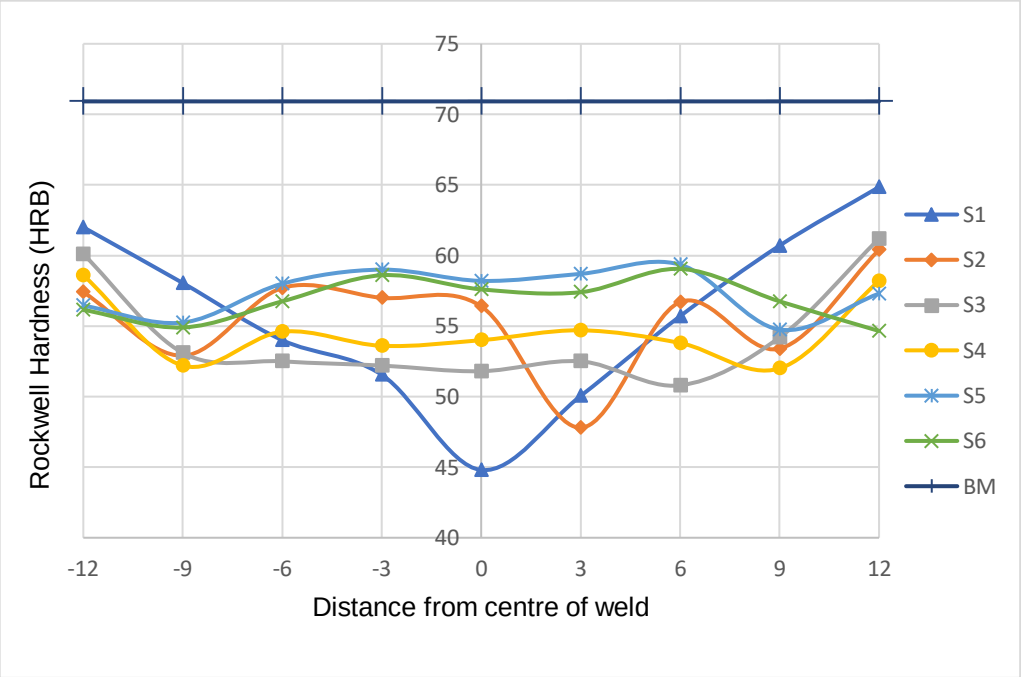

Figure 4.34: Shows Rockwell hardness at the start of the weld for all rotational speeds

The hardness chart for specimens taken from the middle of the weld for all rotational speeds including parent material are presented in figure 4.35. Specimens from 1000 rpm followed by 1200 rpm had the highest average hardness values, with specimen from 600 rpm having the lowest values. At the middle of the weld, rotational speed of 1000 rpm and 1200 rpm had lower tensile properties and bigger grain sizes in the stir zone while rotational speed of 600 rpm had higher tensile properties and smaller grain sizes in the stir zone.

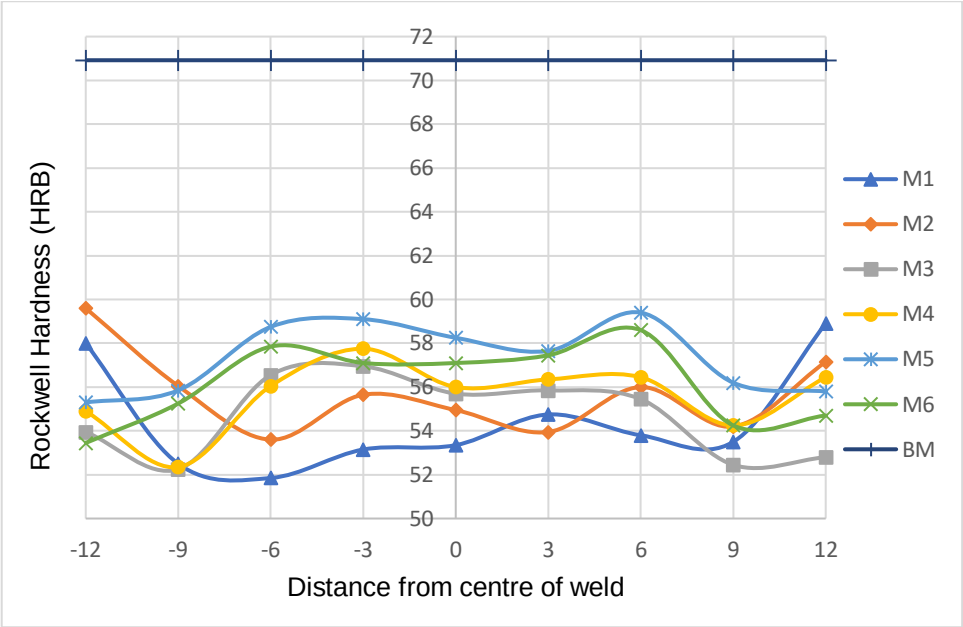

Figure 4.35: Shows Rockwell hardness results at the middle of the weld for all rotational speeds

The hardness value for specimens taken at the end of the weld for all rotational speeds including parent material are presented in figure 4.36. The specimen with highest hardness values is from the rotational speed of 1000 rpm. The rotational speed of 600 rpm has the lowest values in the retreating side, while the rotational speed of 700 rpm has the lowest hardness value in the advancing side of the stir zone. At the end of the weld 1200 rpm had specimens with higher UTS and the smallest average grain sizes and 600 rpm had higher percentage elongation.

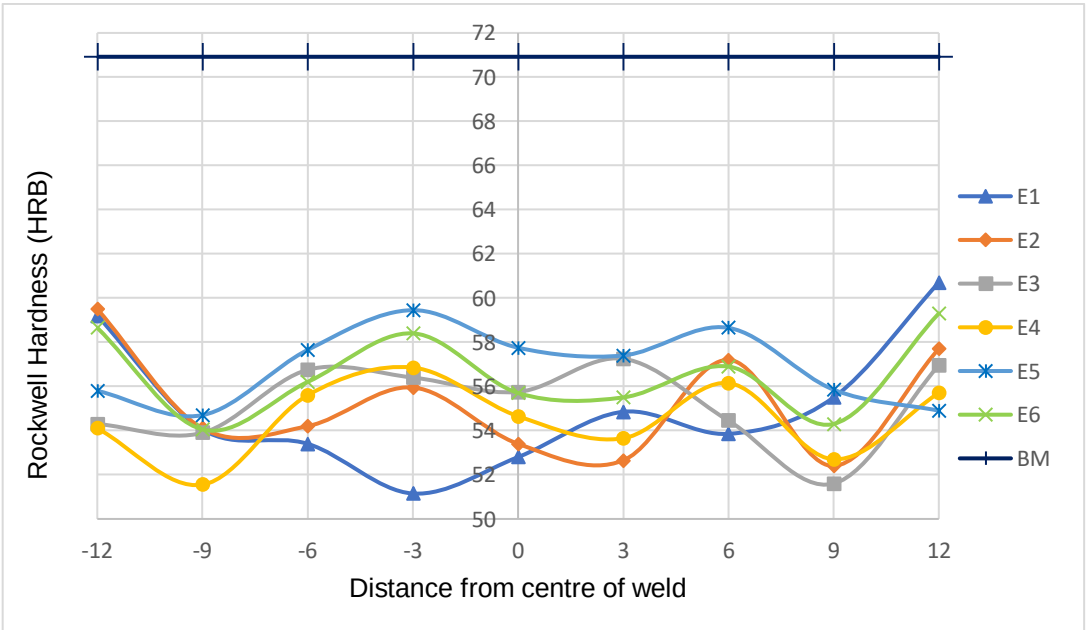

Figure 4.36: Shows Rockwell hardness at the end of the weld for all rotational speeds

The purpose of performing the Rockwell hardness test, was to evaluate which of the FSW rotational speeds has specimens with the highest resistance to plastic deformation or indentation. At the start, middle and end of friction stir welded specimens, specimens S5, M5 and E5 welded with a rotational speed of 1000 rpm shows the highest values in the SZ, TMAZ and HAZ throughout. While specimens from rotational speed 600 rpm which has the lowest grain sizes and higher tensile properties show lower hardness values in the three zones. With rotational speed 1200 rpm having the second highest hardness values throughout the SZ, TMAZ and HAZ.

4.5 Summary

It was observed that grain sizes had a correlation with tensile properties and fractography analysis. The rotational speed (600 rpm) which had the highest tensile properties (ultimate tensile strength and percentage elongation) had the smallest grain sizes even though it comprised of surface grooves, voids and wormholes at the beginning of the weld.

The hardness test results shown no correlation with the tensile properties nor the grain sizes. The specimens with higher average hardness values, had lower tensile properties and bigger grain sizes.

CHAPTER 5: CONCLUSION AND FUTURE WORK

5.1 Conclusion

The objective of this study was to investigate the influence of rotational speeds on the friction stir welding of 6082-T6 aluminium alloy joints using a constant welding speed of 80 mm/min. All of the welded specimens had weaker mechanical properties than that of the parent metal specimen. None-the-less, an optimum rotational speed was found.

In the microstructure of all specimens welded at different rotation speeds and also looking at the grain average sizes in the stir zone. The rotational speed of 600 rpm had smaller grain sizes at the start and middle of the weld. While 1200 rpm had smaller grain sizes at the end of the weld. Rotational speed 600 rpm specimens were also found without defects except specimen S1.

Tensile properties, ultimate tensile strength and percentage elongation were tested and compared at different rotational speeds. For both tensile properties, it was found that rotational speed of 600 rpm had the highest values throughout the weld than other rotational speeds. At the start, middle and end of the weld the UTS values were found to be 187, 189 and 185 MPa respectively. While rotational speed 1200 rpm had the highest UTS value at the end of weld with value 186 MPa. The highest percentage elongation values from start, middle and end were found at rotational speed of 600 rpm with values of 18, 18 and 19 % respectively. When all fractured tensile specimens were put under a Scanning Electron Microscope to evaluate their type of failure by means of fractograghy. It was found that all specimens from rotational speed of 600 rpm had ductile fractures.

Hardness was tested using the Rockwell hardness testing method. The rotational speed that had the closest hardness values to the parent materials was of 1000 rpm. Hardness has shown no correlation to tensile properties and grain sizes, as the rotational speed that had finer microstructure and greater tensile properties had weaker hardness. It was observed that as the rotational speed increases the hardness increased until an optimum rotational speed of 1000rpm was reached and it decreased at 1200 rpm.

Looking at the macrostructure of all specimens it was observed that rotational speed 600 rpm had welds with lesser defects, with specimens M1 and E1 having no defects visible even while specimen S1 had a huge wormhole visible in the stir zone. This speed is the lowest speed tested. As the rotational speeds were increased, they seem to be causing defects to the

specimens; 900 rpm seems to be the only high rotational speed to have fewer defects visible on the macrostructure.

Rotational speed of 600rpm specimen had a huge wormhole at the start but had the highest tensile properties, smaller grain size and a ductile fracture. Specimens at the middle and end had no macrostructural defects. The higher tensile properties on the smallest rotational speed, might be caused by rapid cooling of the specimen as it had lower heat input during welding than higher rotational speeds. Rotaional speed of 600 rpm was selected as the optimum rotational speed when friction stir welding 6 mm thick 6082-T6 aluminium alloy plates with a welding speed of 80mm/min.

5.2 Future work

For future purposes, it will be best to know the force exerted on each workpiece during the plunging period and it should be a constant one throughout. The tensile testing machine should be of newer technology and be able to show the Young's Modulus of each specimen tested.

In order to get higher hardness and tensile values, the specimens could be hardened or made stronger by heat treatment (annealing or quenching), which in the case of 6082 aluminium alloy will be tempering (T6) at high temperatures. Investigating cooling temperatures could be of beneficiary to understanding the effects of rotational speed in friction stir welding of 6082-T6 aluminium alloys.

For fractography and microstructure having a lot of unknown structures a SEM with EDX available in order to identify different chemical composition formed during friction stir welding of 6082-T6 at different rotational speeds and identifying all the unknown structures that should not be used. To also see which rotational speed gives the highest percentage of chemical compounds that are good or not good for the strength and microstructure of 6082-T6 aluminium alloys.

Bibliography

Adamowski, J., Gambaro, C., Lertora, E., Ponte, M. & Szkodo, M. 2007. Analysis of FSW welds made of aluminium alloy AW6082-T6. *Archives of Materials Science and Engineering*, 28(8): 453–460.

Ahmadi, H., Arab, N.B.M., Ghasemi, F.A. & Farsani, R.E. 2012. Influence of Pin Profile on Quality of Friction Stir Lap Welds in Carbon Fiber Reinforced Polypropylene Composite. *International Journal of Mechanics and Applications*, 2(3): 24–28. http://article.sapub.org/10.5923.j.mechanics.20120203.01.html.

Anil Kumar, H.M., Venkata Ramana, V. & Pawar, M. 2018. Experimental Study on Dissimilar Friction Stir welding of Aluminium Alloys (5083-H111 and 6082-T6) to investigate the mechanical properties. *IOP Conference Series: Materials Science and Engineering*, 330: 012076. http://stacks.iop.org/1757-899X/330/i=1/a=012076?key=crossref.a1d1e883e601ff2134ef45c7f3695fad.

Bisadi, H., Tavakoli, A., Tour Sangsaraki, M. & Tour Sangsaraki, K. 2013. The influences of rotational and welding speeds on microstructures and mechanical properties of friction stir welded Al5083 and commercially pure copper sheets lap joints. *Materials and Design*, 43: 80–88. http://dx.doi.org/10.1016/j.matdes.2012.06.029.

Bozorgzadeh, M.A. & Idris, M.H. 2015. Friction stir Welding. *International Journal of Review in Life Sciences*, 5(3 (Jul-Sep)).

Dawood, H.I., Mohammed, K.S. & Wahab, Z.A. 2013. The Effect of Rotational Speed on Flow Behavior and Weld Properties in Friction Stir Welding of Pure Aluminum. *Advanced Materials Research*, 795(May 2016): 182–189.

Elangovan, K. & Balasubramanian, V. 2008. Influences of tool pin profile and welding speed on the formation of friction stir processing zone in AA2219 aluminium alloy. *Journal of Materials Processing Technology*, (459): 7–18.

Esmaily, M., Mortazavi, N., Osikowicz, W., Hindsefelt, H., Svensson, J.E., Halvarsson, M., Martin, J. & Johansson, L.G. 2016. Bobbin and conventional friction stir welding of thick extruded AA6005-T6 profiles. *Materials and Design*, 108: 114–125. http://dx.doi.org/10.1016/j.matdes.2016.06.089.

Farajkhah, V. & Liu, Y. 2017. Effect of clamping area and welding speed on the friction stir welding-induced residual stresses. *International Journal of Advanced Manufacturing Technology*, 90(1–4): 339–348.

Feng, T.T., Zhang, X.H., Fan, G.J. & Xu, L.F. 2017. Effect of the rotational speed of on the surface quality of 6061 Al-alloy welded joint using friction stir welding.

Gemme, F., Verreman, Y., Dubourg, L. & Wanjara, P. 2011. Effect of welding parameters on microstructure and mechanical properties of AA7075-T6 friction stir welded joints. *Fatigue*

and Fracture of Engineering Materials and Structures, 34(11): 877–886.

Ghaffarpour, M., Kolahgar, S., Dariani, B.M. & Dehghani, K. 2013. Evaluation of dissimilar welds of 5083-H12 and 6061-T6 produced by friction stir welding. *Metallurgical and Materials Transactions A: Physical Metallurgy and Materials Science*, 44(8): 3697–3707.

Hao, H.L., Ni, D.R., Huang, H., Wang, D., Xiao, B.L., Nie, Z.R. & Ma, Z.Y. 2013. Effect of welding parameters on microstructure and mechanical properties of friction stir welded Al-Mg-Er alloy. *Materials Science and Engineering A*, 559(January 2013): 889–896.

Hasan, M.M., Ishak, M. & Rejab, M.R.M. 2015. A simplified design of clamping system and fixtures for friction stir welding of aluminium alloys. *Journal of Mechanical Engineering and Sciences (JMES)*, 9(December): 1628–1639.

He, J., Ling, Z. & Li, H. 2016. Effect of tool rotational speed on residual stress , microstructure , and tensile properties of friction stir welded 6061-T6 aluminum alloy thick plate. *The International Journal of Advanced Manufacturing Technology*, (174): 1953–1961.

Hema, P., Sai Kumar Naik, K. & Ravindranath, K. 2017. Prediction of Effect of Process Parameters on Friction Stir Welded Joints ofdissimilar Aluminium Alloy AA2014 & AA6061 Using Taper Pin Profile. *Materials Today: Proceedings*, 4(2): 2174–2183.

Huang, Y., Wang, Y., Wan, L., Liu, H., Shen, J., dos Santos, J.F., Zhou, L. & Feng, J. 2016. Material-flow behavior during friction-stir welding of 6082-T6 aluminum alloy. *International Journal of Advanced Manufacturing Technology*, 87(1–4): 1115–1123. http://dx.doi.org/10.1007/s00170-016-8603-7.

Jenarthanan, M.P., Varun Varma, C. & Krishna Manohar, V. 2018. Impact of friction stir welding (FSW) process parameters on tensile strength during dissimilar welds of AA2014 and AA6061. In *Materials Today: Proceedings*.

Kallee, S.W., Nicholas, E.D. & Thomas, W.M. 2001. Friction Stir Welding- Invention, Innovations and Applications. *8th International Conference on Joints in Aluminium*, 43(11): 1–13. http://www.twi.co.uk/services/technical-information/published-papers/friction-stir-welding-invention-innovations-and-applications-march-2001/%5Cnhttp://www.csa.com/partners/viewrecord.php?requester=gs&collection=TRD&recid=2006025505442MD.

Kaplonek, W. & Nadolny, K. 2013. Advanced desktop SEM used for measurement and analysis of the abrasive tool's active surface. *Acta Microscopica*, 22(3): 278–288.

Klobčar, D., Kosec, L., Pietras, A. & Smolej, A. 2012. Friction-stir welding of aluminium alloy 5083. *Materiali in Tehnologije*, 46(5): 483–488.

Ko, Y., Lee, K. & Baik, K. 2017. Effect of tool rotational speed on mechanical properties and microstructure of friction stir welding joints within Ti – 6Al – 4V alloy sheets. *Advances in Mechanical Engineering*, 9(8): 1–7.

Kumar, B.P. & Noor, S.A. 2012. Design and development of Fixture for Friction Stir Welding. *Innovative Systems Design and Engineering*, 3(12): 305–311.

http://ieeexplore.ieee.org/xpls/abs_all.jsp?arnumber=6216279.

Kumbhar, N.T. & Bhanumurthy, K. 2012. Friction Stir Welding of Al 5052 with Al 6061 Alloys. *Journal of Metallurgy*, 2012: 1–7.

Leitão, C., Leal, R.M., Rodrigues, D.M., Vilaça, P. & Loureiro, A. 2008. Material flow in Friction Stir Welding. *Microscopy and Microanalysis*, 14(S3): 87–90. http://www.journals.cambridge.org/abstract_S1431927608089472.

Liu, H., Hu, Y., Dou, C. & Sekulic, D.P. 2017. An effect of the rotation speed on microstructure and mechanical properties of the friction stir welded 2060-T8 Al-Li alloy. *Materials Characterization*.

Mao, Y., Ke, L., Liu, F., Huang, C., Chen, Y. & Liu, Q. 2015. Effect of welding parameters on microstructure and mechanical properties of friction stir welded joints of 2060 aluminum lithium alloy. *International Journal of Advanced Manufacturing Technology*, 81(5–8): 1419–1431.

Mishra, R.S. & Ma, Z.Y. 2005. Friction stir welding and processing. *Materials Science and Engineering R: Reports*, 50(1–2): 1–78.

Möser, M. 1987. Fractography with the SEM (Failure Analysis). : 366–385.

Nourouzi, S., Shakeri, M., Karimi, N. & Habibnia, M. 2012. Effect of Tool Rotation Speed and Feed Rate on Friction Stir Welding of 1100 Aluminum Alloy to Carbon Steel. *Materials and Manufacturing Technologies XIV*, 445(January): 741–746.

Paik, J.K. 2009. Mechanical properties of friction stir welded aluminum alloys 5083 and 5383. *International Journal of Naval Architecture and Ocean Engineering*, 1(1): 39–49.

Prabha, K.A., Putha, P.K. & Prasad, B.S. 2018. Effect of tool rotational speed on mechanical properties of aluminium alloy 5083 weldments in friction stir welding. In *Materials Today: Proceedings*.

Raja, A.R., Yusufzai, M.Z.K. & Vashista, M. 2016. Characterization of advancing and retreating weld of friction stir welding of aluminium Characterization of advancing and retreating weld of friction stir welding of aluminium. , (December). https://www.researchgate.net/profile/Avinash_Ravi_Raja/publication/311583563_Characterization_of_advancing_and_retreating_weld_of_friction_stir_welding_of_aluminium/links/584f033508aeb989252cb273/Characterization-of-advancing-and-retreating-weld-of-fricti.

Raja, P., Bojanampati, S., Karthikeyan, R. & Ganithi, R. 2018. Effect of rotation speed and welding speed on Friction Stir Welding of AA1100 Aluminium alloy. *IOP Conf. Series: Materials Science and Engineering*, 346.

Raja, S., Hasan, F. & Ansari, A.H. 2016. Effect of Friction Stir Welding on the Hardness of Al-6061 T6 aluminium alloy. : 6–9.

Rajamanickam, N. & Balusamy, V. 2008. Effects of process parameters on mechanical properties of friction stir welds using design of experiments. *Indian Journal of Engineering*

and Materials Sciences, 15(4): 293–299.

Rodrigues, D.M., Leitão, C., Louro, R., Gouveia, H. & Loureiro, A. 2010. High speed friction stir welding of aluminium alloys. *Science and Technology of Welding and Joining*, 15(8): 676–681. http://www.maneyonline.com/doi/abs/10.1179/136217110X12785889550181.

Rose, A.R., Manisekar, K. & Balasubramanian, V. 2012. Influences of welding speed on tensile properties of friction stir welded AZ61A magnesium alloy. *Journal of Materials Engineering and Performance*, 21(2): 257–265.

Safeen, M.W. & Spena, P.R. 2019. Main issues in quality of friction stir welding joints of aluminum alloy and steel sheets. *Metals*, 9(5).

Saini, P., Tayal, S.P., Kumar, A. & Kaushik, V. 2013. Experimental Study of Hardness by Friction Stir Welding of 6061-T6 Aluminium Pieces. : 792–794.

Sakthivel, T., Sengar, G.S. & Mukhopadhyay, J. 2009. Effect of welding speed on microstructure and mechanical properties of friction-stir-welded aluminum. *International Journal of Advanced Manufacturing Technology*, 43(5–6): 468–473.

Sedmak, A., Kumar, R., Chattopadhyaya, S., Hloch, S., Tadic, S., Djurdjevic, A., Cekovic, I. & Donceva, E. 2016. Heat input effect of friction stir welding on aluminium alloy AA 6061-T6 welded joint. *Thermal Science*, 20(2): 637–641. http://www.doiserbia.nb.rs/Article.aspx?ID=0354-98361500147D.

Sharma, C., Dwivedi, D.K. & Kumar, P. 2012. Effect of welding parameters on microstructure and mechanical properties of friction stir welded joints of AA7039 aluminum alloy. *Materials and Design*, 36: 379–390. http://dx.doi.org/10.1016/j.matdes.2011.10.054.

Sharma, G. & Dwivedi, D.K. 2017. Study on microstructure and mechanical properties of dissimilar steel joint developed using friction stir welding. *The International Journal of Advanced Manufacturing Technology*, 88(5–8): 1299–1307. http://link.springer.com/10.1007/s00170-016-8763-5.

Singarapu, U., Adepu, K. & Reddy, S. 2015. Influence of tool material and rotational speed on mechanical properties of friction stir welded AZ31B magnesium alloy. *Journal of Magnesium and Alloys*, 3: 335–344. http://dx.doi.org/10.1016/j.jma.2015.10.001.

Singh, J. & Sharma, P. 2013. Effect of Tool Rotational Speed on Mechanical Properties of Friction Stir Welded Aluminium Alloys. *International Journal of Latest Trends in Engineering and Technology (IJLTET)*, 3(1): 353–357.

Sinha, V.C., Kundu, S. & Chatterjee, S. 2016. Microstructure and mechanical properties of similar and dissimilar joints of aluminium alloy and pure copper by friction stir welding. *Perspectives in Science*, 8: 543–546. http://dx.doi.org/10.1016/j.pisc.2016.06.015.

Soni, N., Chandrashekhar, S., A., K. & V.R., C. 2017. Defects Formation during Friction Stir Welding : A Review. *International Journal of Engineering and Management Research*, 7(3): 121–125.

Srinivasa Rao, M.S., Ravi Kumar, B.V.R. & Manzoor Hussain, M. 2017. Experimental study on

the effect of welding parameters and tool pin profiles on the IS:65032 aluminum alloy FSW joints. In *Materials Today: Proceedings*.

Sun, H., Zhou, Q., Zhu, J. & Peng, Y. 2017. Analysis on the Fracture of Al-Cu Dissimilar Materials Friction Stir Welding Lap Joint. *Journal of Materials Engineering and Performance*, 26(12): 5715–5722.

Taheri, H., Kilpatrick, M., Norvalls, M., Harper, W.J., Koester, L.W., Bigelow, T. & Bond, L.J. 2019. Investigation of nondestructive testing methods for friction stirwelding. *Metals*, 9(6): 1–22.

Tamadon, A., Pons, D.J., Sued, K. & Clucas, D. 2018. Thermomechanical Grain Refinement in AA6082-T6. : 1–20.

Tongne, A., Desrayaud, C., Jahazi, M. & Feulvarch, E. 2016. On material flow in Friction Stir Welded Al alloys. , 239: 273–283.

Torun, O. 2016. Effect of Welding Parameters on Microstructure and Mechanical Properties of Cast Fe-40Al Alloy. *Metals*, 6(10): 229.

Ugender, S. 2018. Influence of tool pin profile and rotational speed on the formation of friction stir welding zone in AZ31 magnesium alloy. *Journal of Magnesium and Alloys*, 6(2): 205–213. https://linkinghub.elsevier.com/retrieve/pii/S2213956718300173.

Ugender, S., Kumar, A. & Somi Reddy, A. 2014. Influence of Friction Stir Welding Parameters on Mechanical Properties of 6061- T6 Aluminum Alloy. *RESEARCH AND REVIEWS: JOURNAL OF ENGINEERING AND TECHNOLOGY*, 3(3): 9–13.

Unnikrishnan, M.A. & Edwin Raja Dhas, J. 2017. A Survey on Friction Stir Welding of Dissimilar Magnesium Alloys. *IOP Conference Series: Materials Science and Engineering*, 247(1).

Venable, R. ; Bucher, J. 2004. Back Actuators for Segmented Mirrors and Other Applications Actuation mechanisms could be simpler . Mechanism for Self-Reacted Friction Stir Welding This mechanism performs better than others that have been tried . , (October): 20–21.

Vijaya Ramnath, B., Elanchezhian, C., Rajesh, S., Jaya Prakash, S., Kumaar, B.M. & Rajeshkannan, K. 2018. Design and Development of Milling Fixture for Friction Stir Welding. *Materials Today: Proceedings*, 5(1): 1832–1838. https://doi.org/10.1016/j.matpr.2017.11.282.

Wan, L., Huang, Y., Guo, W., Lv, S. & Feng, J. 2014. Mechanical Properties and Microstructure of 6082-T6 Aluminum Alloy Joints by Self-support Friction Stir Welding. *Journal of Materials Science and Technology*, 30(12): 1243–1250. http://dx.doi.org/10.1016/j.jmst.2014.04.009.

Wang, F.F., Li, W.Y., Shen, J., Hu, S.Y. & Santos, J.F. 2015. Effect of tool rotational speed on the microstructure and mechanical properties of bobbin tool friction stir welding of Al – Li alloy. , 86: 933–940.

Wen, Q., Yue, Y., Ji, S., Li, Z. & Gao, S. 2016. Effect of Welding Speeds on Mechanical

Properties of Level Compensation Friction Stir Welded 6061-T6 Aluminum Alloy. , 35(4): 375–379.

Widener, C.A., Talia, J.E., Tweedy, B.M. & Burford, D.A. 2006. HIGH-ROTATIONAL SPEED FRICTION STIR WELDING WITH A FIXED SHOULDER. *6th International Symposium on Friction Stir Welding*.

Yovanovich, M. 2006. Micro and Macro Hardness Measurements, Correlations, and Contact Models. *44th AIAA Aerospace Sciences Meeting and Exhibit*, (January): 1–28. http://arc.aiaa.org/doi/10.2514/6.2006-979.

Zhang, L. & Wang, X. 2018. Microstructure Evolution and Properties of Friction Stir Welding Joint for 6082-T6 Aluminum Alloy. , 21(6).

Zhang, Y., Sato, Y.S., Kokawa, H., Park, S.H.C. & Hirano, S. 2008. Stir zone microstructure of commercial purity titanium friction stir welded using pcBN tool. *Materials Science and Engineering A*, 488(1–2): 25–30.

Zipp, R.D., Company, J.I.C., Dahlberg, E.P. & Consultants, M. 1987. Preparation and Preservation of Fracture Specimens. *ASM handbook: Fractography*, 12: 72–77.

APPENDICES

APPENDIX A

FSW Stress-Strain test results at different speeds

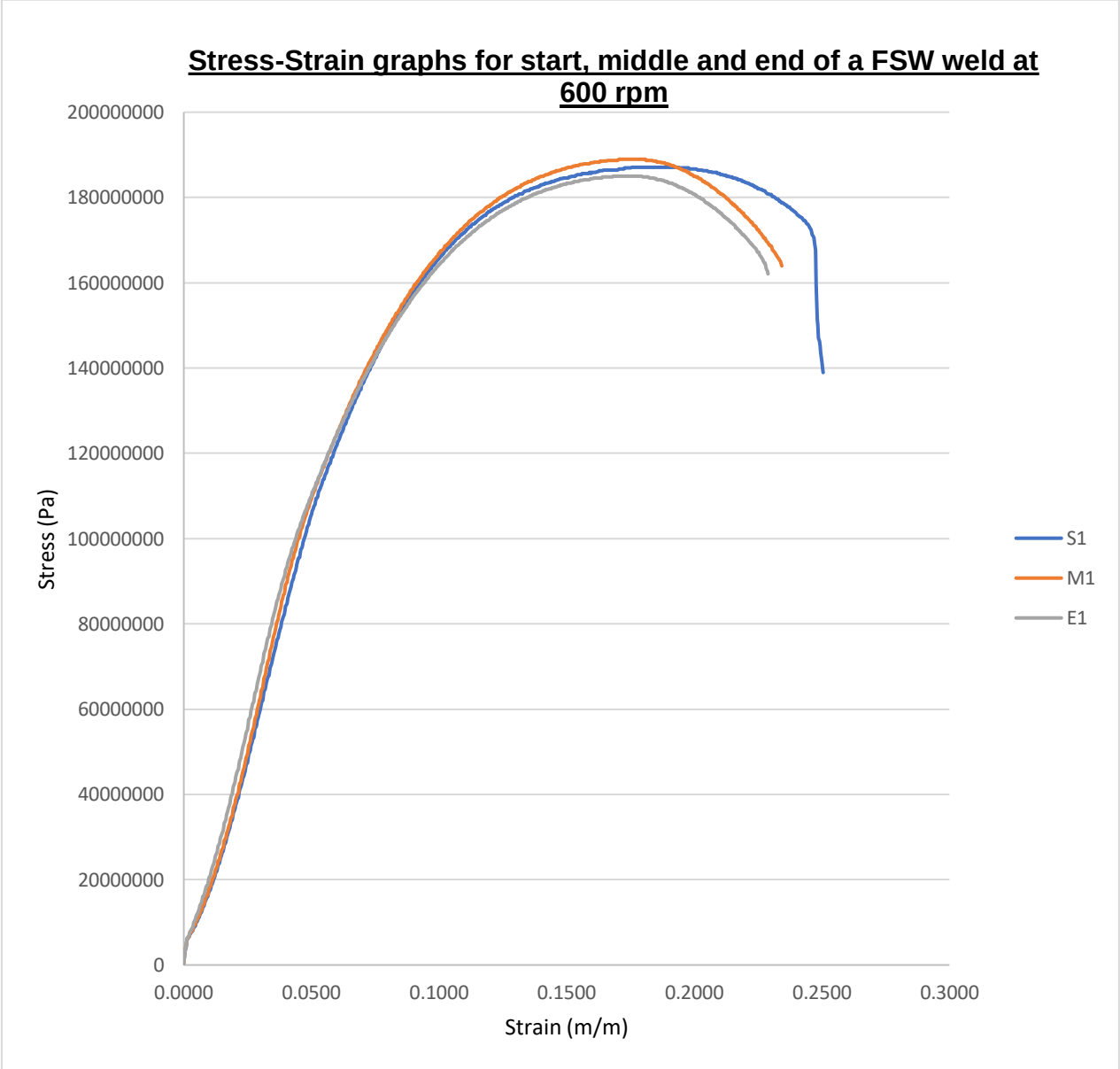

Figure A 1: Stress-strain graphs for start, middle and end of FSW welds at 700 rpm

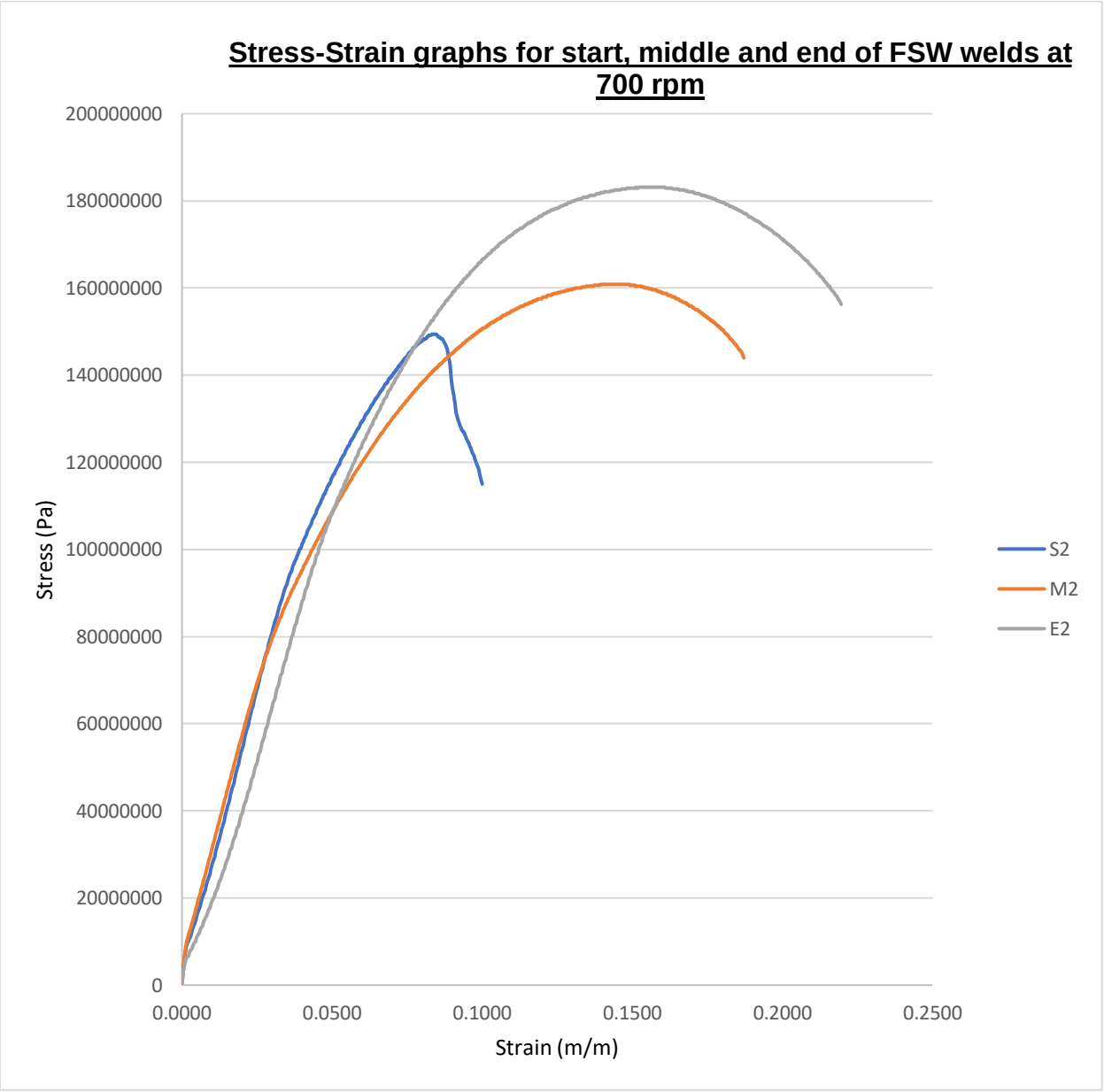

Figure A 2: Stress-strain graphs for start, middle and end of FSW welds at 700 rpm

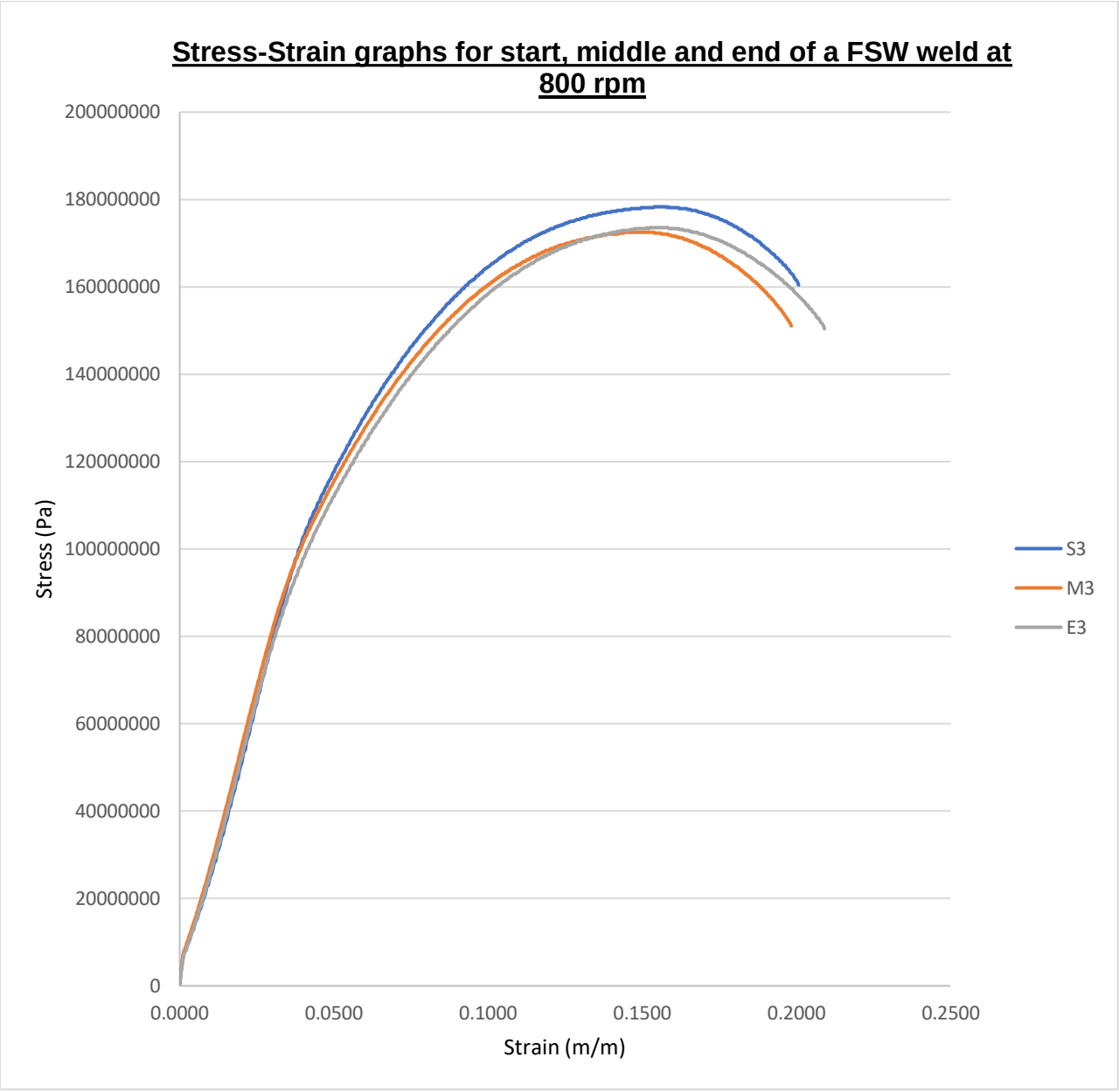

Figure A 3: Stress-strain graphs for start, middle and end of a FSW weld at 800 rpm

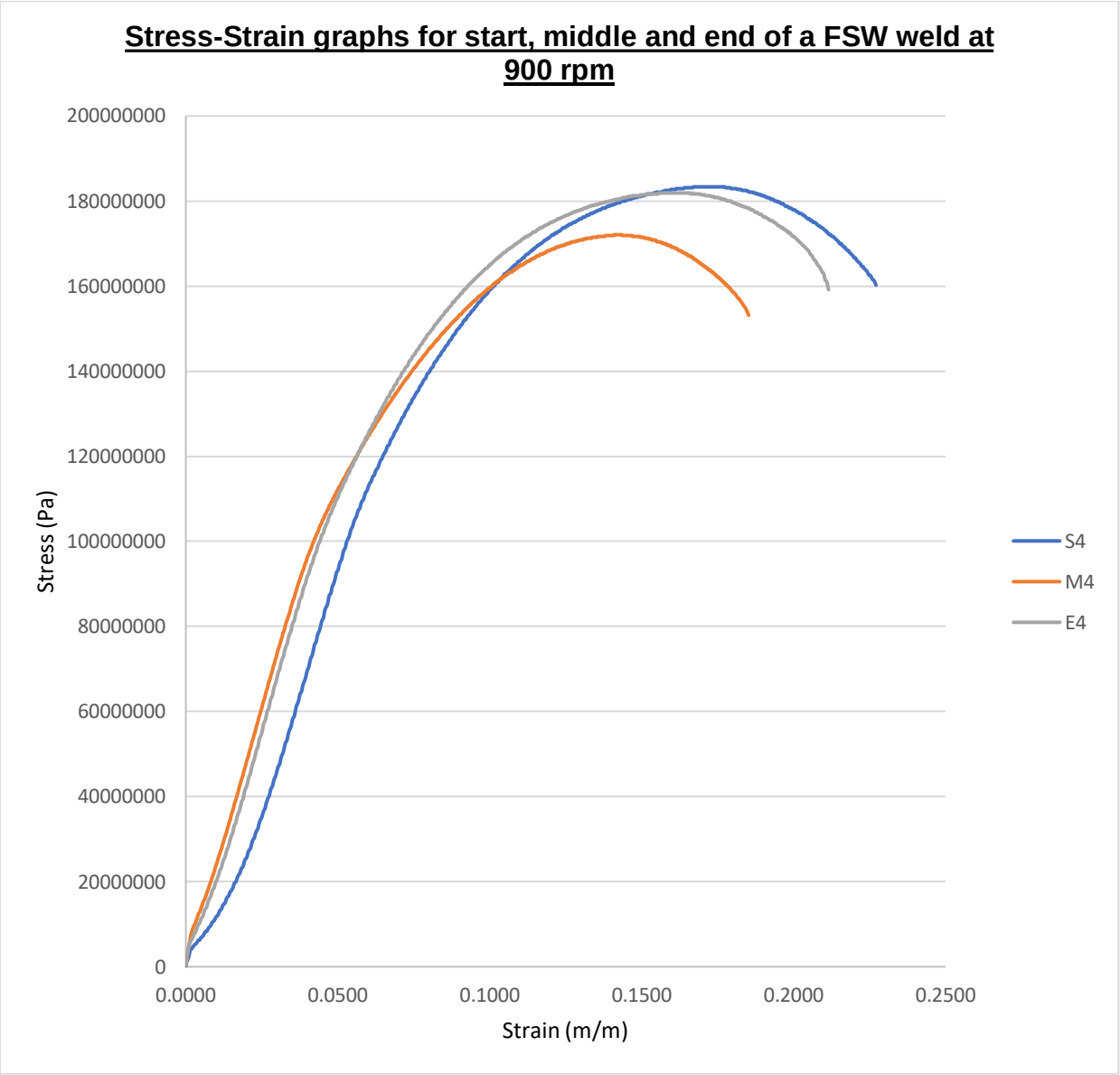

Figure A 4 :Stress-strain graphs for start, middle and end of a FSW weld at 900 rpm

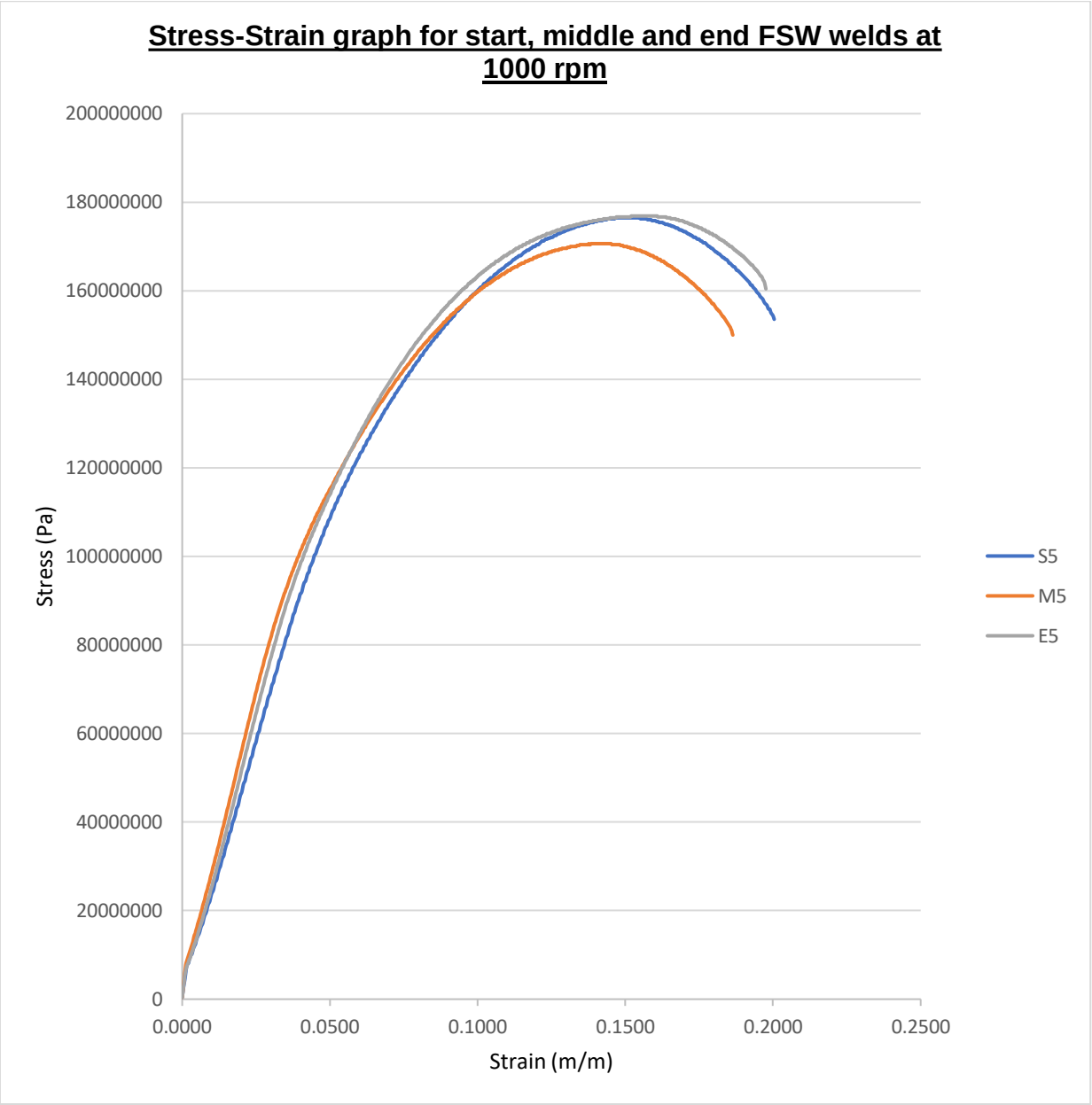

Figure A 5: Stress-strain graphs for start, middle and end of a FSW weld at 1000 rpm

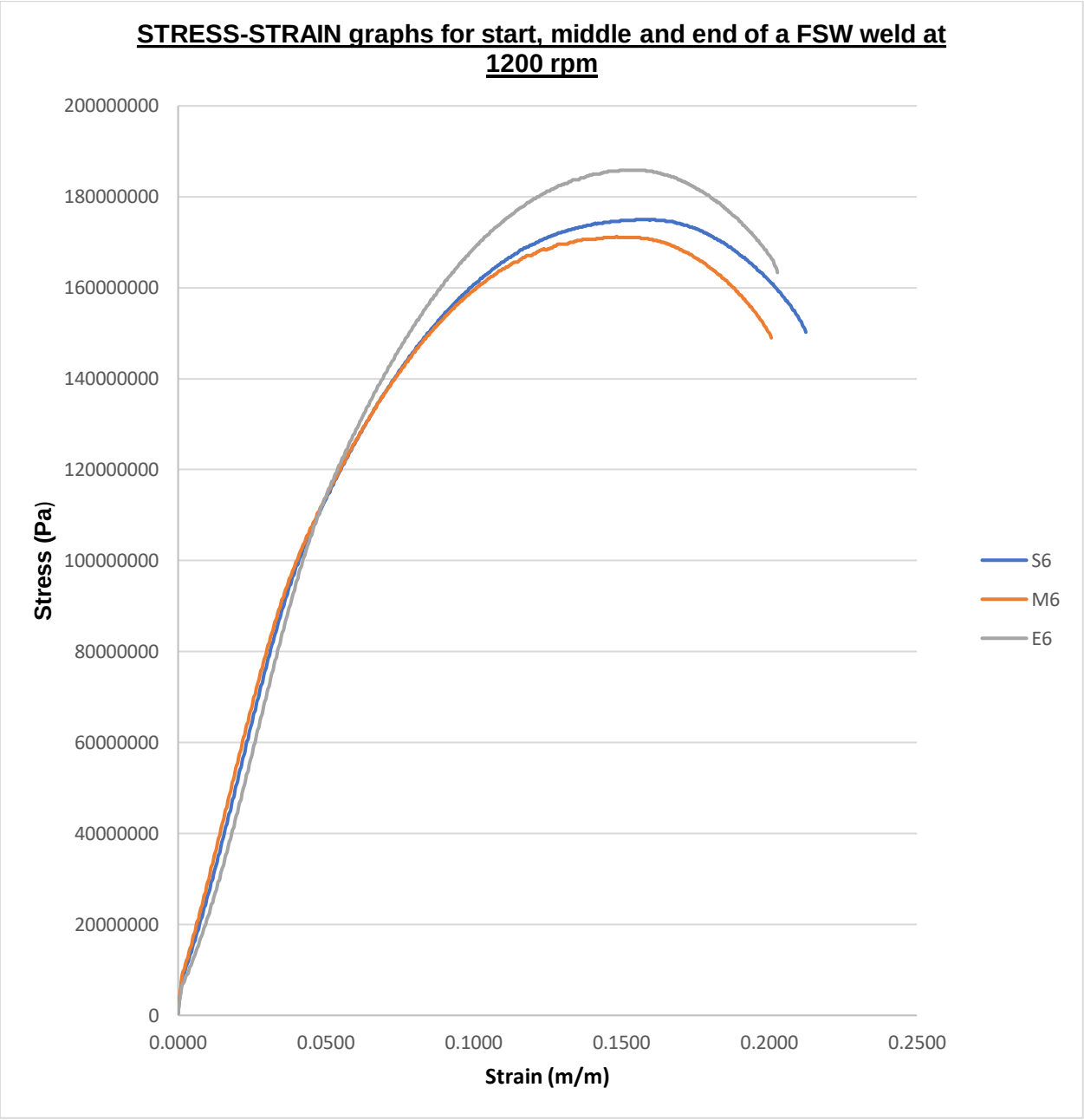

Figure A 6: Stress-strain graphs for start, middle and end of a FSW weld at 1200 rpm

Appendix B

Hardness Scale Conversion Table

HARDNESS SCALE CONVERSION TABLE

Approximate Equivalents of Hardness Scales for Soft Metals

VICKERS DPH	ROCKWELL									BRINELL BHN	
HV/10	B	E	F	G	H	K	15-T	30-T	45-T	500kg	3000kg
254	100			83			93	82	72	201	240
248	99			81			93	82	71	195	234
243	98			79			93	81	70	189	228
238	97			78			92	81	69	184	222
234	97			77			92	80	69	181	218
230	96			76			92	80	68	179	214
226	96			75			92	80	68	177	210
222	95			74			92	79	67	175	208
217	95			73			92	79	67	171	205
213	94			73			91	79	66	169	203
208	93			71			91	78	66	167	200
204	92			70		100	91	78	65	163	195
200	92			69		100	91	77	64	162	193
196	91			68		100	90	77	64	160	190
192	90			66		99	90	76	63	157	185
188	89			64		98	90	76	62	154	180
184	88			63		97	90	75	61	151	176
180	87			61		97	89	75	60	148	172
176	86			59		96	89	74	59	145	169
172	85			58		95	89	74	58	142	165
168	84			56		94	88	73	57	140	162

164	83			54		93	88	72	56	137	159
160	82			53		92	88	72	55	135	156
156	81			51		91	87	71	54	133	153
152	80			49		91	87	70	53	130	150
148	79			48		90	87	70	52	128	147
144	78			46		89	86	69	51	126	144
141	77			44		88	86	68	50	124	141
139	76			43		87	86	68	49	122	139
137	75		100	41		86	85	67	49	120	137
135	74		99	39		85	85	66	48	118	135
132	73		99	38		85	85	66	47	116	132
130	72		98	36		84	84	65	46	114	130
127	71	100	98	35		83	84	64	45	112	127
125	70	100	97	33		82	84	64	44	110	125
123	69	99	96	31		81	83	63	43	109	123
120	68	98	96	30		80	83	62	42	107	121
118	67	98	95	28		79	83	62	41	106	119
116	66	97	95	27		78	82	61	40	104	117
115	65	96	94	25		78	82	60	39	102	116
114	64	96	94	24		77	82	60	38	101	114
113	63	95	93	22		76	81	59	37	99	112
112	62	95	92	21		75	81	58	36	98	110
111	61	94	92	19		74	81	57	35	96	108
110	60	93	91	18		73	81	57	34	95	107
108	59	93	91	16		72	80	56	32	94	106
107	58	92	90	15		71	80	55	31	92	104
106	57	91	90	13		71	80	55	30	91	102
105	56	91	89	12		70	79	54	29	90	101
104	55	90	88	10		69	79	53	28	89	99
103	54	90	88	9		68	79	53	27	87	
102	53	89	87	7		67	78	52	26	86	
101	52	88	87	6		66	78	51	25	85	
100	51	88	86	4		65	78	51	24	84	
100	50	87	86	3		65	77	50	23	83	
99	49	87	85			64	77	49	22	82	
98	48	86	85			63	77	49	21	81	
97	47	85	84			62	76	48	20	80	

96	46	85	83			61	76	47	19	79	
95	45	84	83			60	76	46	18	79	
95	44	84	82			59	75	46	17	78	
94	43	83	82			58	75	45	16	77	
93	42	82	81			58	75	44	15	76	
92	41	82	81			57	74	44	14	75	
91	40	81	80			56	74	43	13	74	
90	39	80	79			55	74	42	11	74	
90	38	80	79			54	73	42	10	73	
89	37	79	78			53	73	41	9	72	
88	36	79	78		100	52	73	40	8	71	
88	35	78	77		100	52	72	40	7	71	
87	34	77	77		99	51	72	39	6	70	
87	33	77	76		99	50	72	38	5	69	
86	32	76	75		99	49	71	38	4	68	
86	31	76	75		98	48	71	37	3	68	
85	30	75	74		98	47	71	36	2	67	
85	29	74	74		98	46	70	36	1	66	
84	28	74	73		97	45	70	35		66	
84	27	73	73		97	45	70	34		65	
83	26	73	72		97	44	69	33		65	
83	25	72	71		96	42	69	33		64	
82	24	71	71		96	42	69	32		64	
82	23	71	70		96	41	68	31		63	
81	22	70	70		95	40	68	31		63	
81	21	70	69		95	39	68	30		62	
80	20	69	69		95	38	68	29		62	
80	19	68	68		94	38	67	29		61	
79	18	68	67		94	37	67	28		61	
79	17	67	67		93	36	67	27		60	
78	16	67	66		93	35	66	26		60	
78	15	66	66		93	34	66	26		59	
77	14	65	65		92	33	66	25		59	
77	13	65	65		92	32	65	24		58	
76	12	64	64		92	32	65	24		58	
76	11	64	64		91	31	65	23		57	
75	10	63	63		91	30	64	22		57	

75	9	62	62		91	29	64	22		56	
74	8	62	62		90	28	64	21		56	
74	7	61	61		90	27	63	20		56	
73	6	61	61		90	26	63	20		55	
73	5	60	60		89	26	63	19		55	
72	4	59	60		89	25	62	18		55	
72	3	59	59		88	24	62	17		54	
71	2	58	58		88	23	62	17		54	
71	1	58	58		88	22	61	16		53	
70	0	57	57		87	21	61	15		53	
HV/10	**B**	**E**	**F**	**G**	**H**	**K**	**15-T**	**30-T**	**45-T**	**500kg**	**3000kg**
VICKERS DPH	**ROCKWELL**									**BRINELL BHN**	